GSBS Dissertations and Theses   Graduate School of Biomedical Sciences

2016-05-05

Characterizing the Disorder in Tristetraprolin and its Contribution to Post-Transcriptional Gene Regulation: A Dissertation

Laura M. Deveau
University of Massachusetts Medical School

Let us know how access to this document benefits you.

CHARACTERIZING THE DISORDER IN TRISTETRAPROLIN AND ITS
CONTRIBUTION TO POST-TRANSCRIPTIONAL GENE REGULATION

A Dissertation Presented

By

LAURA DEVEAU

Submitted to the Faculty of the
University of Massachusetts Graduate School of Biomedical Sciences, Worcester
in partial fulfillment of the requirements for the degree of

DOCTOR OF PHILOSOPHY

May 5th, 2016

Biochemistry and Molecular Pharmacology

Signature Page

CHARACTERIZING THE DISORDER IN TRISTETRAPROLIN AND ITS
CONTRIBUTION TO POST-TRANSCRIPTIONAL GENE REGULATION

A Dissertation Presented By

LAURA DEVEAU

The signatures of the Dissertation Defense Committee signify completion and approval
as to style and content of the Dissertation

_____
Francesca Massi, PhD, Thesis Advisor

_____
Jill Zitzewitz, PhD, Member of Committee

_____
Laurence Stern, PhD, Member of Committee

_____
Kendall Knight, PhD, Member of Committee

_____
Philip Bevilacqua, PhD, Member of Committee

The signature of the Chair of the Committee signifies that the written dissertation meets
the requirements of the Dissertation Committee

_____
Celia Schiffer, PhD, Chair of Committee

The signature of the Dean of the Graduate School of Biomedical Sciences signifies that
the student has met all graduation requirements of the school.

_____
Anthony Carruthers, PhD,
Dean of the Graduate School of Biomedical Sciences

Program in Biochemistry and Molecular Pharmacology

May 5th, 2016

Dedication

This work is dedicated to my little girl, Olivia.

I hope my work inspires you as much as your love inspires me.

I love you!

Acknowledgements

Nothing can quite compare to the outpouring of love, support, and encouragement that I've received while preparing my dissertation and defending my thesis. Thank you to my thesis advisor, Francesca Massi, family and friends for all of your support and help while preparing for my defense. Overwhelmed and at a loss for the perfect words, so I will just say thank you from the bottom of my heart. There's no way I could have gotten this far without ALL of you!

Abstract

RNA-binding proteins (RBPs) are important for a wide variety of biological processes involved in gene regulation. However, the structural and dynamic contributions to their biological activity are poorly understood. The tristetraprolin (TTP) family of RBPs, including TTP, TIS11b and TIS11d, regulate the stability of mRNA transcripts encoding for key cancer-related proteins, such as tumor necrosis factor-α and vascular endothelial growth factor. Biophysical studies have shown that the RNA binding domain, consisting of two CCCH zinc fingers (ZFs), is folded in the absence of RNA in TIS11d and TIS11b. In TTP, however, only ZF1 adopts a stable fold, while RNA is required to completely fold the tandem zinc finger (TZF). The focus of this research was to understand the origin and biological significance of the structural differences observed for the TZF domains of TTP and TIS11d. Three residues were shown to control the affinity for the structural Zn^{2+} and determine the folding of ZF2 in the absence of RNA. The partially-folded TZF domain of TTP has greater selectivity for RNA sequences than the fully folded TZF domain of TIS11d. The mRNA destabilizing activity of TTP was increased when the partially disordered RBD of TTP was replaced with the fully structured TZF domain of TIS11d. Disruption of the structure and/or dynamics of the TZF domain observed in the disease-associated mutations of TIS11d, P190L and D219E, results in aberrant cytoplasmic localization. This work demonstrates that the extent of RBD folding in the TTP family is important for differential RNA recognition, mRNA turnover, and protein localization *in vivo*.

Table of Contents

List of Tables

List of Figures

List of Copyrighted Materials Produced by Author

Most of the text for Chapter III is published in American Chemical Society (ACS)

Chemical Biology. No permission needed for authors to use this material.

DeveauLM., and MassiF. (2015). Three residues make an evolutionary switch for folding and RNA-destabilizing activity in the TTP family of proteins ACS Chem. Biol. 11(2) 435-43.

List of Symbols, Abbreviations, or Nomenclature

3' UTR, 3' untranslated region; HEK, Human embryonic kidney; HMQC, heteronuclear multiple-quantum coherence; HSQC, heteronuclear single-quantum coherence; MD, molecular dynamics; NOESY, nuclear Overhauser effect spectroscopy; NMR, nuclear magnetic resonance; PDB, Protein Data Bank; RBD, RNA-binding domain; TNFα, tumor necrosis factor α; TTP, tristetraprolin; TTP$_{TZF\ TIS11d}$, TTP containing the TZF domain of TIS11d; TZF, tandem zinc finger; ZF, zinc finger; ZF1, N-terminal zinc finger; ZF2, C-terminal zinc finger; WT, wild type, FP, fluorescence polarization.

Preface

All of the work presented here was completed in Dr. Francesca Massi's Laboratory at the

University of Massachusetts Medical School.

Chapter III is adapted from:
DeveauLM., and MassiF. (2015). Three residues make an evolutionary switch for folding
and RNA-destabilizing activity in the TTP family of proteins ACS Chem. Biol. 11(2)
435-43.

Work from the following publications was not included in this dissertation:

1) Probing the structural and dynamical effects of the charged residues of the TZF
domain of TIS11d. Morgan BR, **LM Deveau**, and Massi F. *Biophy J.* 2015.

2) Investigating the origin of the partially unstructured tandem zinc finger domain in
TTP. Tavella D, **Deveau LM**, Massi F. (in review ACS JCTC)

3) Networks of charged side chains shape the complex folding free energy surface of a *de
novo* designed protein. **Deveau LM** and Nobrega RP, Koga N, Tatsumi-Koga R, Baker
D, Massi F, Matthews CR. (submitted to PNAS)

4) Allosteric inhibition of a stem cell RNA-binding protein by an intermediary
metabolite. Clingman CC, **Deveau LM**, Hay SA, Genga RM, Shandilya SM, Massi F,
Ryder SP. *Elife* 2014. `

5) A conserved three-nucleotide core motif defines Musashi RNA-binding specificity.
Zearfoss NR, **Deveau LM**, Clingman CC, Massi F, and Ryder SP. *J Biol Chem* 2014.

6) The molecular basis of drug resistance against hepatitis C virus NS3/4A protease
inhibitors. Romano KP, Ali A, Aydin C, Soumana D, Ozen A, **Deveau LM**, Silver C,
Cao H, Newton A, Petropoulos CJ, Huang W, Schiffer CA. *PLoS Pathog.* 2012.

7) Molecular mechanisms of viral and host cell substrate recognition by hepatitis C virus
NS3/4A protease. Romano KP, Laine JM, **Deveau LM**, Cao H, Massi F, Schiffer CA. *J
Virol.* 2011.

8) A Hydrophobic Core Stabilizes the Residual Structure in the RRM2 Intermediate State
of TDP-43. Mackness BC, Morgan BR, **Deveau LM**, Tran MT, Kathuria SV, Massi F,
Zitzewitz JA. (intended submission PNAS)

Chapter I: Introduction

The eukaryotic cell needs to rapidly modify the expression levels of many proteins in response to cues from the extracellular environment. Although traditionally much work has focused on transcriptional control, one major mechanism for regulating protein expression is through post-transcriptional regulation of their encoding mRNAs. This regulatory mechanism is particularly important during development when transcription is typically repressed[1-5] and during inflammatory responses[6] when multiple genes are coordinated rapidly in response to external cues. During these processes, RNA-binding proteins (RBPs) function to control mRNA stability, editing, localization, and translational efficiency [7,8]. Accordingly, dysregulation of these processes causes multiple diseases, including amyloid lateral sclerosis (ALS)[9], fragile X retardation[10], acute inflammatory disease[11] and cancer [12,13]. Therefore, examining the relationship between the structure and function of RBPs and their cellular targets is essential for understanding their role in human physiology.

Post-transcriptional gene regulation is dependent on protein and RNA structure

Post-transcriptional regulation begins during RNA synthesis in the nucleus and continues through translation in the cytoplasm. Many mRNA processing steps, including mRNA capping, splicing, polyadenylation, and editing as well as mRNA localization and stability, are regulated at the post-transcriptional level through the function of RBPs[14,15] (Figure 1.1).

Because RBPs are the main facilitators of post-transcriptional regulation, it is imperative to understand how these proteins recognize and bind to their RNA targets.

RBPs contain multiple structural motifs, such as the RNA recognition motifs (RRMs)[16,17], double stranded RNA-binding domain (dsRBD)[18,19], K Homology (KH) domains[20,21], and zinc fingers (ZFs)[22-24] (Table 1.1).

Just as the primary amino acid sequence and secondary structure of RBPs are important for RNA-mediated

Figure 3.1 Post-transcriptional Regulation is controlled by RBPs. A model of the eukaryotic cell. Post-transcriptional regulation is facilitated by RNA binding proteins (small circles) at many mRNA processing steps, including mRNA capping, splicing, polyadenylation and editing. Many factors remain associated with mRNA and are exported out of the nucleus into the cytoplasm to facilitate mRNA localization, translation and degradation.

post-transcriptional control, so are the primary sequence integrities and folds of the target RNAs; most RBPs –even those among the same class of RBP domains– have sequence and RNA structure preferences. For example, some proteins have high sequence specific requirements, such as MuscleBlind Like (MBNL)-1 CCCH protein that binds specifically to CUG or CCUG repeats to regulate tissue specific alternative splicing[25]. Additionally, some proteins have specific RNA shape requirements, such as the RNA editing enzyme ADAR2[26], which is a dsRBP that binds specifically to the minor- major – minor-groove surface of RNA. Typically, post-transcriptional regulation is achieved through the

interaction of RBPs to the 5′ or 3′ untranslated regions (UTRs) of the RNA[27]. These

RNAs can be single or double stranded, have secondary structure, such as hairpin and

stem loops that can interact to form tertiary structure and/or be modified via methylation,

each of which changes the structure and biochemical properties of the RNAs[28]. These

changes can have dramatic effects on a specific RBP′s recognition and binding of the

target RNA[29].

Table 1.1: RBPs contain multiple structural motifs

Name of domain	Structural description	Protein-RNA interface	Representative structure
RRM	~90 residue polypeptide chain folded into two alpha helices and four-antiparellel beta-strands	Aromatic residues stack specifically with ssRNA bases	MSI1[205]
dsRBD	~70 amino acids folded with two alpha-helices packed against a three stranded beta-sheet.	Shape specific recognition of dsRNA minor-major-minor groove patterns with sugar phosphate backbone	ADAR2[26]
KH	~70 amino acids and fold into three antiparallel beta sheets packed against three alpha helices	Binds to ds/ssRNA through aromatic stacking at the cleft formed between the first and second alpha helix and variable loop	NOVA2[20]
ZF	~70 amino acid peptide chain containing minimal secondary structure; fold according to the coordination of three cystines and a histidine residue by a zinc ion	ssRNA binding interactions occur through protein backbone and side chain hydrogen bond contacts and aromatic stacking.	MBNL1[25]

Post-transcriptional mRNA turnover

The fate of a particular mRNA is tightly regulated from transcription in the nucleus through translation and degradation in the cytoplasm. In the cytoplasm, mRNAs can be: (1) stored in a particular sub-cellular localization,[30] (2) assembled with ribosomes for protein synthesis[31], or (3) degraded[32]. One of the most important of these is mRNA decay, which acts as a quality control mechanism for aberrant transcripts and protein/mRNA levels in the cell[33]. Research in the last 3 decades has defined multiple pathways of mRNA turnover (Figure 1.2)[34]. Transcripts containing pre-mature stop codons due to incomplete splicing, transcription errors, or RNA mutations are subject to nonsense mediated decay[35]. In this process, mRNA degradation is triggered by 5′ decapping, 3′ poly(A) tail removal, and cleavage by endonucleases. All mRNA transcripts that pass quality control surveillance have a limited lifetime. In eukaryote cells, mRNA turnover occurs through deadenylated-mediated decay[36]. During this process, the nacent poly(A) tail is first removed via one of three processes. 1) The poly(A)-specific ribonuclease (PARN) complex that binds directly to the 5′cap of transcripts and removes nucleotides from its poly (A) tail. 2) The Ccr4/Caf1/Not complex forms a multimeric CCR4-NOT1 complex which binds to factors associated with the RNA. The association of CCR4-NOT1 complex with the RNA positions the CAF1 deadenylase for poly (A) tail removal. 3) In a few cases, the Pan2/Pan3 exonuclease complex has been shown to be important for initial poly (A) shortening. These processes of deadenylation destabilizes the cap binding complex, and triggers 3′ to 5′ mRNA degradation via a 3′ exoribonuclease multi-protein complex called the exosome.

Alternatively, deadenylation can trigger Lsm1-7 protein complex binding to the 3′ end of the RNA leading to decapping via the Dcp1/Dcp2-complex, which in turn causes the degradation of the mRNA by the 5′–3′ exonuclease Xrn1 (Figure 1.2).
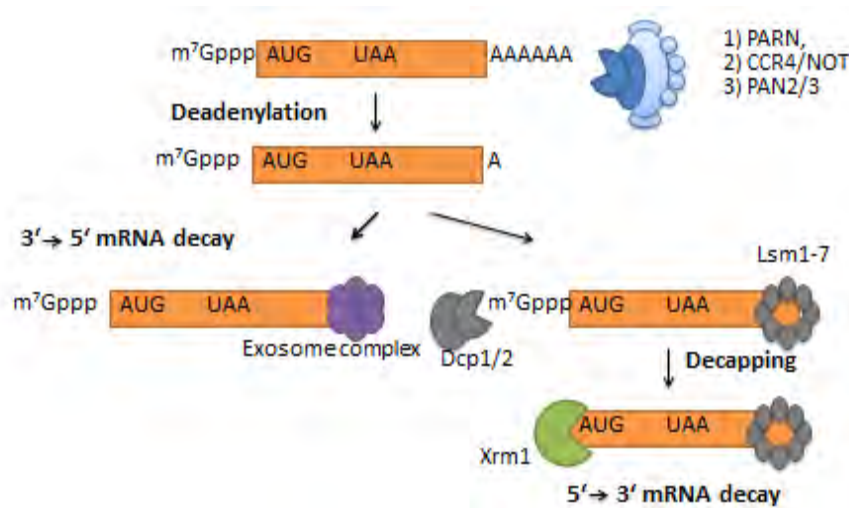
Figure 1.2: Post-transcriptional mRNA decay mechanisms. A model of eukaryotic mRNA turnover. Nacent mRNAs (orange) have a 5′cap and 3′ poly (A) tail. Deadenylation by 1) the poly (A)-specific ribonuclease (PARN) 2) the Ccr4/Not complex or 3) the Pan2/Pan3 exonuclease initiate poly (A) shortening. Deadenylation triggers 3´ to 5′ mRNA degradation uses a 3′exosome complex. Alternatively, deadenylation triggers Lsm1-7 protein complex binding to the 3′ end of the RNA which triggers the removal of the 5´ cap of RNA by Dcp1/Dcp2-complex, which in turn causes the degradation of the mRNA by the 5′–3′ exonuclease Xrn1.

mRNA decay rates can vary substantially between mRNAs[37,38]. In mammalian cells, the average rate of decay is 8 hours; however, it can be as fast as 15 minutes (TNF-α) or as slow as 17 hours (β-globin)[39,40]. One feature that controls mRNA decay is stability elements, short sequence elements within mRNAs that control the rate of mRNA turnover[38]. One of the most well characterized instability elements controlled post-transcriptionally is the adenine and uracil rich sequence element (ARE) identified in 1986 by Cerami *et al*. AREs are sequence elements of 50-150 nucleotides located in the 3′-UTRs of mRNA with short half-lives[41]. Indeed, chimeric mRNAs containing an ARE

instead of their endogenous 3′-UTR have increased turnover in cells, suggesting that the

presence of these sequence elements leads to mRNA instability (Figure 1.3)[42]. ARE

motifs are enriched in essential inflammatory mediators, such as the cytokines tumor

necrosis factor (TNF)-α and interleukin (IL)-1α/ β, the lymphokine granulocyte-

macrophage colony stimulating factor (GM-CSF), highlighting the role these motifs play

in transient biological processes[41,43,44].
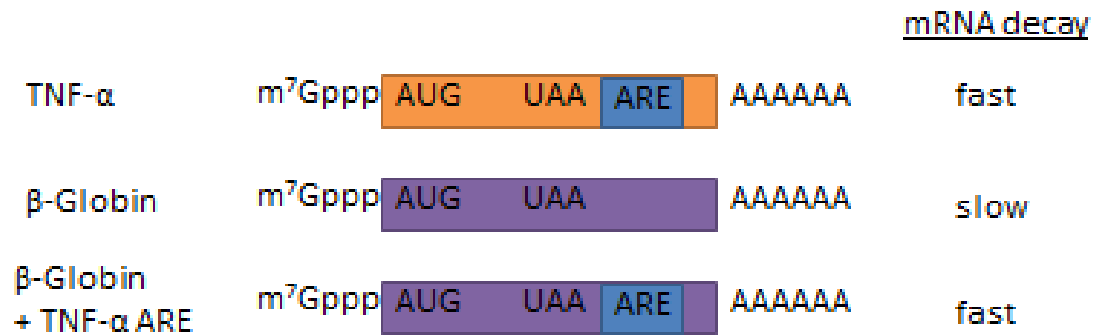
Figure 1.3: AREs controls mRNA decay. Schematic representation of the effects of the adenine-uridine rich stability element (ARE), short sequence elements (blue) within mRNAs that control the rate of mRNA turnover. ARE elements are located at the 3′ UTR of the TNF-α mRNA (orange) which trigger its fast deadenylation proceded with rapid degradation. β globin mRNAs (purple) are long lived (lifetime of 17 hours). Chimeras which replace β globin 3′ UTR with that of TNF-α rapidly degrade, indicating that it is the ARE feature on mRNA that dictates turnover[42].

Recent computational analysis estimates that 8% of human transcripts contain

AREs[45]. In fact, AREs are also found in many oncogenes, such as *c-fos, COX-2,* and *c-myc*. Mutation of the single ARE in *c-fos* does not decrease the ARE′s ability to

destabilize the mRNA, suggesting that the ARE motif is essential for only a subset of

transcripts[46]. Later studies showed that the stability of the ARE of the 3′ UTR is governed

through a host of RBPs (more than 20, including TTP) to either promote or inhibit the

ARE degradation machinery or influence their cellular localization[47]. Interestingly, the

RBD of these post-transcriptional regulators have different folds and binding site

preferences (Table 1.2).

Table 1.2: ARE binding proteins function, fold, and binding site preference

Protein family	Function in mRNA metabolism	Fold	Binding site
ELAV/Hu family	Stabilize	RRM	U and CU-rich sequences[48,49]
TTP family	Destabilize	CCCH	UUAUUUAUU[50]
HRNPD/AUF1 family	Stabilize	RRM	AUGUAUUGUUUAUACAU (hairpin)[51]
TIA1/TIAR	translational repressors	RRM	uridylate stretches[52]
KSRP	mRNA splicing/ destabilizing	KH	low sequence specificity[53]

Many of these ARE binding proteins compete for the same RNA sequence. For

example, Growth Associated Protein (GAP)-34 is a protein in the cell that controls axonal

outgrowth. KSRP binds to GAP-43 ARE mRNA to promote its decay in cells, while HuD

binds to and stabilizes this same mRNA. Given their antagonistic behavior, much work

has been done to investigate the competition between these proteins for ARE 3′UTRs.

Competition binding experiments have shown that HuD binds to the mRNA with a lower

affinity than KSRP. This results in the displacement of HuD upon KSRP overexpression

and subsequently leads to in an inhibition of axonal outgrowth. This example highlights

how the complex network of interactions between RBPs must be explored in order to

fully understand how these proteins regulate their mRNA targets *in vivo*[54].

Tristetraprolin

Of the many proteins that bind to AREs at 3′ UTRs, the most well characterized is tristetraprolin (TTP). TTP was originally identified as an early response gene whose expression is induced in response to many different stimuli, such as the pro-/anti-inflammatory factors TNF-α[55], IL-1β[56], and lipopolysaccharide (LPS)[57]. The role of TTP was first identified in a study involving the early expression of genes in 3T3 fibroblasts after treatment with insulin. The Blackshear group found that after exposing these cells for ten minutes to insulin, an increase in transcription levels was observed corresponding to the biogenesis of 25 proteins[58]. Of the transcripts sequenced, only one had a unique protein sequence, which contained 3 groups of 4 consecutive proline rich patches. They coined this early response gene "Tristetraprolin" (TTP). Since then TTP has been noted for its regulation of the short lived mRNA encoding the inflammatory cytokine, TNF-α. Early studies demonstrated that TTP-deficient mice suffer from systematic inflammatory syndrome, due to over-expression of TNF-α. Increased TNF-α concentrations seem to be directly linked to inflammatory syndrome in mice since symptoms are alleviated if TTP-deficient mice are injected with antibodies specific for TNF-α. Directed truncation experiments of the coding and noncoding sequences of TNF-α map TTPs binding to its 3′UTR highlighting a mechanism by which loss of TTP-mediated gene regulation can lead to chronic inflammatory diseases[59].

TTP mRNA decay is controlled through the recruitment of multimeric

polyadenylation decay enzymes

Tristetraprolin acts to limit cytokine toxicity by initiating mRNA decay through direct interactions between its N- and C- terminal domains and various deadenylases (Figure 1.4)[60]. Truncation and coimmunoprecipitation assays have determined that TTP associates with many of the known multimeric mRNA decay pathway enzymes, highlighted above[60]. Specifically, the Ccr4/Caf1/Not complex is recruited through an interaction between the conserved C-terminus of TTP with NOT1[61]. Recently, a C-terminal peptide of TTP, comprised of residues 312-326, was crystallized with the CCR4-NOT1 complex[62]. Although only a small fragment of the TTP sequence, mutations in this region of full-length TTP result in impaired RNA decay, further demonstrating CCR4-NOT1 interaction with the TTP family. However, this function of TTP (interactions with mRNA decay machinery) is tightly controlled through its mRNA/protein expression, phosphorylation, and subcellular localization as discussed below.

Figure 1.4: TTP is an RBP that facilitates rapid mRNA decay. A model of mRNA degradation initiated by TTP binding to ARE-containing mRNA. Binding of TTP promotes degradation of the mRNA transcripts, thus decreasing protein production of TNF-α.
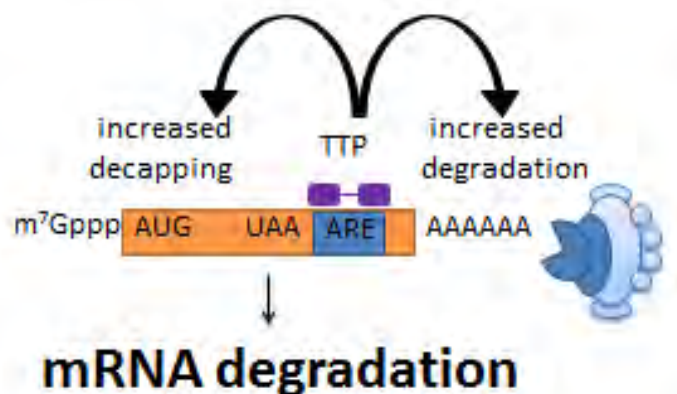
Regulation of the post-transcriptional regulator TTP

TTP controlled expression

In normally cultured fibroblast cells, TTP gene expression is low to undetectable and the protein is localized predominantly in the nucleus[63]. Transcription and subsequent translation of TTP can be induced when cells are exposed to stimuli, such as LPS[57]. LPS exposure activates the mitogen activated protein kinase (MAP-Kinase) family, initiating a cascade of signaling events to activate transcription factors specific for the rapid accumulation of mRNA encoding TTP[57]. TTP mRNA overexpression is seen as early as 15 minutes and basal levels are achieved within 2 hours after cells are stimulated[64]. This overexpression of TTP is necessary to prevent cellular damage from the toxic accumulation of cytokines.

TTP activity is spatiotemporally regulated

TTP's ability to target transcripts for rapid cytoplasmic degradation is positively regulated via its phosphorylation, specifically at residues S60 and S186 by MAPK-AP kinase-2 (MK2)[65]. Although mass spectroscopy has determined that both S60 and S186 are phosphorylated by MK2, binding assays demonstrate that phosphorylation of only S186 is critical for TTP association with the adapter protein 14-3-3. This interaction is necessary for the TTP/RNA complex translocation into processing bodies (P-bodies), the site of mRNA degradation, as the 14-3-3 acts as a chaperone to protect TTP from proteasomal degradation. Mutant S60A TTP has a moderate effect on 14-3-3 association, while mutant S186A completely abrogates binding to 14-3-3 adaptor protein. TTP's

interaction with the dimeric face of the 14-3-3 proteins is thought to preclude CAF1 association of the CCR4-CAF1-NOT1 complex for mRNA deadenylation and subsequent degradation. Therefore, in its phosphorylated state, TTP is rendered inactive for mRNA decay. Additional evidence suggests that the phosphorylation of TTP also decreases it relative affinity for the ARE sequence (Figure 1.5)[66].
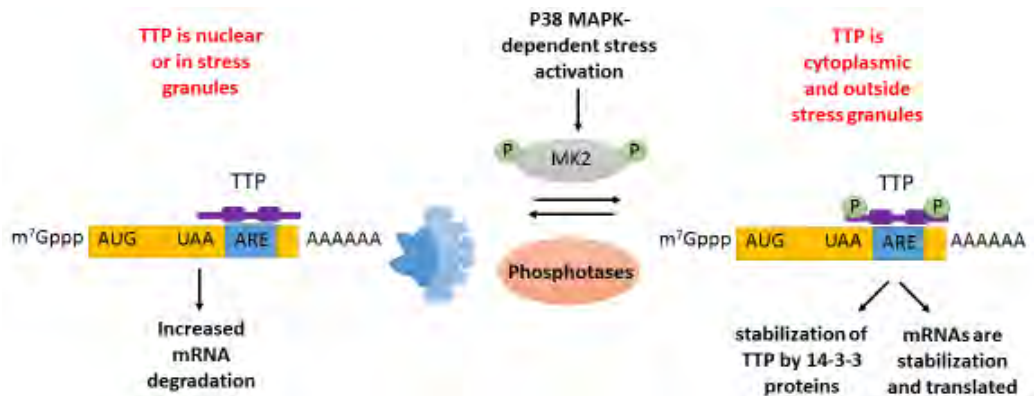
Figure 1.5: Phosphorylation regulates TTP activity in the cell. In TTP unphosphorylated state it binds to the 3'UTR of mRNA at the ARE for the rapid turnover of transcripts. Phosphorylation of TTP by MAPK-AP kinase-2 (MK2) allows for 14-3-3 adaptor protein association prevents the recruitment of degradation enzymes recruited by TTP. TTP is activated upon dephosphorylating by protein phosphatase 2A (PP2A). Phosphorylation of TTP also influences its subcellular localization (red text).

Phosphorylation is necessary for the temporal and spatial regulation of TTP in order to ensure the accurate turnover of TTP mRNA targets. Early experiments on fibroblast cells transfected with GFP-TTP suggested the protein was mostly nuclear[67]. When these cells are exposed to stress or an abundance of mitogens, such as LPS, TTP was seen to be translocated into the cytoplasm. Further evidence that TTP is a nucleocytoplasmic shuttling protein came with the identification of the N- terminal $L_{xxx}L_{xx}L_xL$ sequence that is characteristic of a nuclear export signal (NES)[68]. The nuclear export receptor Exportin 1 (XPO1), also known as chromosomal maintenance 1 (CRM-1), is responsible for binding to this sequence on TTP for it proper translocation out of

the nucleus[69]to subcellular foci containing mRNA decay enzymes. A separate study was done to map the nuclear localization sequence (NLS) of TTP. In this study, two basic residues, R134 and R137 of TTP RBD were shown to be critical for its association with Importin α/β[70]. Mutations of these arginines to alanines results in the mislocalization of TTP. Importin's association with the TTP/RNA complex suggests that TTP RNA binding may be required for its proper translocation into the cytoplasm. mRNA turnover occurs mainly in the cytoplasm and changing TTP′s primary sequence results in its mislocalization into cytoplasmic foci, suggesting RNA binding may provide another mechanism by which cells regulate TTP activity.

Alternative spatiotemporal regulation of TTP occurs in response to cellular stress (Figure 1.5). Under these conditions, unphosphorylated TTP colocalizes with ARE transcripts, forming transient foci in the cytoplasm called stress granules[32]. Stress granules are thought to sequester TTP from RNA decay enzymes, thereby providing another level of regulation of TTP′s activity in the cell. Only when TTP is phosphorylated is it excluded from stress granules and released into the site of mRNA turnover, P-bodies[71,72]. The interplay between RNA binding, phosphorylation, and subcellular localization is critical for TTP's function to keep the concentration of cytokines, such as TNF-α, low in the cell.

TTP and cancer

As described above, TTP activity is coordinated through multiple processes to regulate gene expression in order to control normal cellular homeostasis. Dysregulation of TTP at any of these steps has the potential to cause cancer in addition to chronic

inflammation, as TTP binds to many critical ARE-rich containing genes aberrantly

overexpressed in cancer (Table 1.3). Many immortalized cancer cell lines (brain, breast,

liver, colon, cervix) and tumors of the lung, ovary, prostrate, and thyroid have been

shown to have decreased expression levels of TTP[73]. In fact, decreased TTP gene

expression is now known to be a common prognostic indicator for breast cancer[74].

Other studies demonstrate that TTP plays a role in suppressing factors that

promote vascularization that lead to tumorigenesis. TTP-knockout mice injected with

cells containing TTP under control of an inducible promoter formed large tumors when

TTP was not expressed. However, when TTP expression was induced with doxycycline,

tumor size was reduced significantly. Furthermore, vascular endothelial growth factor

(VEGF) protein levels in these tumor cells decreased in response to increasing TTP gene

expression. Decreased VEGF levels, resulted in tumors with diminished

vascularization[100]. Presenting TTP as a tumor suppressor protein resulted in a multitude

of experiments to identify more cancer related mRNA targets (Table 1.2).

TTP loss-of-function mutations and their profound physiological effects on

disease manifestation and progression have opened up the characterization of the entire

TTP family, which includes TIS11d and TIS11b. Mutations in TIS11d and TIS11b have

also been associated with the pathogenesis of certain types of human cancers[101,102].

Frameshift and point mutations throughout the TIS11d gene locus have been identified in

tissues taken from leukemia patients[103]. In 2010, Hodson *et al.* identified Notch1 as a

direct target of TIS11d and TIS11b[104]. Additionally, the angiogenic gene DII4 is the only

known *in vivo* target of TIS11b[105]. The critical involvement of TIS11d and TIS11b in

cancer progression motivates detailed analysis to understand how these RNA-binding

proteins recognize and bind to their particular mRNA transcripts.

Table 1.3 Reported mRNA targets of TTP

Reported gene target	References	Cellular Process
TNF-α	55	Inflammation/Cancer
GM-CSF	75	
IL-2, IL-10 IL3, IL-6, IL-12	76,77	
Ier3	78	
Polo-like kinase 3	79	
Ccl2/3	80	
CD86	81	
c-fos	82	
cIAPs	83	
c-myc	84	
COX-2	85	
DUSP1	86	
E6-AP	87	
E47	88	
IDO	86	
IFN-gamma	89	
iNOS	90	
LATS2	91	
MHC (Class 1B and F)	86	
MMP-1	92	
PAI type 2	93	
TTP	94	
uPA	92	
uPAR	92	
VEGF	95	
Cyclin D1	84	Cell cycle
MIP-2	96	
p21	82	
1,4-galactosyltransferase	97	Other
PITX2	98	

*Targets in bold are classified as "physiological" targets - confirmed through assays with cells from knock-out mice. Genome wide analysis through microarray [98], (RIP)-Chip[77], and (PAR-Clip)[99] have also identified 250, 137, and 1,313 TTP mRNA targets, respectively.

TTP family members are not redundant

TTP family members, TIS11b and TIS11d were identified though tetradecanoyl phorbol acetate- (TPA-) induced expression in fibroblast cells in 1991[106]. TIS11b and TIS11d have TTP-like activity and bind to ARE-rich sequence elements in the 3′UTR of TNF-α, causing rapid deadenylation and triggering mRNA decay[107]. The fact that they all are located on different chromosomes; TTP chromosome 19q13.1, TIS11b chromosome 14q22-24, and TIS11d chromosome 2p22.3-p21, suggests that these proteins may be redundant[108]. However, TTP, TIS11b, and TIS11d knockout mice exhibit different phenotypes, suggesting these proteins cannot replace each other's function. Additionally, mRNA expression patterns of TTP, TIS11b, and TIS11d are different[109-111]. Where TTP mRNA expression is greatest in cervical tissue, TIS11b and TIS11d mRNA expression is greatest in the pancreas and thymus[112]. Therefore although TTP, TIS11b, and TIS11d perform the same function by operating to facilitate mRNA degradation, their different transcriptional regulation and the differences in their tissue specific expression suggests that they regulate different mRNA targets (Table 1.4).

Table 1.4: Summary of phenotypes observed in TTP family knockout mice

TTP family member	Phenotype of knockout mice
TTP	Death within 7-16 months as a result of systemic inflammatory syndrome
TIS11b	Embryonic lethality from embryonic vascular abnormalities and heart defects
TIS11d	Survive for approximately 2 weeks after birth, but suddenly die as a result defective hematopoiesis

Sequence alignments of TTP with its family members, TIS11d and TIS11b, show the highest sequence similarity at their CCCH tandem zinc finger (TZF) with TIS11d and TIS11b being 71% identical to TTP and 91% identical to each other, with most variations found in the N- and C-terminal domains (Figure 1.6)[113]. The minimal RNA binding unit of TTP was mapped through truncation experiments to contain the 72 amino acid (residues 102-174) CCCH tandem zinc finger (TZF) motif. The conservation of the CCCH motif therefore identified the RBD of TIS11d and TIS11b as well. Both the N- and C-terminal domains are necessary for the recruitment of enzymes essential for mRNA degradation and regulation of TTP activity though phosphorylation and localization[108]. Primary sequence predictions on the N-terminal and C-terminal domains determine that these domains are intrinsically disordered[114]. Given the high sequence conservation of the RNA-binding domains of TTP and TIS11 proteins, structural studies would help elucidate how these proteins recognize and bind distinct mRNAs, targeting them for mRNA decay.

```
hTTP        ------MANRYTM-DLTAIYESLLS-LSPDV--------PVPSDHGGTESS---PGW---
hTIS11b     MTTTLVSATIFDLSEVLCKGNKMLNYSAPSAGGCLLDRKAVGTPAGG--------GFPRR
hTIS11d     MSTTLLSA-FYDV-DFLCKTEKSLANLNLNN---MLDKKAVGTPVAAAPSSGFAPGFLRR
                 *  : ::  :. . . :. *      .    .* :  ..        *:

hTTP        -GSSGPWSLSPSDSSPSGVTSRLPGRSTSLVEGRSCGWV-------------PPPPG----
hTIS11b     HSVTLPSSKFHQNQLLSS------------LKG-----------------EPAPA----
hTIS11d     HSASNLHALAHPAPSPGSCSPKFPGA----ANGSSCGSAAAGGPTSYGTLKEPSGGGGTA
               . :   :        ..           :*              *. .

hTTP        FAPLAPRL---------GPE------LSPSPTSPTATSTTPSRYKTELCRTFSESGRCRYG
hTIS11b     LSSRDSRFRDRSFSEGGER------LLPTQKQPGGGQVNSSRYKTELCRPFEENGACKYG
hTIS11d     LLNKENKFRDRSFSENGDRSQHLLHLQQQQKGGGGSQINSTRYKTELCRPFEESGTCKYG
            :      .:        *       *    .   . . ..:********.*.*.* *.**

hTTP        AKCQFAHGLGELRQANRHPKYKTELCHKFYLQGRCPYGSRCHFIHNPSEDLAAP------
hTIS11b     DKCQFAHGIHELRSLTRHPKYKTELCRTFHTIGFCPYGPRCHFIHNAEERRALA------
hTIS11d     EKCQFAHGFHELRSLTRHPKYKTELCRTFHTIGFCPYGPRCHFIHNADERRPAPSGGASG
             *******: ***. .**********..*:  * ****.*******..*   . .

hTTP        ----------------GHPPVLRQSISFSGLPSGRRTSPPPPGLAGPSLSSSSFSPSSS
hTIS11b     -----GARDL-------SADRPRLQHSFSFAGFPSAAATAAATG------LLD---SPTSI
hTIS11d     DLRAFGTRDALHLGFPREPRPKLHHSLSFSGFPSGHHQ--PPGGLESPLLLD---SPTSR
                        * *.:*:**:*:**.      ..       *.    **:*

hTTP        PPPP----------------------------------------------GDLPLSP
hTIS11b     TPPP-------------------------------------IL----SADDLL--
hTIS11d     TPPPPSCSSASSCSSSASSCSSASAASTPSGAPTCCASAAAAAAAALLYGTGGAEDLLAP
            .***                                              .: *

hTTP        SAFSAAPGTPLARRDPTPVCC----------------------------------
hTIS11b     GSP----TLPDGTNNPFAFSSQELASLFA--------------------------
hTIS11d     GAPCAACSSASCANNAFAFGP-ELSSLITPLAIQTHNFAAVAAAAYYRSQQQQQQQGLAP
            .:         .    .:. ..

hTTP        -------PSCRRAT--------PIS--VWGPLGG----LVRTPSVQSLGSDPDEYAS---
hTIS11b     -------PSMGLPGGGS-----PTTF-LFRPMSESPHMFDSPPSPQDSLSDQEGYLSS--
hTIS11d     PAQPPAPPSATLPAGAAAPPSPPFSFQLPRRLSDSP-VFDAPPSPPDSLSDRDSYLSGSL
                   **   .         * : :   :.     :  .**  . ** :  * *

hTTP        SGSSLGGSDSPVFEAGVFAPPQPVAAPRRLPIFNRISVSE-
hTIS11b     SSSSHSGSDSPTLDNS-----------RRLPIFSRLSISDD
hTIS11d     SSGSLSGSESPSLDPG-----------RRLPIFSRLSISDD
            *..* .**:** ::  .          ******.*:*:*:
```

Figure 1.6: Sequence alignment of the human TTP family members. Identical residues (*), conserved (:) and semi-conserved (.) residues are denoted below each line of the alignment.

Differences in RNA binding for TIS11d and TTP are observed through NMR

Heteronuclear single quantum coherence (HSQC) spectra are the most common nuclear magnetic resonance (NMR) approach to observe changes in the secondary structure of proteins upon addition of substrate. This NMR experiment allows scientists to correlate the chemical shifts of covalently bond nuclei, often ^{15}N and ^{1}H, through measuring the direct transfer of magnetization from the proton to the bound amide nitrogen. The correlation of each amide ^{15}N and ^{1}H can be plotted to generate a two dimensional spectrum, where each amide peak, with the exception of proline, which does not have an amide group, can be assigned. HSQC experiments can provide information regarding whether a protein is folded, a molten globule, or unfolded[115]. Proteins that are well folded are characterized as having well dispersed and sharp peaks of every amino acid, whereas unfolded proteins give a signature of sharp, overlapping peaks at the 8 ppm region of the spectrum due to all amide protons being equally solvent exposed and sharing a similar chemical environment. A highly dynamic/flexible, molten globular protein spectrum shows significant line broadening of signals, and these cross peaks are not visible in the HSQC.

The HSQC spectrum of the TZF domain (100-174) of TTP has been published[116]. In this structure, only the amino terminal zinc finger and linker were clearly resolved and all cross peaks from its C- terminal zinc finger are missing, indicating that this region samples an ensemble of states and as consequence cross peaks are broadened beyond the detection limit. However, with the addition of RNA (5′UUUUAUUUAUUUU′3) cross-peaks were observed in the spectra that correspond to residues in the linker and zinc

finger 2 (ZF2) that were absent in the RNA-free spectra, but in the presence of zinc

(Zn^{2+}). The appearance of resonances from ZF2 indicates that a large conformational

change occurs upon RNA binding, which stabilizes the second zinc finger. Taken

together, these findings demonstrate that only the N-terminal TZF domain of TTP adopts

a stable fold in the unbound state in the presence of zinc (Zn^{2+}), and that RNA binding

induces folding of ZF2 (Figure 1.7).
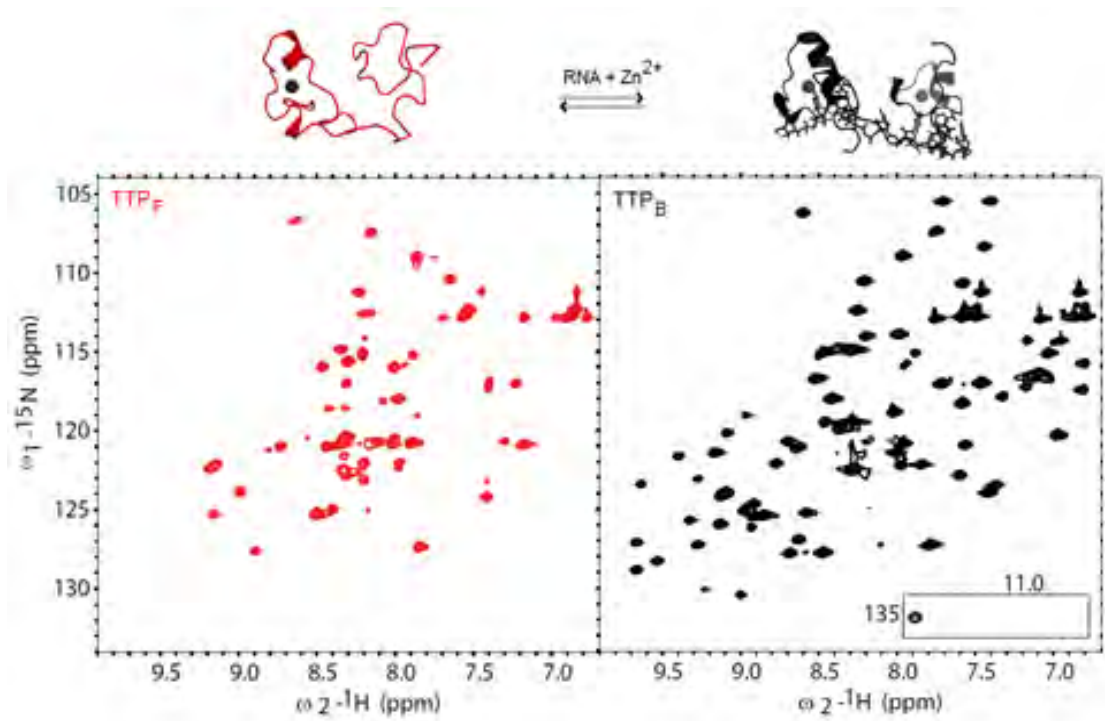
Figure 1.7: Only the N-terminal TZF domain of TTP adopts a stable fold in its unbound state; RNA binding induces complete TZF fold. HSQC spectra of free and bound TTP (red and black, respectively). Above each HSQC is a cartoon representation of TTP binding of the cognate RNA sequence. TTP undergoes an unfolding/ folded transition upon RNA binding.
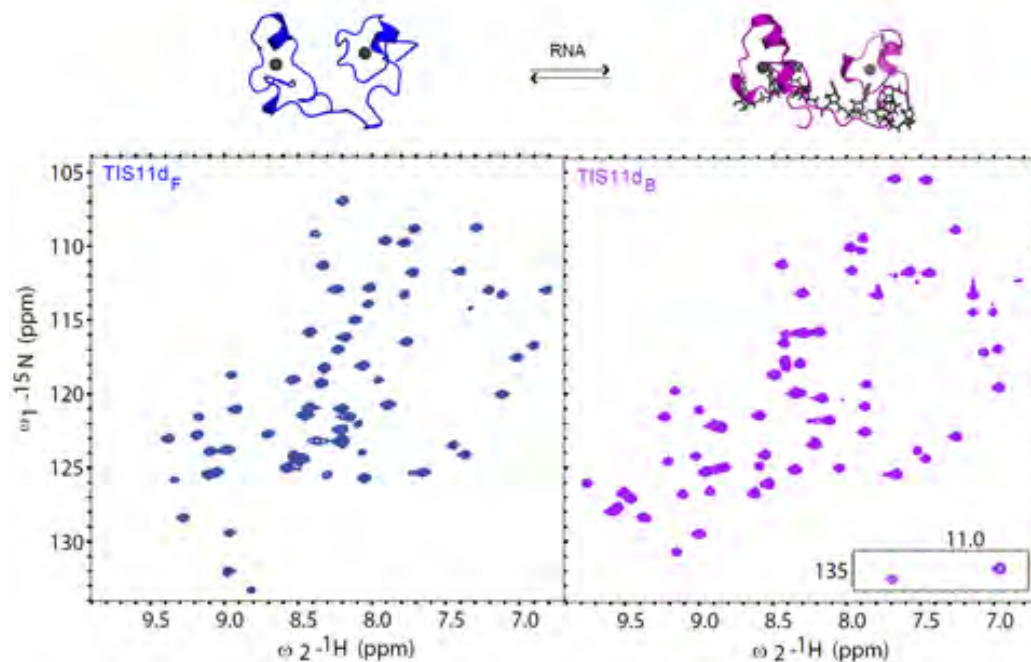
Figure 1.8: NMR and computational studies have shown that in the absence of RNA the structure of the two zinc fingers of TIS11d are maintained, although their orientation changes. HSQC spectra of free and bound TIS11d (blue and magenta, respectively). Above each HSQC is a cartoon representation of TIS11d binding of the cognate RNA sequence.

The structural rearrangement upon binding RNA is unique to the TZF of TTP.

Structural studies of TIS11d bound to the single stranded RNA sequence

5′UUAUUUAUU3′ (PDB code:1RGO) depicts two well folded zinc fingers, different

than what we observed for TTP[117]. NMR and computational studies have shown that in

the absence of RNA the structure of the two zinc fingers of TIS11d is maintained,

although their orientation changes due to the flexible nature of the linker region (Figure

1.8). The solved solution structure of the TIS11d/ RNA (U1-U2-A3-U4-U5-U6-A7-U8-

U9) complex is held together mainly through backbone (not side chain) hydrogen bonds,

van der Waals forces, and base stacking interactions along Watson-Crick edges of each

nucleotide. Additionally, side chain residues E157, C174, and C212 form hydrogen bonds with RNA bases. The RNA lies along one face of the TZF, with ZF1 interacting with the 3' U6 and A7 nucleotides and ZF2 with the 5' U2 and A3 nucleotides. The linker region of TIS11d is also involved in hydrogen bonding with the bases of the RNA, resulting in a more rigid protein/RNA complex. Comparisons of the TIS11 family show that many of the aromatic associations (Y170, F176, Y208, and F218) with the RNA are conserved (Figure 1.6)[118]. Mutations of these residues in TTP to non-aromatic amino acids abrogates RNA-binding. High sequence similarity of residues at the protein-RNA interface and the zinc coordinating residues for both TTP and TIS11d suggests that the TZFs may present similar binding conformations to the 5′UUAUUUAUU3′ RNA. The residues that differ at these positions (K169 in the first finger of TIS11d is an arginine in TTP, and R198 is a histidine in TTP) are basic residues in both proteins and therefore should be able to make similar contacts with the RNA. The positively charged amino acids along the protein/RNA interface neutralize the negatively charged phosphate backbone of the RNA allowing the binding of the TZFs to the single stranded RNA.

TTP family members are the main facilitators of post transcriptional mRNA decay. Although all of the family members have the same type of CCCH tandem zinc finger RNA binding domain, the structure of this domain differs among family members. We hypothesize that the structure of these proteins dictates its binding activity *in vitro* and *in vivo*. RNA recognition and binding by the TTP family is crucial as several human diseases, such as acute inflammatory disease and cancer are linked to post-transcriptional

dysfunction of these RBPs, we want to investigate how the TTP family members discriminate their mRNA targets.

Scope of thesis project

Tristetraprolin (TTP) is a prototype of the CCCH-type zinc finger proteins. Binding of TTP to AU-rich elements in the 3ʹUTR of many mRNA transcripts promotes deadenylation and consequent degradation of transcripts. This process provides an important mechanism for reducing the mRNA synthesis of key cytokines and growth factors associated with chronic inflammation and cancer. The TTP protein family in humans includes two other proteins, TIS11b and TIS11d. The TIS11b and TIS11d RNA binding domain (RBD) that consists of two CCCH zinc fingers (ZFs) shares a high degree of sequence identity to TTP and have TTP-like activity, yet neither TIS11b nor TIS11d can replace TTP function in TTP knockout mice. Additionally, TTP, TIS11b, and TIS11b have unique cell- and tissue specific expression, suggesting that they regulate different mRNA targets. Therefore, examining how the primary sequences of individual TTP family members influence cellular targets is essential for understanding their role in human physiology.

Biophysical characterization of the TTP family members, TIS11b and TIS11d shows that both ZFs are folded in the absence of RNA in TIS11d and TIS11b. In TTP, however, only ZF1 adopts a stable fold. Through this work, we have identified the origin of disorder/order for TTP/TIS11d, respectively. We constructed chimeric proteins of the TZF domains of TTP and TIS11d and characterized their structure and RNA-binding activity. We found that three residues located at the C-terminal end of the α-helix in ZF2

23

determine the structure of TZF domain. Additionally, we observed that the mRNA destabilizing activity of TTP was increased when the partially disordered TZF domain of TTP was replaced with the fully structured domain of TIS11d. These results show that the degree of structure of the TZF domain affects the function of the protein in the cell and indicates that the protein can modulate its activity through its structure.

This data was further supported through experiments on missense mutations localized in the RBD of TIS11d (P190L and D219E) that have been associated with acute myeloid leukemia and acute lymphoblastic leukemia, respectively. We observed that both mutations affect the structure and dynamics of the RBD of TIS11d. This result suggest how these mutations play a role in disease pathogenesis. Taken together, these results highlight how small variations in amino acid composition contribute to protein function both *in vivo* and *in vitro*.

In Chapter II, we demonstrate how the structural differences in TTP and TIS11ds RBDs affect their RNA binding activity using fluorescence polarization (FP) to measure RNA binding and NMR to observe to characterize structural differences. Together, these data suggest that the structure and flexibility of the TTP family of proteins affects the selection of mRNA targets.

In Chapter III, we evaluate the effects of mutations on the conserved six residue motif, the R(K)YKTXL sequence, preceding each zinc finger. Mutation of residue X in MEX5, from arginine or lysine to glutamic acid, results in increased RNA specificity of the TZF; for this reason this residue was identified as the discriminator residue. In this chapter we test whether or not the fifth residue is sufficient to act as a determinant of

RNA binding specificity in the TTP family. In TTP and TIS11d this is not the case, mutation of glutamic acid to arginine in ZF1 decreases the affinity of the protein for RNA, without making it more promiscuous. Mutation of glutamine to lysine in ZF2 does not affect the RNA binding affinity or specificity of TTP or TIS11d.

Chapter IV, focuses on understanding the origin and biological significance of the structural differences between TTP and TIS11d. We identified three residues located in the α-helix of TTP required for the folding of ZF2 in the absence of RNA. Despite their different folding propensities, TTP, TIS11d, and chimeras bound to RNA with similar affinity. In contrast, the mRNA destabilizing activity of TTP was increased when the partially disordered RBD of TTP was replaced with the fully structured RBD of TIS11d. These results indicate that differences in the folded state of the RBD, while not affecting the *in vitro* RNA-binding affinity, have a large effect on the biological activity of the proteins in the cell.

In Chapter V, we investigate two missense mutations localized in the RBD of TIS11d (P190L and D219E) that have been associated with acute myeloid leukemia and acute lymphoblastic leukemia, respectively. We observed that both mutations affect the structural flexibility of the RBD of TIS11d, yet the mutant variants bind similarly to the cognate RNA sequence. Confocal images taken for HEK293 cells of GFP tagged TIS11d show disperse cytoplasmic expression while the P190L and D219E mutants display puncta within the cytoplasm. This result suggests that the structure of the RBD of TIS11d affects its subcellular localization, which may explain its role in disease pathogenesis.

The final chapter details how NMR and other biophysical techniques can be used to identify mutations in the TTP family that cause abnormalities in folding and RNA binding properties that result in TTP's dysfunction leading to inflammatory disorder and cancer. Understanding the source of the TTP family dysfunction can aid in the development of potential therapeutics for disease.

Chapter II: Characterizing the differential RNA binding activity of the human TTP family

Abstract

The cell modifies gene expression in response to cues from its extracellular environment. Post-transcriptional regulation allows cells to control the production of various growth factors, inflammation mediators, and pro-oncogenic proteins at the RNA level. RNA-binding proteins (RBPs) ensure accurate post-transcriptional regulation by recognizing specific mRNA targets from a convoluted pool of cellular transcripts through stable sequence and/or structural interactions. One such RBP, tristetraprolin (TTP), binds the 3′ UTR of transcripts containing adenine/uracil rich elements (AREs). Binding of TTP to these transcripts promotes their rapid degradation within the cell. TTP is a member of a small family of proteins, whose mammalian members include TIS11b and TIS11d, which have TTP-like activity. However, neither TIS11b nor TIS11d can reproduce TTP function in TTP knockout mice indicating that they are not functionally equivalent. Our lab has shown that the RNA binding domain (RBD) of TIS11d and TIS11b are well folded in the absence of RNA. However, the RBD of TTP is only partially folded in its RNA-free state. Here we show that stable coordination of the adenine in TTP ZF1 promotes the folding transition of ZF2 in TTP to bind to RNA following an induced-fit model. In TIS11d where both ZF1 and ZF2 are folded in the absence of RNA, such a strong preference for RNA-binding is not observed. Therefore, the different structure and stability observed for the RBD domains of TTP and TIS11d affect how these proteins bind RNA sequences. These results highlight how proteins in the same family can recognize and regulate different transcripts in the cell.

Introduction

The eukaryotic cell needs to modify the expression levels of many proteins in response to cues from the extracellular environment. One such mechanism for fine-tuning gene expression is through post-transcriptional regulation. By definition post-transcriptional regulation control begins once the RNA polymerase begins RNA synthesis in the nucleus and continues until translation of the gene in the cytoplasm. During the process of mRNA biogenesis in the nucleus a number of factors begin to associate with the mRNA, including RBPs. Many RBPs associate with their target mRNA, and this complex is exported out of the nucleus into the cytoplasm where it alters the localization, translation and/or degradation of the mRNA. Despite much previous effort, we still lack a thorough understanding of how many RBPs recognize and regulate their target mRNAs to control their cellular fate[119].

Tristetraprolin (TTP) is one post-transcriptional regulator that binds specifically to AU rich sequence elements (ARE) in the 3′–untranslated region (3′UTR)[120] of many mRNAs encoding essential inflammatory mediators, including TNFα[121], fibronectin[122], interleukin-1α/ β[122], and granulocyte-macrophage colony stimulating factor (GM-CSF)[75]. Recent computational analysis estimates that 8% of human transcripts contain AREs[45]. In 1986, Cerami *et al*. determined that these common ARE sequences confer mRNA instability[41]. TTP is one of the post transcriptional regulators responsible for governing the lifetime of these ARE containing mRNAs, inhibiting the expression of many essential cytokine and growth factor proteins by recruiting degradation machinery to their bound mRNAs.

Although the seminal member of this protein family (TTP) is well characterized, less is known about the other family members, TIS11d and TIS11b. These two family members were identified through increased expression after exposure to the tumor promoter, tetradecanoyl phorbol acetate (TPA), coining their name TPA Inducible Sequence 11 (TIS11) proteins[123]. The family is defined by a conserved RBD that is a CCCH tandem zinc finger. In this RBD these proteins share high sequence identity; TIS11b and TIS11d are approximately 70% identical to TTP, and 91% identical to each other. Outside of the RBD the family members share little sequence similarity (Figure 2.1). The N- and C-terminal domains (NTD/CTD) of these proteins are necessary to ensure proper recruitment of the enzymes in the mRNA degradation pathway[124]. TTP activity is modulated spatially and temporally through protein-protein interactions at the NTD and CTD. Phosphorylation of these domains decreases TTP RNA binding[125]. Further TTP is a nucleocytoplasmic shuttling protein containing an N-terminal $L_{xxx}L_{xx}L_xL$ sequence that serves as a nuclear export signal (NES)[68]. Software to predict secondary structure from primary sequence suggests that the NTD and CTD contain minimal stable structural elements[118]. Regions lacking stable structures are difficult to study *in vitro* and so we focused on the conserved RBD of TTP and TIS11d to determine how each protein binds distinct mRNAs, targeting them for degradation.
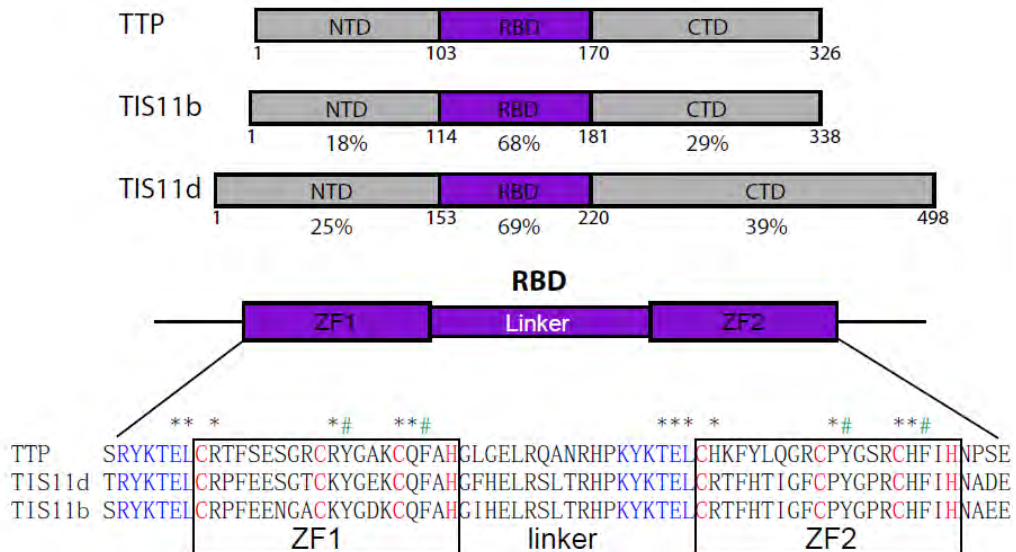
Figure 2.1: The TTP family of proteins. Schematic representation of the human TTP family members, TTP, TIS11b, and TIS11d. The N-terminal domain (NTD) and C-terminal domain (CTD) are colored in gray and the RNA binding domain (RBD) is in purple. The percent homology of each domain to TTP and its nucleotide length is denoted below each domain. The TTP family share homology at their RBD, a tandem zinc finger connected by an 18 amino acid linker. The two zinc finger motifs, ZF1 and ZF2, have a characteristic CX8CX5CX3H zinc coordination (highlighted in red). Conserved R(K)YKTEL sequences preceding each finger are highlighted in blue. Residues directly involved in hydrogen bonds with RNA are highlighted are indicated with asterisks (*), those that stack with RNA bases are denoted with a green pound (#) sign.

Despite being members of the same family and containing highly homologous

RBDs, TTP and TIS11b/d are not functionally redundant. Genetic studies revealed

further functional differences among TTP/TIS11 family members. Although TIS11b and

TIS11d have TTP-like activity neither TIS11b nor TIS11d replaces TTP function in TTP

knockout mice[107]. TTP knockout (KO) mice develop systemic inflammatory syndrome; cachexia, dermatitis, patchy alopecia, erosive arthritis, conjunctivitis, myeloid hyperplasia, and extramedullary hematopoiesis[126]. In contrast,
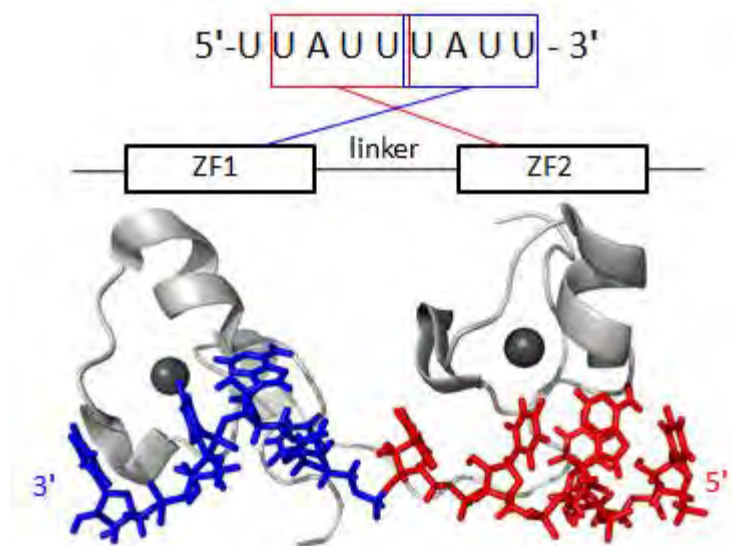
Figure 4.2: Structure of the TIS11d in complex with RNA. NMR structure of TIS11d depicts its antiparallel binding to its 5′UUAUUUAUU3′ RNA substrate. ZF1 binds to the 3′ UAUU half site (blue), while ZF2 binds to the 5′ UAUU half site (red).

TIS11b KO mice are embryonic lethal by day 11 due to vascular abnormalities and heart defects. TIS11d KO mice survive for approximately two weeks after birth, but then die of intestinal hemorrhage, pancytopenia, and reduced numbers of definitive multilineage and lineage-committed hematopoietic progenitors[111]. The differing mRNA expression patterns of TTP[112] are expressed mainly in cervical tissue, and TIS11b/d, which are expressed in the pancreas and thymus, as well as differences in transcriptional regulation strongly suggest that the TTP family of proteins regulate different mRNA targets in the cell.

The structure of the RBD of TIS11d in complex with single stranded RNA sequence 5′U1-U2-A3-U4-U5-U6-A7-U8-U9-3′was solved using nuclear magnetic resonance (NMR) spectroscopy (PDB code:1RGO)[127]. The structure depicts two well folded zinc fingers. The TIS11d/RNA complex binds to RNA mainly though protein

backbone hydrogen bonds and base stacking interactions along Watson-Crick edges of each nucleotide, with zinc finger 1 (ZF1) interacting with the 3′ U6-A7-U8-U9 halfsite and zinc finger 2 (ZF2) interacts with the 5′ U2-A3-U4-U5 halfsite (Figure 2.2). The linker region of TIS11d forms an extensive hydrogen bond network with the bases of the RNA, resulting in a rigid protein/RNA complex.

The residues interacting with RNA are well conserved between TIS11d and TTP. The sequence differences are minimal at these positions; K169 and R198 of TIS11d correspond to R119 and H148 in TTP. These residues should maintain similar electrostatic contacts with the RNA. Mutations of many of these conserved residues affect TTP family RNA binding. For example, mutations to either the aromatic residues Y170 (Y120), F176 (F126), Y208 (Y158), and F218 (F168) in TIS11d (or their corresponding TTP residues) critical for forming base stacking interactions with the RNA and/or the zinc coordinating residues C159 (C109), C168 (C118), C174 (C124), and H178 (H128) in ZF1 and C197 (C147), C206 (C156), C212 (C162) and H216 (H166) result in complete abrogation of RNA binding[118]. Other important interactions in the TTP family RBD are with the conserved KTEL sequence preceding each finger (Figure 2.1 blue). Mutations of this motif in TTP *C.elegans* family member MEX5 have been shown to confer specificity to the 5′UUUUAUUUAUUUU3′ sequence as adenine coordination is accomplished through hydrogen bonds of E157, L158, and R160 in ZF1, while E195, L196, and R198 bind with the adenine in ZF2 of the KTEL motif[128,129].

NMR and computational studies of TIS11d show that in the absence of RNA the structure of the two zinc fingers are maintain, although their orientation relative to one

another changes due to the flexible nature of the linker. Despite their high sequence identity (Figure 2.3a), the structure of the RBD differs between TTP/TIS11d in the ligand-free state[127,128]. Biophysical studies of the TTP TZF domain reveal that it is partially unstructured in the free state and undergoes folding only upon binding RNA (Figure 2.3b)[130,131]. We hypothesize that difference in TTP and TIS11d ligand-free structures affect their selectivity for mRNA targets *in vitro*.

Previous work from our lab and others has used two dimensional NMR spectroscopy to observe changes in TTP and TIS11d RBDs upon binding their 5′UUAUUUAUU3′ targets using an experiment referred to as ^{15}N-^{1}H heteronuclear single quantum coherence (HSQC) spectroscopy[127,130,131]. This two-dimensional NMR characterization provides us with an understanding of substrate binding at the atomistic level, not offered by other spectroscopic techniques. Since chemical shift is a measure of changes in local environment, we use it to map substrate binding onto each RNA binding domain, as binding RNA influences the distribution of electrons around the nucleus. Chemical shift differences in TTP upon RNA binding, $\Delta\delta = [(10\Delta\delta_H)^2 + \Delta\delta_N^2]^{1/2}$, is plotted as a function of the residue number. $\Delta\delta_H$ and $\Delta\delta_N$ are the chemical shift changes observed for the ^{1}H and ^{15}N resonances in ppm, respectively. It is important to note that we cannot deconvolve whether the observed changes in chemical shifts are due to a conformational change of the protein or direct RNA contacts. However it does provide insights regarding what residues are undergoing changes in their local environment as a consequence of RNA-binding.
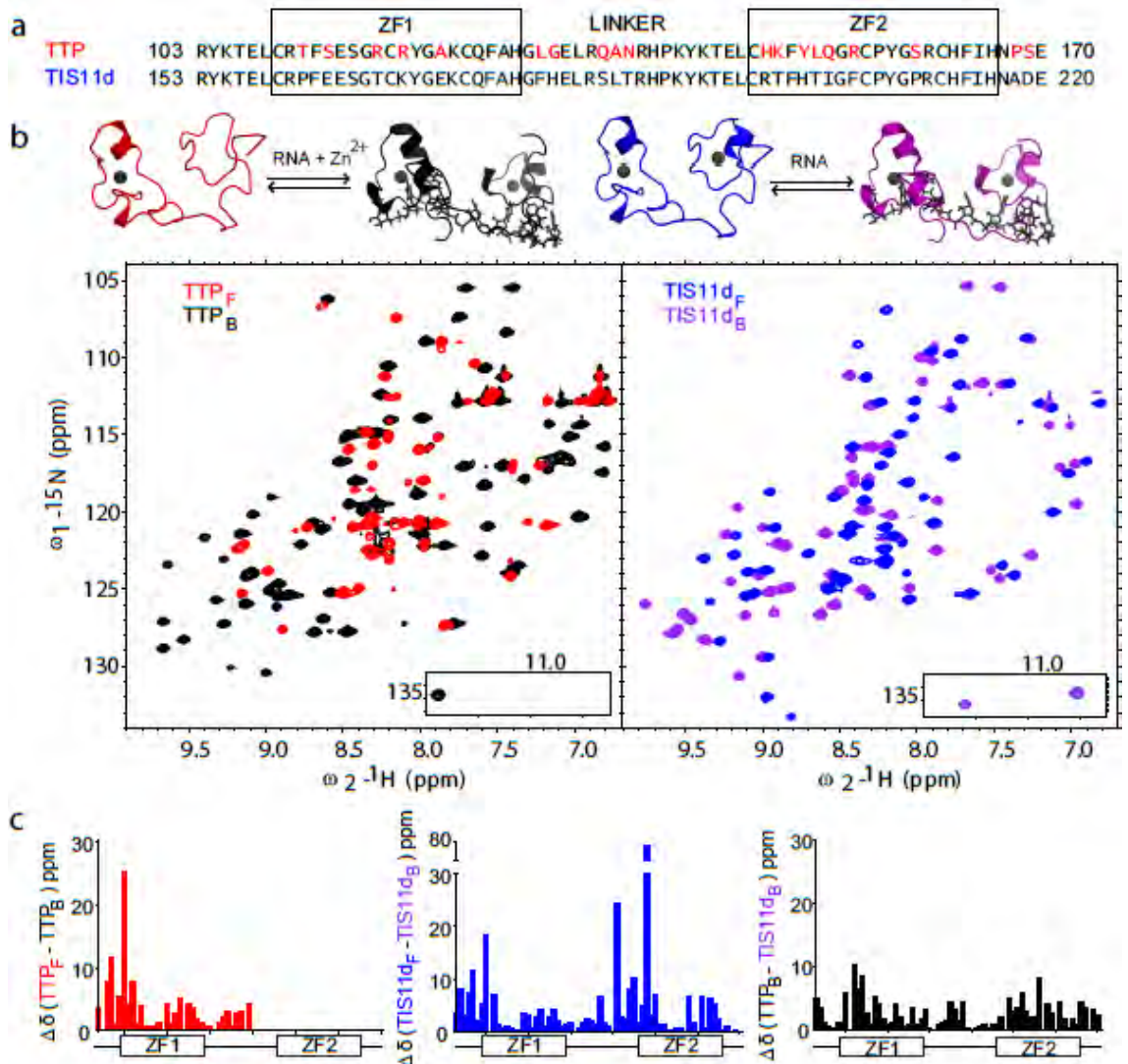
Figure 2.3: The RBD of TTP and TIS11d are highly homologous, bind to cognate RNA similarly, yet differ in their RNA free states. A) A sequence alignment of the TZF of TTP and TIS11d. The TZF consists of two CCCH zinc fingers (ZF1 and ZF2 represented in boxes) and an 18 amino acid linker. The conserved R(K)YTEL motif is underlined. Residues that differ between the two proteins are shown in red. Residues directly involved in RNA binding in the NMR solution structure (PDB file 1RGO) are indicated with asterisks; black = hydrogen bonds, green = base stacking interactions. B) HSQC spectra of free and bound TTP (red and black respectively) and free and bound TIS11d (blue and magenta respectively). Proteins are bound to their cognate RNA (5′UUUUAUUUAUUUU3′) sequence. Above each HSQC is a cartoon representation of TTP and TIS11d binding of the cognate RNA sequence. TTP undergoes an unfolding/ folded transition, while TIS11d reorganizes its structure. C) Chemical shifts difference (Δσ) plots for (Left, red) TTP free (TTP_F) to TTP bound to 5′UUUUAUUUAUUUU3′ (TTP_B). In this panel we can only calculate differences for ZF1 and part of the linker since peaks are missing in the HSQC spectrum for ZF2 due to intermediate exchange line broadening; (Middle, blue) TIS11d free ($TIS11d_F$) to TIS11d bound to 5′UUUUAUUUAUUUU3′ ($TIS11d_B$); (Right, black) TIS11d RNA bound ($TIS11d_B$) and TTP RNA bound spectra (TTP_B).

^{15}N-^{1}H HSQC experiments were collected for TTP and TIS11d in the presence

and absence of their target 5′UUUUAUUUAUUUU3′RNA sequence and chemical shift

differences were calculated for ZF1 of TTP and TIS11d. Chemical shift difference plots

for ZF1 RNA binding were similar, suggesting that TTP and TIS11d ZF bind their target

mRNA in a similar manner (Figure 2.3C, top and middle). Additionally, we calculated

the chemical shift variation of the 5′UUUUAUUUAUUUU3′ bound form of TTP and

TIS11d (Figure 2.3C, bottom) and found that their chemical shift differences are

minimal. Secondary structure prediction software using these chemical shifts determined

that their protein structures are similar with the exception of the helix in the second finger

where TTP forms one helical turn and TIS11d forms an extra turn. We therefore

hypothesized that different structures of TTP and TIS11d unliganded states influence

their RNA binding specificity for the UAUU half site at each finger.

In this study, we use fluorescence polarization (FP) coupled with NMR to

investigate the mechanism of RNA recognition by TTP and TIS11d. Together, these data

suggest that the structure and flexibility of the TTP family of proteins has a large effect

on RNA recognition and the selection of mRNA targets.

Results and Discussion

The site specific interaction of TTP and TIS11d to variants of ARE13

To understand TTP and TIS11d binding determinants, the binding of TTP and

TIS11d were measured and compared to a series of fluorescently labeled ARE13

(5′FAM-UUUUAUUUAUUU3′) RNA mutations that substitute the two adenosines to

uracils individually and together (Table 2.1 and 2.2). Red indicates the position mutated

in the RNA sequence relative to the high affinity ARE13 sequence.

Table 2.1: Equilibrium binding of TTP TZF to RNA substrates

RNA	Sequence 5′ to 3′	$K_{d\ apparent}$ (nM)	ΔG (kcal mol $^{-1}$)	ARE Preference
ARE13	UUUUAUUUAUUUU	10.1 ± 0.7	-10.7	1
5U13	UUUUUUUUAUUUU	56 ± 4	-9.7	6
3U13	UUUUAUUUUUUUU	63 ± 3	-9.7	6
U13	UUUUUUUUUUUUU	340 ± 30	-8.7	34
14mer	UUUUUUAUUUUUUU	56 ± 2	-9.7	6
ARE7	UAUUUAU	128 ± 2	-9.2	13

Table 2.2: Equilibrium binding of TIS11d TZF to RNA substrates

RNA	Sequence 5′ to 3′	$K_{d\ apparent}$ (nM)	ΔG (kcal mol $^{-1}$)	ARE Preference
ARE13	UUUUAUUUAUUUU	11 ± 2	-10.7	1
5U13	UUUUUUUUAUUUU	35 ± 5	-10.0	3
3U13	UUUUAUUUUUUUU	41 ± 9	-9.9	4
U13	UUUUUUUUUUUUU	101 ± 1	-8.0	9
14mer	UUUUUUAUUUUUUU	32.2 ± 0.4	-10.0	3
ARE7	UAUUUAU	121 ± 4	-9.3	11

Through use of fluorescence polarization assays, we determined that TTP forms

high affinity complexes with its preferred substrate ($K_{d\ app}$ = 10.1 ± 0.7nM) while it

bound to 5′-UUUUUUUUUUUUU-3′ (U13) sequence with a 34-fold weaker affinity (K_d

$_{app}$ = 340 ± 30nM), consistent with published data[132]. TIS11d, in contrast, does not seem

as selective as TTP; it binds to the ARE13 target with a similar affinity to TTP ($K_{d\ app}$ =

11± 2 nM), while it bound to U13 sequences with only a 9-fold weaker affinity ($K_{d\ app}$ =

101± 1nM).

Both RBDs bind with the highest affinity when ZF1 and ZF2 are coordinated by a UAUU halfsite, with TTP showing the greater specificity. Substitution at either adenine nucleotide results in decreased affinity to both TTP and TIS11d. Substituting the 5′ (5U13) or 3′ (3U13) adenine for a uridine yields a 3- to 4-fold reduction in affinity for TIS11d, respectively. TTP experiences a 6-fold loss in affinity for either of these RNA variants as compared to the ARE13 sequence. Although, uridine substituted RNA sequences bind to TTP and TIS11d with less affinity than the cognate 5′UUUUAUUUAUUUU3′ sequence, they still bind with high affinity. These data suggests that TTP and TIS11d bind to other RNA targets besides ARE13 with high affinity.

Investigating the effect of mutations in the cognate RNA sequence on TIS11d binding

The solution structure of the TIS11d/RNA complex shows that ZF1 of TIS11d interacts with the 3′ U6-A7-U8-U9 halfsite and ZF2 interacts with the 3′ U2-A3-U4-U5 halfsite[127]. Therefore, TIS11d ZF1 binds the 3′ adenine (A7) and ZF2 binds the 5′ adenine (A3). We examined how the chemical shifts change upon binding to various RNA sequences- ARE13, U13, 5U13, and 3U13 (Table 2.1 and 2.2), to see if TIS11d recognizes these RNAs in a similar structural manner to its bound ARE13 sequence.
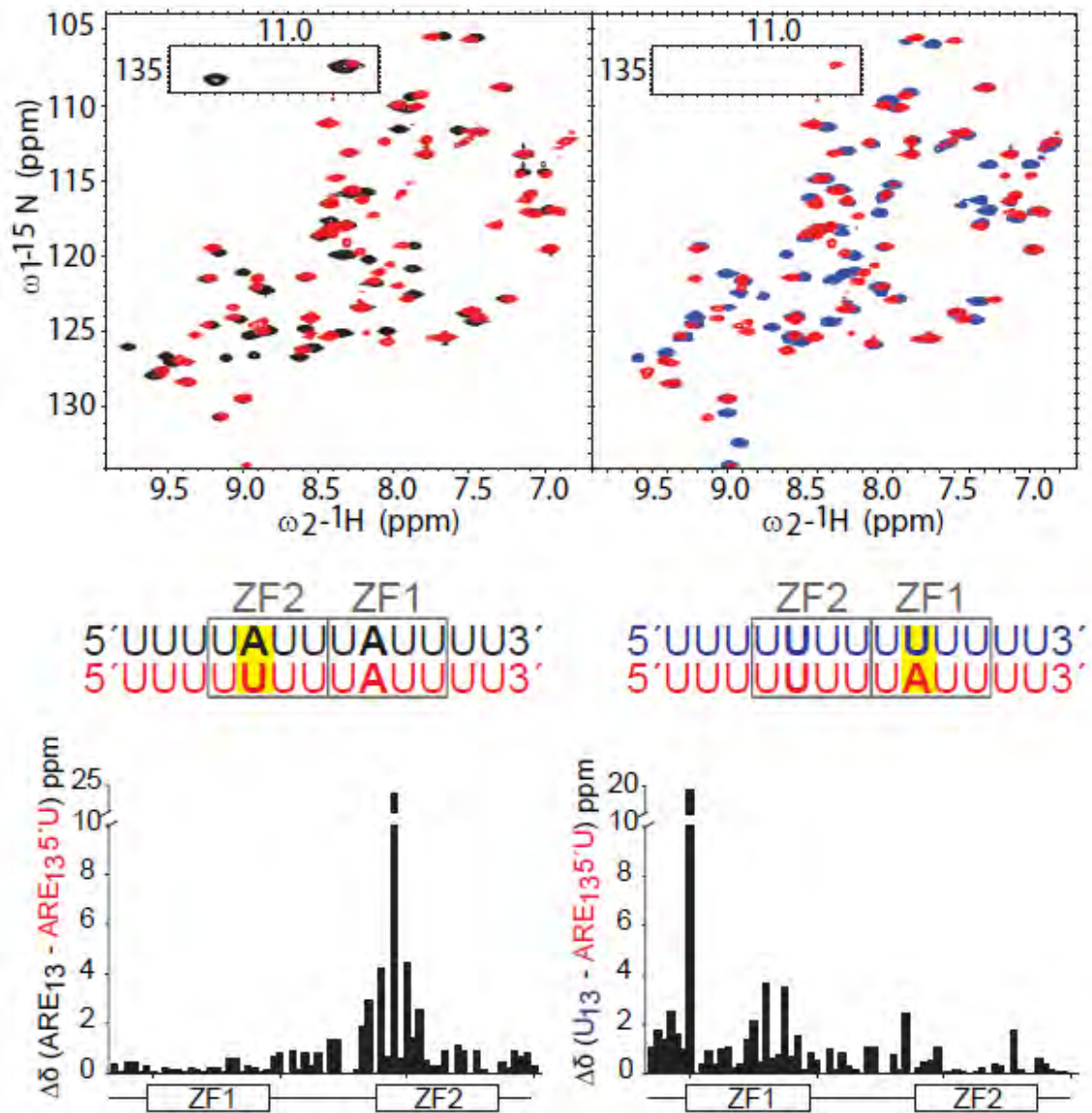
Figure 2.4: Investigating the binding of cognate RNA variants on TIS11d binding by NMR.
HSQC spectra of TIS11d bound to 5U13 - 5′UUUU**U**UUU**A**UUUU3′ (red) overlaid with either TIS11d in complex with its high affinity ARE13 - 5′UUUU**A**UUU**A**UUUU3′ (black) binding partner, or with its low affinity U13 – 5′ UUUU**U**UUU**U**UUUU3′ (blue) binding partner. Beneath each HSQC are their respective chemical shift perturbation plots, each with a schematic representation of the TZF motif of TIS11d.

Figure 2.5: Investigating the binding of cognate RNA variants on TIS11d binding by NMR. HSQCs of TIS11d bound to 3U13 - 5′UUUUAUUUUUUUU3′ (cyan) overlaid with either TIS11d in complex with ARE13 - 5′UUUUAUUUAUUUU3′ (black), or with the U13 – 5′ UUUUUUUUUUUUU3′ (blue) binding partner. Beneath each HSQC are their respective chemical shift perturbation plots, each with a schematic representation of the TZF motif of TIS11d.
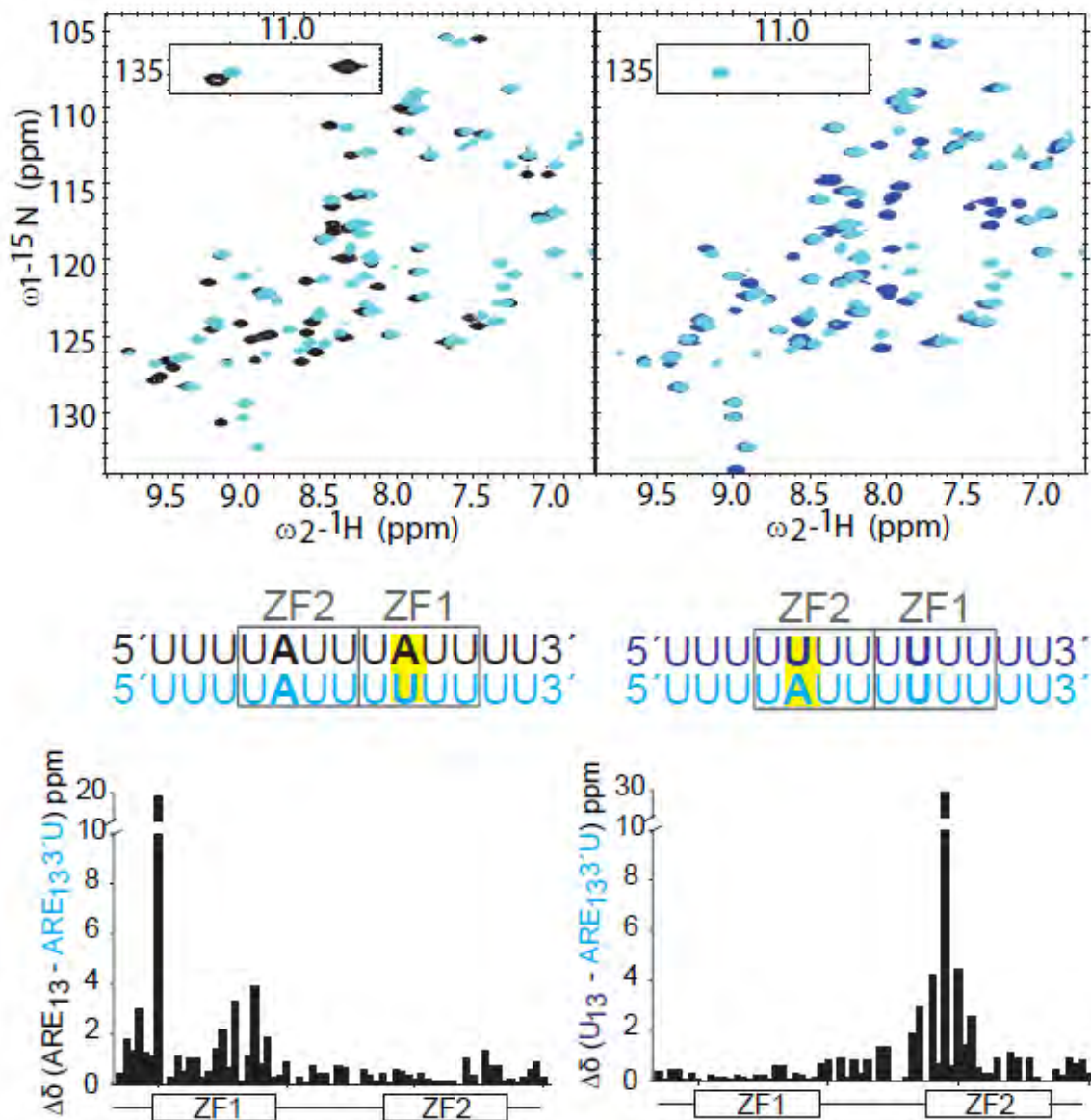
As expected, TIS11d in complex with 5U13 shows larger chemical shift changes at ZF2 when compared to its binding of ARE13 (Figure 2.4), while chemical shift changes at ZF1 are larger when compared to U13 binding (Figure 2.4). TIS11d in complex with 3U13 show larger chemical shift changes at ZF2 when compared to its binding of ARE13 (Figure 2.5), while chemical shift changes at ZF1 are larger when compared to U13 binding (Figure 2.5). These results are consistent with TIS11d binding the 3′ half site with ZF1 and the 5′ half site with ZF2 regardless of the RNA sequences that were used in these experiments (Figure 2.2).

Investigating the effect of mutations in the cognate RNA sequence to TTP binding

In order to determine if TTP binds RNA with the same registry as observed with TIS11d, where ZF1 binds to the 3′ U6-A7-U8-U9 halfsite and ZF2 coordinates the 3′ U2-A3-U4-U5 halfsite, we collected ^{15}N-^{1}H heteronuclear single quantum coherence (HSQC) spectra of TTP with the same sequences. Chemical shift difference maps were generated for the ZF1, linker, and ZF2 regions comparing binding to the ARE13 and U13 sequences. As with TIS11d, TTP binding to 5U13 shows larger chemical shift changes at ZF2 when compared to ARE13 binding, and binding to 5U13 shows larger chemical shift changes in ZF1 compared to binding to U13 (Figure 2.6). However, TTP binding to 3U13 is more complex --- in the ^{15}N-^{1}H HSQC spectrum we observe peak disappearances corresponding to several residues of the adenine recognition pocket. In ZF1 crosspeaks from C109, R110, T111, F112, E114, R119, and A122 are not observed, and E107, L108, and S113 crosspeaks are weak. In ZF2, K143, T144, E145, C147, and K149 are absent while K143 and L152 are weak and barely above the noise level. Peak intensity

differences in the ^{15}N-^{1}H HSQC spectrum mapped to the adenine coordination sites of TTP TZF suggested degeneracy in TTP binding not observed with TIS11d (Figure 2.7).
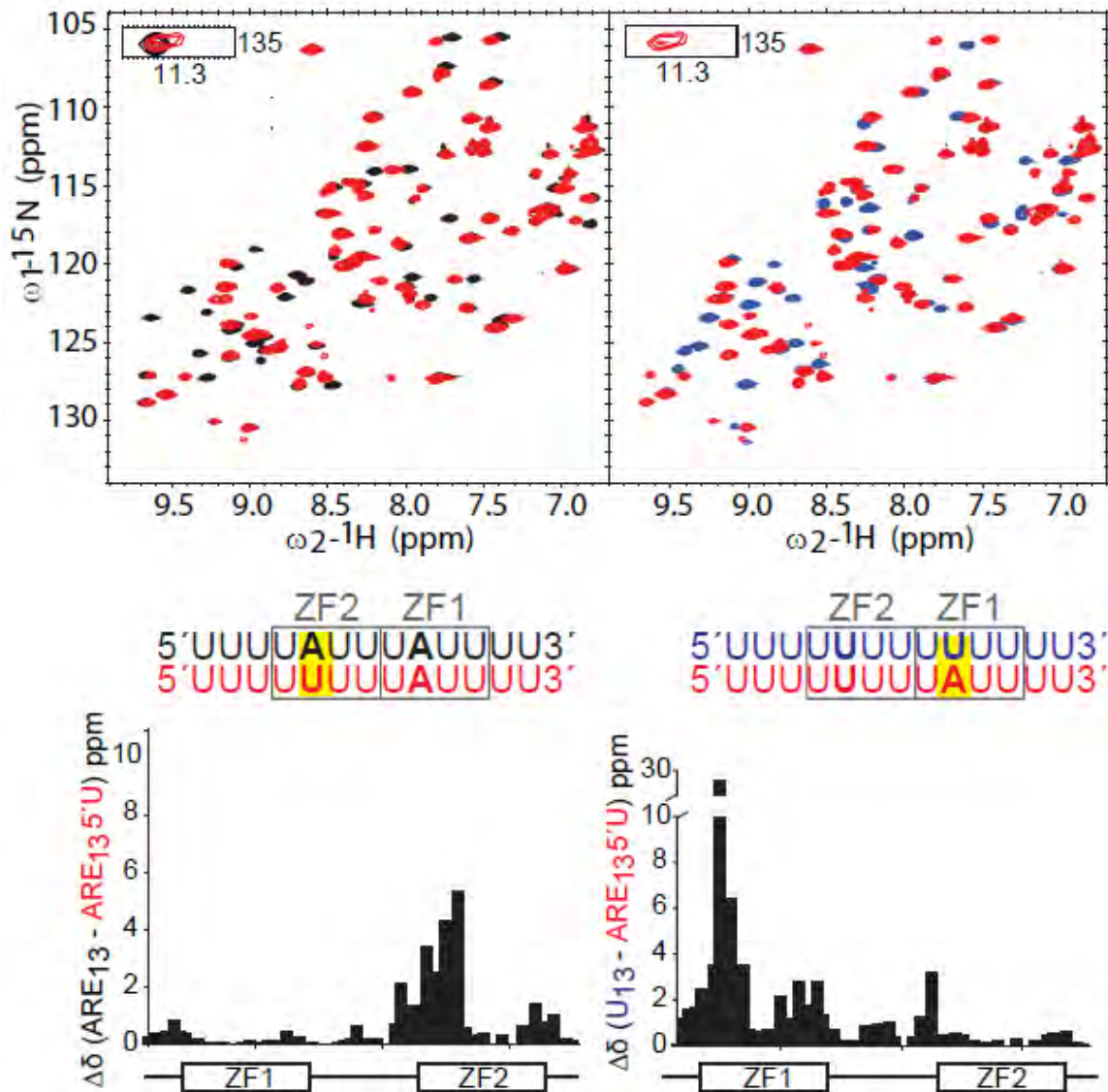
Figure 2.6: Investigating the binding of cognate RNA variants on TTP binding by NMR. HSQC spectra of TTP bound to 5U13 - 5′UUUUUUUUAUUUU3′ (red) overlaid with TTP in complex with its high affinity ARE13 - 5′UUUUAUUUAUUUU3′ (black) binding partner or its low affinity U13 – 5′ UUUUUUUUUUUUU3′ (blue) binding partner. Beneath each HSQC is their respective chemical shift perturbation plots with a schematic representation of the TZF motif of TTP.
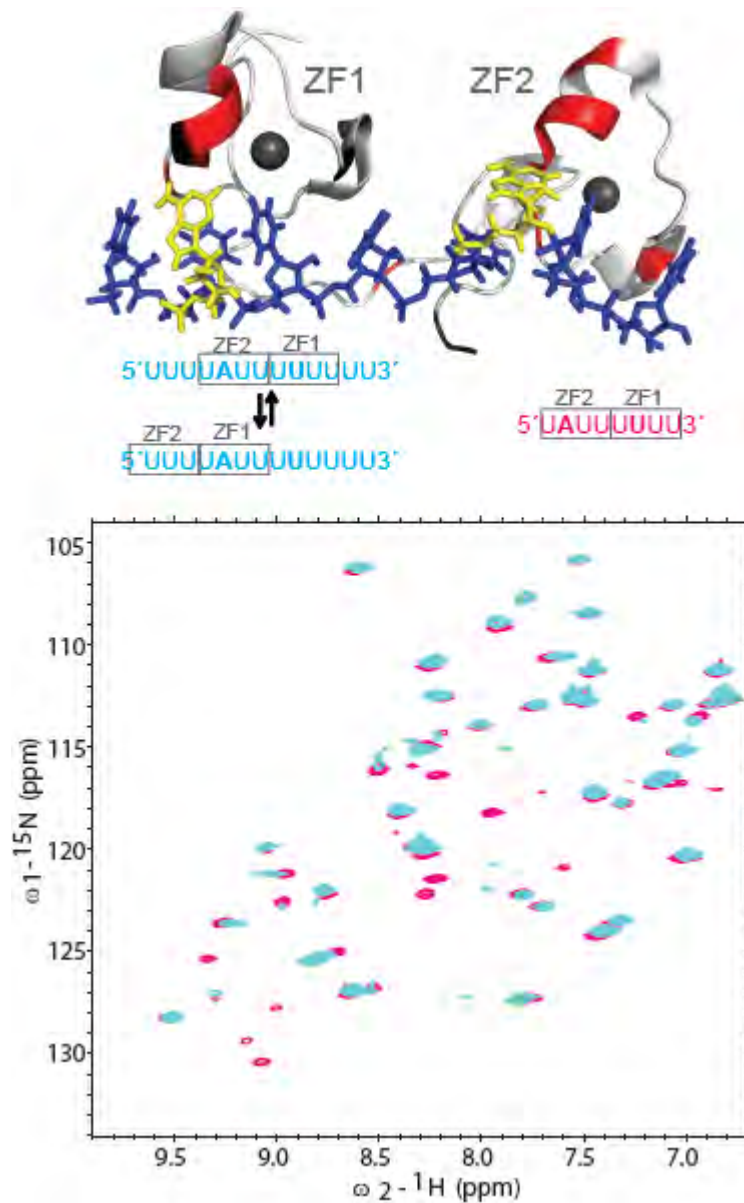
**Figure 2.7: Peak disappearance associated with TTP binding to ARE13 3′U -
5′UUUUAUUUUUUUU3′**. Below, HSQC spectra demonstrate that binding of TTP
5′UUUU**A**UUUUUUUU3′ (cyan) causes signal loss to the adenine binding pocket. Peak heights are
restored upon binding TTP to a shorter RNA sequence, ARE3U8, 5′U**A**UUU**U**UUU3′ (magenta), which
restrains TTPs ability to slide to other RNA binding sites. Above, schematic of chemical exchange
process associated with binding each RNA. Additionally, peaks that are lost upon TTP binding to 3U13
RNA sequence are mapped onto the NMR structure in red (PDB file: 1RGO) using PyMOL. Also
displayed are zinc atoms (grey spheres), uracils (blue), and adenines (yellow) bound to TTP.

We hypothesized that the cross peaks of the adenine binding pocket disappeared because of a chemical exchange process that is intermediate in the NMR timescale that leads to extensive line broadening. This may be caused by TTP binding this RNA sequence with 2 different registers (Figure 2.7). In order to test this hypothesis, we used a shorter RNA sequence, ARE-3U8 (5′UAUUUUUU3′), which contains no RNA bases other than those shown to directly hydrogen bond with the published TIS11d structure. By constraining TTP ZF1 to bind to the UUUU half site and ZF2 to the UAUU half site, we increased the number of cross peaks observed in the ^{15}N-^{1}H HSQC that mapped to the adenine binding pocket (Figure 2.7). When we then mapped these chemical shifts onto ZF1, the linker, and ZF2, we see that TTP binding to ARE3U8 is similar to that of TIS11d binding to 3U13. Namely, we observed larger chemical shift changes for ZF2 when compared to binding to ARE13 and larger chemical shift changes are observed for ZF1 when compared to binding to U13 (Figure 2.8). This result indicates that in TTP, its folded ZF1 has higher affinity for the UAUU half site than its unfolded ZF2.
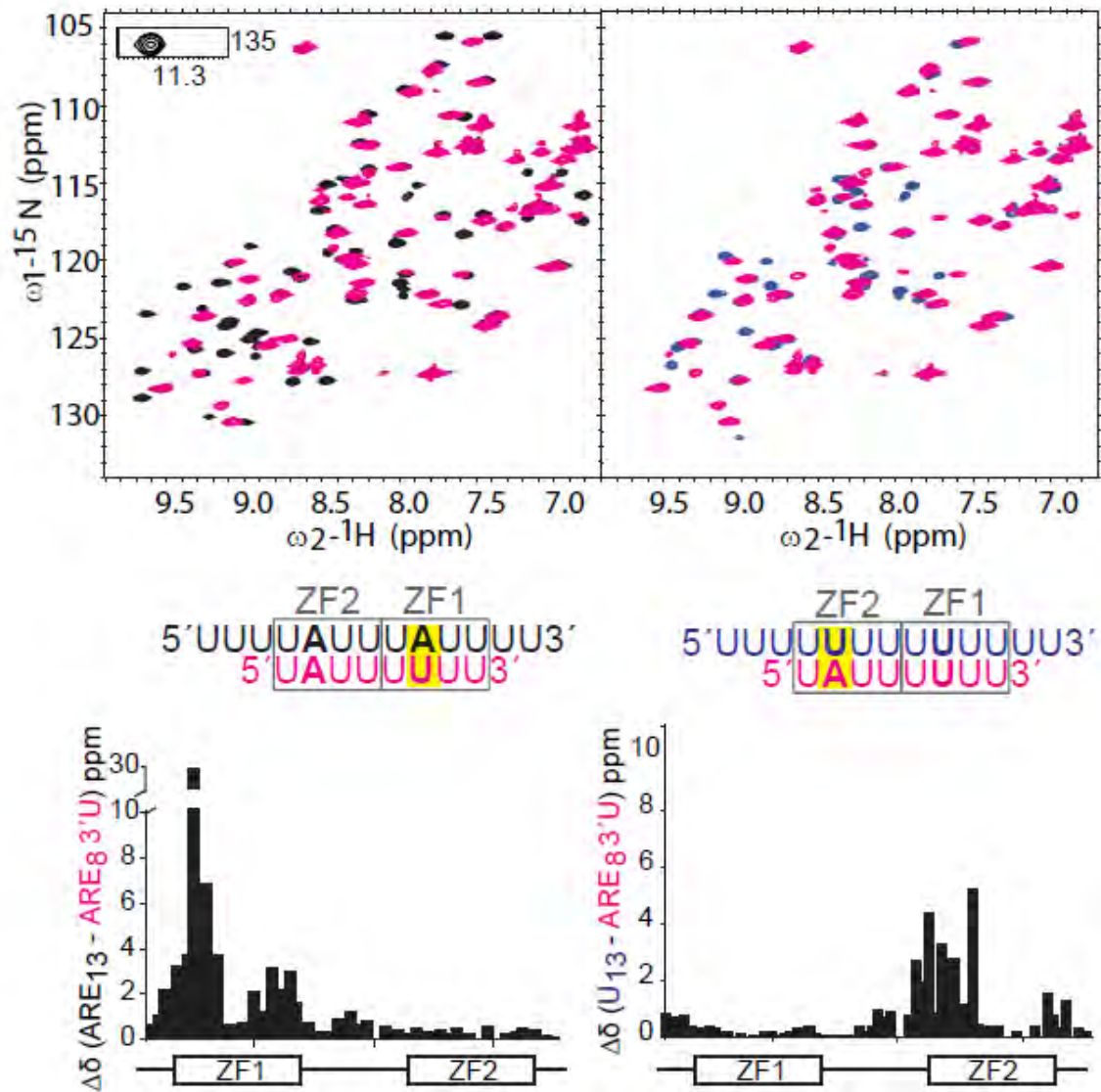
Figure 2.8: Investigating the binding of cognate RNA variants on TTP binding by NMR. HSQC spectra of TTP bound to ARE-3U8 - 5′UAUUUUUU3′ (magenta) overlaid with TTP in complex with ARE13 - 5′UUUUAUUUAUUUU3′ (black) or U13 – 5′ UUUUUUUUUUUUU3′ (blue) binding partner. Beneath each HSQC are their respective chemical shift perturbation plots, each with a schematic representation of the TZF motif of TTP.

TTP ZF1 preference for the 6UAUU9 subsite

Binding of TTP to 3U13 causes signal loss in residues of both adenosine binding pockets, and we predict this is a result of the TTP ZF1 higher affinity for the UAUU sequence. In order to test this, we performed NMR experiments where TZF binds to a longer RNA sequence, 14mer- 5′UUUUUUAUUUUUUU3′ (Figure 2.9), which can accommodate ZF1 binding to the UUUU or the UAUU subsite. ^{15}N-^{1}H HSQC spectrum of TIS11d bound to this longer RNA sequence shows that TIS11d binds to the 3U13 (5′UUUUAUUUUUUU3′) and 5U13 (5′UUUUUUUUAUUUU3′) as crosspeaks corresponding to both binding registers are present. Furthermore, the crosspeaks we observed corresponding to these two binding registers are of the same intensity, demonstrating that TIS11d binds to 5U13 and 3U13 equally (Figure 2.9). These results emphasize that RBPs from the same family, such TTP and TIS11d, can recognize and bind different cellular mRNA transcripts despite sharing significant sequence identity.

Figure 2.9: HSQCs using longer variant ARE13 RNA show that TTP ZF1 favors the UAUU half site, whereas TIS11d has no preference. (Left) HSQC overlay of TIS11d bound to 5′-UUUUUUAUUUUUUU3′ (black), 5U13 - 5′UUUUUUUUUAUUUU3′ (red), and 3U13 – 5′ UUUUAUUUUUUUU3′ (blue). (Right) HSQC TTP bound to 5′-UUUUUUAUUUUUUU3′ (black) overlaid with 5U13 -5′UUUUUUUUUAUUUU3′ (red). Atop each HSQC is a schematic representation of ZF1 and ZF2 RNA binding. TIS11d binds to this RNA sequence with 2 registries equally, whereas TTP binds in one registry where its ZF1 binds to the UAUU half site displaying TTP preference for the UAUU half sites.
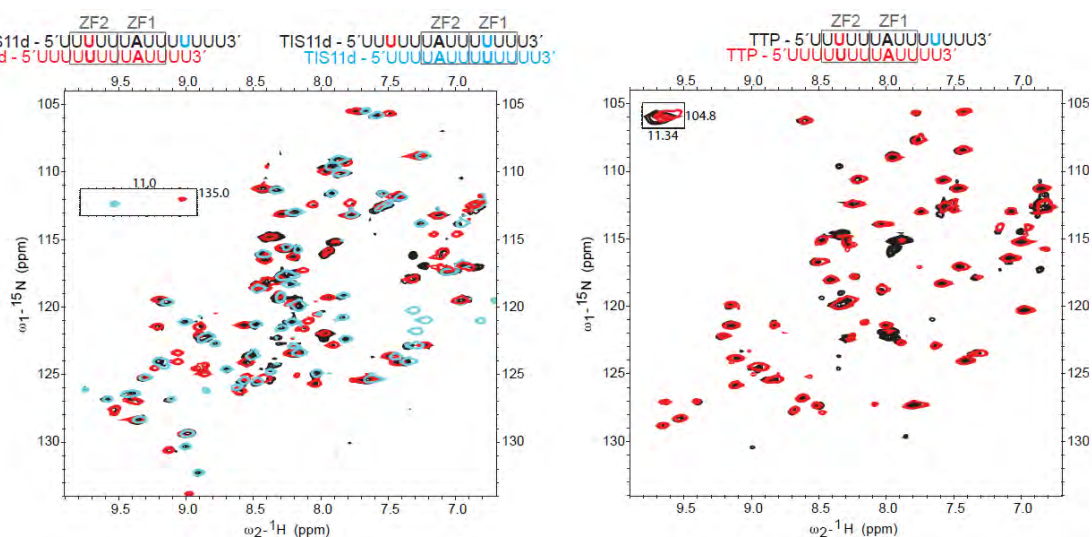
For TTP in the absence of RNA, only ZF1 is stably folded. Only until TTP stably binds its RNA substrate will ZF2 fold. In these experiments we show that coordinating ZF1 of TTP to an adenine containing halfsite, UAUU, allow for a more stable interaction with the RNA for the folding of ZF2. In the solution structure of TIS11d there is an extra hydrogen bond formed by E157 in the adenine binding pocket of ZF1 that formed with the RNA (Figure 2.10). This hydrogen bond seems is necessary for TTP high affinity RNA binding since FP data analysis determined that ZF1 of TTP has a slightly higher affinity for the adenine than ZF2 (Table 2.2). This data suggests a possible model of TTP RNA binding where ZF1 hydrogen bonds with adenine to create a stable protein-RNA

complex for the folding of ZF2. Although we conclude an induced fit model of RNA

binding, this does not preclude a small percentage of TTP that folds fully in its RNA free

form and then binds RNA, similar to what we observe for TIS11d. In TIS11d both ZF1

and ZF2 are folded in the absence of RNA and therefore the additional hydrogen bond

associated with adenine coordination is not necessary for it to form a stable protein-RNA

interaction. Altogether, this data supports that the different structure and stability

observed for RBD TIS11d and TTP affect how they bind their RNA targets *in vitro*.
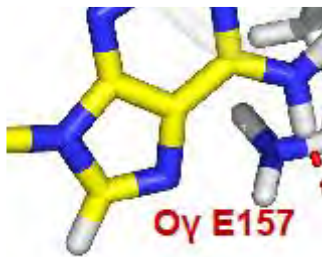
Figure 2.10: Adenine binding pocket. A) A surface image of TIS11d (gray) in complex with ARE9-5′UUAUUUAUU3′ (yellow) (PDB access code: 1RGO). The red box highlights TIS11d ZF1 adenine recognition pocket. B) Close up view of the adenine binding pocket of TIS11d ZF1. The adenosine base is in yellow. E157 is represented in green. E157 side chain carboxyl forms a hydrogen bond (red) with the exocyclic amine of the adenosine base. Backbone carboxyl of L158, L196 and backbone amide of R160, R198 also form hydrogen bonds (black) with the adenosine.

Figure 2.11: Binding of the UAUU half-site to the N-terminal zinc finger is not sufficient to promote complete folding of the TZF domain. Top: HSQC of TTP bound to ARE 5′UAUUAUU3′ (green) overlaid with ARE13 bound TTP (black). Middle: HSQC of TTP bound to 5′UAUUUAU3′ (purple) overlaid with ARE13 bound TTP (left, black) and the unliganded form of TTP (right, red). Bottom: HSQC of TTP bound to 5′UUAUUUU3′ (cyan) overlaid with ARE13 bound TTP (left, black) and the unliganded form of TTP (right, red). Sandwiched between 5′UAUUUAU3′ and 5′UUAUUUU3′ binding HSQCs are frames taken from with HSQCs of unliganded TTP (red) and HSQCs of TTP bound to 5′UUAUUUU3′ (cyan), ARE13 (black), and 5′UAUUUAU3′ (purple) of amino acids of the first finger to follow chemical shifts associated with RNA binding. Conclusion: Binding of the half site fails to promote complete TTP TZF folding.
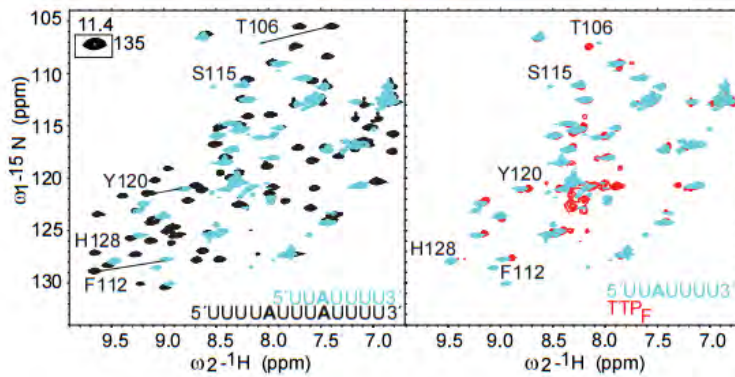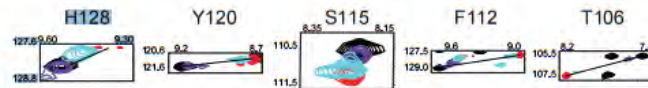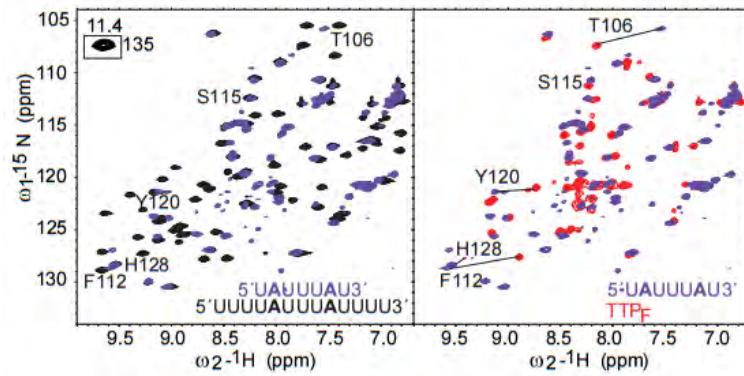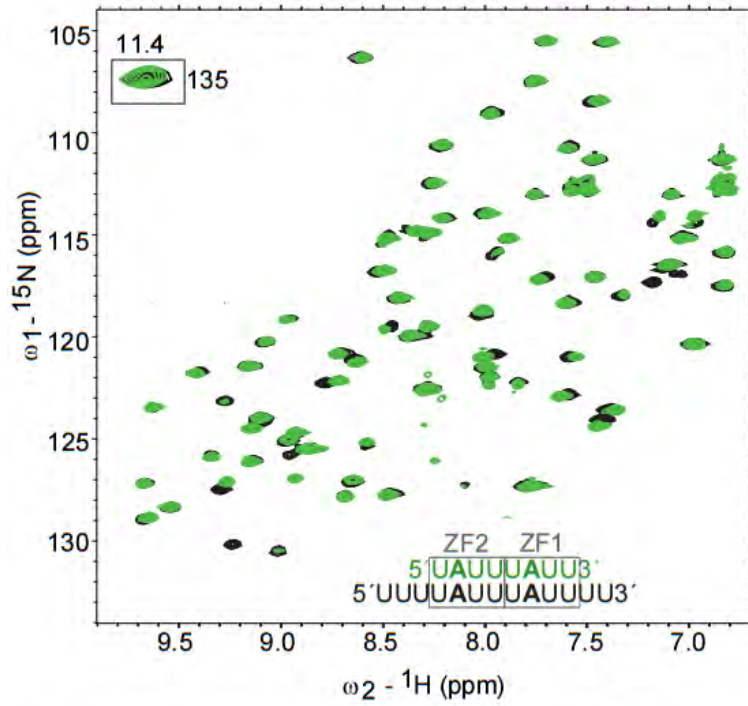
Binding an RNA octamer completes folding of the TTP TZF domain

NMR studies performed by our lab and others demonstrated that only ZF1 and the linker are clearly resolved in the ^{15}N-^{1}H HSQC spectrum of the ligand-free form of TTP. However, cross-peaks are observed upon binding to its cognate RNA sequence, ARE13- 5′UUUUAUUUAUUUU3.′ These cross peaks correspond to the residues of the linker and ZF2 that were absent in the initial RNA-free spectra. The ^{15}N-^{1}H HSQC spectrum of TTP bound to RNA does not change when the RNA sequence is shortened to eight nucleotides in length, 5′UAUUUAUU3,′ (ARE8)- RNAs of this length will not disrupt any hydrogen bonds associated with ZF1 and ZF2 RNA binding (Figure 2.11). In fact, the ^{15}N-^{1}H HSQC spectrum of TTP bound to ARE8 overlays with the longer ARE13 sequence with exception of cross-peaks assigned to residues A122, S160, and H163 of the linker and ZF2 which do decrease in intensity (Figure 2.11). When we examined TTP bound to RNA heptamers, ARE7- 5′UAUUUAU3′, we found that many additional peaks lost intensity in the ^{15}N-^{1}H HSQC spectrum. In these experiments, peaks associated with ZF2 binding were found to have very low intensity, approaching the signal-to-noise-limit. However, the spectrum associated with ZF1 binding to ARE7 is similar to what we observe for ARE13 binding. Loss of ZF2 interactions with the high affinity UAUU halfsite may also explain why we calculate a dissociation constant for the bound TTP: ARE7 complex ($K_{d,app}$ = 128 ± 2nM) that is an order of magnitude smaller than that calculated for TTP:ARE13 complex ($K_{d,app}$ = 10.1 ± 0.7nM). Additionally, TTP and TIS11d do not bind another RNA variant, 5′UUUUAUU3′, which lacks the 5′ halfsite required for ZF2 binding. In fact, the ^{15}N-^{1}H HSQC spectrum taken of TTP binding to
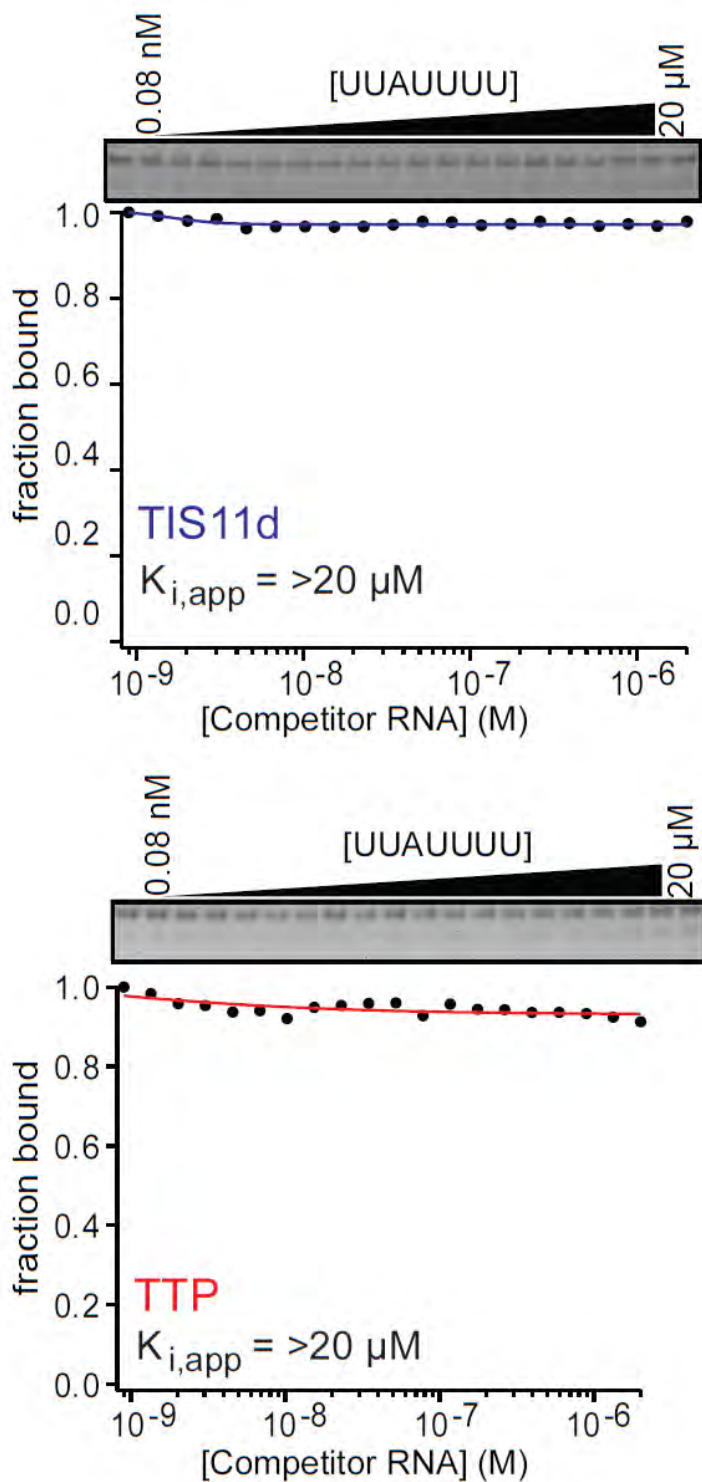
this sequence closely mimics that of the ligand-free form of TTP. The binding affinity of TIS11d and TTP for 5′UUUUAUU3′ was also found to be low in competition gel shift assays. Therefore, only the lower limit of the binding range could be determined where $K_{i\ (apparent)}$ was found to be $>20\ \mu M$ (Figure 2.12). Overall, this data indicates that binding to the 5′UAUUUAU3′ RNA sequence is not sufficient to fully stabilize the structure of ZF2.

Figure 2.12: RNA competition of TTP and TIS11d bound to fluorescence labeled ARE$_{13}$ with unlabeled 5′UUAUUUU3′. The fraction of TIS11d (top, blue) and TTP (bottom, red) bound to fluorescently labeled ARE$_{13}$ (bound RNA = top band) is competed off with increasing concentrations of unlabeled 5′UUAUUUU3′ (free RNA = bottom band) with maximum concentration 20 μM. The unlabeled 5′UUAUUUU3′ RNA was unable to completely compete off the fluorescently labeled ARE$_{13}$. Therefore we assume that the Ki, app > 20 μM.

Conclusions

In this study we used a combination of NMR and FP to gain a more complete understanding of how two proteins of the same family, TTP and TIS11d, bind to RNA sequences differently *in vitro*. Contrary to the intuitive expectation that increase in the flexibility of a protein leads to promiscuity in binding behaviors[133-139], we found that the partially folded TTP TZF is more selective for binding the UAUU half site at ZF1 than its fully folded counterpart TIS11d. As discussed above, TIS11d binds 3U13 (5′UUUUAUUUUUUU3′) and 5U13 (5′UUUUUUUUAUUUU3′) sequences equally well. Meanwhile, we observed that TTP RNA binding being coupled to folding of a portion of its RBD increases its selectivity for the 5U13 sequence. Our results highlight that the TTP binding to an adenylate residue with ZF1 creates a stable scaffold upon which ZF2 can fold onto the remainder of the RNA through an induced fit mechanism. These results strongly indicate that TTP and TIS11d might have different mRNA targets in the cell and that this could account for the inability of TIS11d to rescue TTP knockout mice[140].

The high affinity binding of TIS11d and TTP to ARE13, 5U13, 3U13, and U13 *in vitro* suggests that these RNAs may also be *in vivo* targets. Experiments investigating TTP associated mRNA targets in HEK cells using Photoactivatable-Ribonucleoside-Enhanced Crosslinking and Immunoprecipitation (PAR-Clip) identified TTPs interaction with 1,313 ARE rich sequences, many of which were interrupted by uridylated stretches[141]. These experiments, when considered in conjunction with our findings above, suggest that TTP may be able to bind to more RNA targets *in vivo* than just TTP's

reported 5′UUAUUUAUU3′ target sequence. Furthermore, our research highlights the need for the identification of TIS11d biological targets, potentially through a more stringent search like PAR-Clip as our data shows that TIS11d and TTP have different affinities for the same sequences *in vitro*. More studies are needed to determine if they have distinct or overlapping targets *in vivo*.

In the cell, the stability of the ARE containing 3′ UTR is governed through a host of post-transcriptional regulators to either promote or inhibit the ARE degradation machinery[142]. For example, human antigen R (HuR) is an ARE regulatory protein that enhances RNA stability by binding to U and CU-rich sequences while TTP binds to ARE to decrease mRNA stability[143]. Given their antagonistic behavior, much work has been done to investigate competition of these proteins for ARE 3ʹUTRs. The current model posits that in response to cellular stress HuR binds to stabilize transcripts and promote their translation while TTP is being synthesized and phosphorylated by MAP kinase-activated protein kinase 2 (MK2). Phosphorylation of TTP results in its interaction with the chaperone 14-3-3 dimer complex sequestering it away from RNA. Dephosphorylation of TTP by protein phosphatase 2A (PP2A), allows for TTP association with ARE containing RNA, displacing HuR and leading to mRNA degradation[144]. In this study we demonstrated that TTP binds to HuR binding sites (uridine stretches - U13 Table 1) with only a moderate affinity (340 ± 30 nM) while TIS11d binds the same sequence with a higher affinity (101 ± 1 nM), suggesting that TIS11d may be able to compete for uridinylated stretches more effectively than TTP and result in increased turnover of mRNA transcripts in cells. Indeed, previous research in our lab has determined that

replacing the TTP RBD with those of TIS11d leads to increased turnover of a reporter

transcript containing the ARE 3′UTR. Differences in the ability of TTP and TIS11d to

compete for mRNA targets provide an alternative explanation for the different

phenotypes in TTP and TIS11d knockout mice.

One interesting finding from this work was that mutations in ZF2 of TTP that

have a significant impact on TTP′s protein folding actually have little effect on the total

free energy of RNA binding for the canonical 5′UUAUUUAUU3′ sequence. It is possible

that TTP RNA binding is an enthalpically favorable process due to the overall charge of

the protein (TIS11d: +3, TTP: +8), compensating for the entropic penalty associated with

RNA binding that is a result of the increased flexibility of TTP relative to TIS11d.

Performing RNA binding titrations at different temperatures can be used to determine the

enthalpic and entropic contributions to RNA binding through global analysis using

Gibbs-Helmhotz relationship as done in previous work performed in our lab to

characterize RNA binding of truncation mutations in TIS11d RBD that increase its

protein dynamics.

Understanding the physical forces that drive TTP and TIS11d discrimination for

their mRNA targets is critical for understanding how they regulate RNA turnover in the

cell. Many other factors bind TTP affecting its activation/inactivation, localization, and

mRNA degradation activity. Whether RNA induced folding is involved in many of TTPs

biological functions is still a mystery and will be an exciting area of research in the

future.

Materials and Methods

Sample preparation

The sequence encoding amino acids 100-170 (150-220), which includes the TZF

domain of TTP (TIS11d), was expressed using pet21a expression vector. TTP and

TIS11d were expressed in *E. coli* strain BL21-Codonplus (DE3) (Stratagene). Isotopic

labeling with ^{15}N was performed by growing the cells in M9 enriched with 1 g of

$^{15}NH_4Cl$ per liter. ^{13}C labeling is performed by growing cells in ^{13}C-glucose. The cells

were grown at 37° C to an OD_{600} of 0.8 and then induced for 4 hours with 1 mM

Isopropyl β-D-1 thiogalactopyranoside (IPTG) and 0.1 mM $ZnSO_4$ at the same

temperature. Harvested cells were passed through a cell disrupter in 50 mL lysis buffer

containing 50 mM Tris HCl, pH 8.0, 50 mM NaCl, 2 mM dithiothreitol (DTT) and 1

EDTA free Complete protease inhibitor tablet (Roche). Lysates were centrifuged at

19500 RPM for 1 hr at 4° C and passed through a 20 mL DEAE column pre-equilibrated

with 50 mM Tris HCl, pH 8.0, 50 mM NaCl and 2 mM DTT. The flow through was

dialyzed overnight in 25 mM sodium phosphate, pH 6.5, 50 mM NaCl and 2 mM DTT

and passed through a *HiTRAP SP* 10mL column (GE healthcare Life Science)

preequilibrated with in 25 mM sodium phosphate, pH 6.5, 50 mM NaCl and 2 mM DTT.

The peptides were eluted with a gradient of NaCl from 0-1 M; the peptides typically

eluted at 0.2-0.6 M NaCl. Fractions with peptide were combined and concentrated to 2

mL using a 3 KDa Centriprep (Millipore) and further purified using a 1.6 X 60 cm

Superdex-75 size exclusion column (Amersham Biosciences) equilibrated with 50 mM

Tris HCL pH 7, 300 mM NaCl, 2 mM DTT. For NMR analysis fractions with TTP,

TIS11d or chimeras were buffer exchanged into 10 mM Tris pH 6.2, 20 mM KCl, 2 mM DTT, 0.1 mM $ZnSO_4$.

Measurements of RNA-binding affinity

The RNA-binding activity of the samples was determined using fluorescent polarization with fluorescein 5′ end labeled RNA as previously described briefly by Pagano *et al*. The affinities of TTP and TIS11d for variants of the cognate RNA sequence: 5′-UUUUAUUUAUUUU-3′ (ARE_{13}) were measured by direct titration of 3 nM labeled RNA with increasing concentrations of protein. Varying concentrations of the protein were incubated for 3 hours at room temperature with 3 nM fluorescently labeled RNA in a buffer solution containing 10 mM TRIS (pH 8), 100 μM $Zn(OAc)_2$, 100 mM NaCl, 0.01 mg tRNA, 0.01% (v/v) IGEPAL, and 2 mM TCEP. To detect the fluorescently labeled RNA, the gel was imaged using a Fuji FLA-5000 laser imager. The apparent dissociation constant $K_{d,app}$ was determined by fitting to the quadratic equation

$$f = \frac{m-b}{2R}\left(K_d + P + R - \sqrt{[K_d + P + R]^2 - 4RP}\right) + b,$$

where m and b are the maximum and base signals, K_d is the dissociation constant, and P and R are the concentrations of protein and labeled RNA in the sample, respectively.

NMR spectroscopy

Three dimensional triple resonance (^{1}H-^{13}C-^{15}N) experiments, including HNCO, HN(CA)CO, HNCA, HN(CO)CA, HNCACB, and CBCA(CO)NH, have been collected at 14.1 T and 298 K to assign the backbone ^{1}H, ^{13}C, and ^{15}N resonances of [U-^{13}C, U-

[15N] TTP and TIS11d in 92% H_2O/8% D_2O buffer solution (10 mM Tris, 20 mM KCl, 2 mM DTT, 0.1 mM $ZnSO_4$ at pH 6.2). Additional 3D [15N] edited ^1H–^1H NOESY and HMQC-NOESY-HSQC experiments were collected at 14.1 T and 298 K and used to aid in the backbone resonance assignment of each free and RNA bound RBD. All NMR triple-resonance and [15N]-^1H HSQC experiments were collected on a Varian Innova spectrometer operating at 600 MHz equipped with a triple-resonance cold probe. The temperature was calibrated using a sample of 100% methanol. Data processing was performed using NMRPipe [145] and Sparky software[146]. The chemical shift differences, Δ, were determined using $\Delta = (\delta_H^2 + (\delta_N \gamma_N/\gamma_H)^2)^{1/2}$, where δ_H is the chemical shift difference of ^1H, δ_N is the chemical shift difference of [15N] and γ_N, γ_H are the gyromagnetic ratio of ^1H and [15N] atoms.

Chapter III: Identifying deleterious mutations associated with conserved sequences in the TZF of the TTP family

Abstract

The TTP family of proteins is required to accurately recognize mRNAs encoding inflammation mediators and oncogenic proteins, resulting in their precise turnover in the cell. Many of these protein-RNA interactions occur at a conserved 6 residue R(K)YKTEL sequence preceding each zinc finger (ZF) in the tandem zinc finger (TZF), including the coordination of the adenosines of its ARE13- UUUUAUUUAUUUU target RNA sequence. Missense mutations in the TIS11d ZF1 R(K)YKTEL motif are known to correlate with bladder, breast, liver and lung carcinomas. In the *C.elegans* RNA binding protein MEX-5, this motif is maintained except for a substitution of the glutamate at position five for an arginine in zinc finger 1 (ZF1) and a lysine in zinc finger 2 (ZF2) (Figure 3.1). Unlike the TTP family of proteins, MEX-5 is a promiscuous RNA binding protein that recognizes uridine-rich RNA sequences. However, in MEX-5 upon mutation of the R, K residues of the motifs to E as in TTP motif, MEX-5 gains TTP-like specificity and binds an adenine-uridine rich element (ARE) with higher affinity than a sequence of polyuridine. To explore the role of the primary sequence on the binding specificity of TIS11d and TTP, we mutated the glutamate of the R(K)YKTEL motifs in TIS11d and TTP to Arg/Lys in ZF1/ZF2, respectively, to mimic the sequence of MEX-5. We found that replacing the glutamate residue of the R(K)YKTEL motif with an arginine in the ZF1 of TIS11d and TTP impairs RNA binding, likely due to conformational distortions of the adenine binding pocket of ZF1, more severely in TTP than in TIS11d. Additionally, we found that the arginine mutation at ZF1 in TTP decreased its mRNA turnover activity,

consistent with impaired RNA binding. Mutation of the Glu to Lys in ZF2 does not affect the RNA-binding affinity nor the specificity of TTP and TIS11d.

Introduction

RNA binding proteins (RBPs) are the main facilitators of many biological processes, including post transcriptional regulation. Therefore, it is important to understand how these proteins recognize and bind to their RNA targets. RBPs bind to RNA using a variety of structural motifs called RNA binding domains (RBDs). Some of the most-abundant RBDs are RNA recognition motifs (RRMs)[16,17], double stranded RNA-binding domain (dsRBD)[18,19], K Homology (KH) domains[20,21], and tandem zinc fingers (TZFs)[22-24]. One of the most selective RBDs is the CCCH TZF domain; a small domain, approximately 70 amino acids in length. The CCCH TZF contains minimal secondary structure elements and folds according to the coordination of three cystines and a histidine residue by a zinc ion[147]. Proper RNA recognition and binding by TZF proteins is crucial during development when transcription is typically repressed[1-5] and during inflammatory responses[6] when multiple genes are coordinated rapidly in response to external cues. Therefore, examining how the primary sequence of the TZF influences a protein′s cellular targets is essential for understanding their role in human physiology.

In work done by Pagano *et al*. and our lab have shown that small changes in a conserved R(K)YKTXL sequence preceding each finger motif (Figure 3.1) are responsible for the specificity of targets seen across other CCCH TZF RBPs (Table 3.1)[148]. Previous studies on the TZF protein from *C. elegans* MEX-5 suggested that

changes to the primary R(K)YKTR(K)L sequence result in different RNA binding specificities. Wild type MEX-5 binds to RNA with high affinity and low specificity, binding to RNA with stretches of six or more uridines within an eight nucleotide window[148]. The TTP family binds to the AU rich sequence elements (ARE), UUAUUUAUU, with high specificity[149]. Upon mutation of the MEX-5 binding motif R(K)YKTR(K)L to mimic the canonical TTP family binding sequence R(K)YKTEL, MEX-5 gains TTP-like specificity, binding AU rich elements with higher affinity than a sequence of polyuridine. This suggests that the basic residues provide the lower specificity observed in the MEX-5 binding site. Based on these studies of MEX-5 the fifth residue position has been coined the "discriminator residue[148]."

```
TTP_ZF1        RYKTELCRTFSE--SGRCRYGAKCQFAH
TIS11d_ZF1     RYKTELCRPFEE--SGTCKYGEKCQFAH
TIS11b_ZF1     RYKTELCRPFEE--NGACKYGDKCQFAH
MEX-5_ZF1      NYKTRLCMMHAS-GIKPCDMGARCKFAH
MEX-6_ZF1      NFKTRLCMTHAA-GINPCALGARCKFAH
MEX-1_ZF1      AFKTALCDAFKR--SGSCPYGEACRFAH
OMA-1_ZF1      SYKTVICQAWLE--SKTCSFADNCRFAH
OMA-2_ZF1      SYKTVICQAWLE--SKTCAFAENCRFAH
MOE-3_ZF1      SYKTVICQAWLE--SKTCTFAENCRFAH
POS-1_ZF1      AFKTALCDAYKR--SQACSYGDQCRFAH


TTP_ZF2        KYKTELCHKFYL--QGRCPYGSRCHFIH
TIS11d_ZF2     KYKTELCRTFHT--IGFCPYGPRCHFIH
TIS11b_ZF2     KYKTELCRTFHT--IGFCPYGPRCHFIH
MEX-5_ZF2      KYKTKLCKNFARGGTGFCPYGLRCEFVH
MEX-6_ZF2      KYKTKLCKNFARGGSGVCPYGLRCEFVH
MEX-1_ZF2      KYKTQLCDKFSN--FGQCPYGPRCQFIH
OMA-1_ZF2      KYKTKLCDKYTT--TGLCPYGKRCLFIH
OMA-2_ZF2      KYRTKLCDKYTT--TGLCPYGKRCLFIH
MOE-3_ZF2      KYKTKLCDKYTT--TGLCPYGKRCLFIH
POS-1_ZF2      KYKTVLCDKFSM--TGNCKYGTRCQFIH
```

Figure 3.1: Sequence alignment of human and C. elegans CCCH tandem zinc fingers. Alignment of ZF1 (top) and ZF2 (bottom) of the human TTP family and C.elegans CCCH members. Top of each sequence alignment highlights residues directly involved in RNA binding in 1RGO solution NMR structure which are indicated with asterisks; black = hydrogen bonds, green = base stacking interactions. The three cysteines and histidine involved in zinc coordination are bolded in black. The conserved R(K)YKT**X**L sequence preceding the ZF is boxed in gray. Sequence differences of the R(K)YKT**X**L region are colored for positively charged (red), negatively chared (blue), and hydrophobic (orange) side chains.

Table 3.1: Differences in discriminator residues and their RNA recognition sequence

CCCH protein	ZF1	ZF2	Recognition sequence *R=AorG, G=A,G,orT, N=any nucleotide
TTP	E	E	UUAUUUAUU[127]
POS-1	A	V	UAUURDNNG[150]
OMA-1	V	K	UA(A/U) repeat[151]
MEX-5	R	K	U rich repeats[148]

The RNA binding protein tristetraprolin (TTP), and its homologues TIS11b and TIS11d, are required for post-transcriptional repression of many different genes associated with inflammation and cancer initiation/progression in mammals[152]. TTP family members mediate post-transcriptional repression by specifically binding to ARE containing mRNA targets to promote their degradation[153]. The origin of mRNA binding specificity of the TTP family has not yet been determined. We hypothesize that the glutamate in the conserved R(K)YKTEL motif is critical for the RNA binding specificity of the TTP family.

Studies in our lab and others have shown that the TTP family binds with the highest affinity to RNAs containing two UAUU half sites (Table 3.1). The NMR solution structure of TIS11d bound to ARE9 UUAUUUAUU depicts an adenine binding pocket residues involving residues of the conserved R(K)YKTEL sequence preceding each finger (Figure 3.1). The TIS11d/RNA complex is held together mainly though protein

backbone hydrogen bonds, with exception of the side chain residues E157, C174, and C212. Previous work in our lab determined that hydrogen bonds with E157 (E107) in TIS11d (TTP) help to stabilize its interaction with RNA. These results suggest that residues in this motif are critical for the high affinity RNA binding and specificity observed in the TTP family. In support of this hypothesis, mutation of the third position of the motif (K105) in TTP is linked to bladder urothelial carcinomas, and mutation of the fifth motif position in TIS11d (E157) is observed in patients with bladder, breast, liver and lung carcinomas[102].

In order to determine if the ionic charge dictates RNA discrimination of TTP and MEX-5 R(K)YKTEL motif, we mutated the acidic glutamate residues in TTP and TIS11d to arginine in ZF1 and lysine in ZF2, similar to those residues found in MEX-5. The RNA binding activities of the mutant proteins, both the single and double mutant, were measured via fluorescence polarization using variant RNA sequences (Tables 3.2 and 3.3). Additionally, we used nuclear magnetic resonance (NMR) spectroscopy to determine the structural differences that occur upon RNA binding. Finally, we performed an *in vivo* luciferase assay to study how changes in the R(K)YKTEL motif of TTP alters its activity in the cell. We found that mutation of the R(K)YKTEL in ZF1 are detrimental to TIS11d and TTP RNA binding activity, but has a larger effect on TTP. Mutation of the Glu in ZF2 to Lys does not affect the RNA binding affinity of TTP and TIS11d.

Results and Discussion

Changes in the conserved R(K)YTEL motif results in decreased RNA binding affinity of TTP and TIS11d

The solution structure of TIS11d/ARE9 (U1-U2-A3-U4-U5-U6-A7-U8-U9) complex determined that ZF1 of TIS11d interacts with the U6-A7-U8-U9 halfsite and ZF2 interacts with the U2-A3-U4-U5 halfsite. Therefore, TIS11d ZF1 binds the adenine located at the 3′ end and ZF2 binds the adenine located at the 5′ end of the RNA. We substituted uracil residues for adenines in the high affinity ARE13 (UUUUAUUUAUUUU) to elucidate the putative role of the R(K)YKTEL sequence in determining the binding specificity of the TTP family. Using fluorescence polarization (FP) we measured RNA binding after substituting ZF1 glutamate residues for arginine (TTP E107R, TIS11d E157R) and ZF2 glutamate residues for lysine (TTP E145K, TIS11d E195K)

In the tables below the halfsite bound by ZF2 is italicized and shown in bold face, while the halfsite bound by ZF1 is underlined.

Table 3.2: Comparison of mutant TIS11d binding equilibrium FP measurements

RNA	WT TIS11d	(ZF1)E157R	*(ZF2)E195K*	(ZF1)E157R/ *(ZF2)E195K*
UUU*UAUU*UAUUUU	8 ± 0.4 nM	21 ± 2 nM	11 ± 1 nM	16 ± 1 nM
UUU*UUUU*UAUUUU	45 ± 8 nM	102 ± 20 nM	50 ± 3 nM	103 ± 23 nM
UUU*UAUU*UUUUUU	39 ± 6 nM	74 ± 4 nM	58 ± 5 nM	60 ± 4 nM

Table 3.3: Comparison of mutant TTP binding equilibrium FP measurements

RNA	WT TTP	(ZF1)E107R	*(ZF2)E145K*	(ZF1)E107R/ *(ZF2)E145K*
UUU*UAUU*UAUUUU	9 ± 0.5 nM	64 ± 6 nM	9 ± 1 nM	48 ± 3 nM
UUU*UUUU*UAUUUU	62 ± 2 nM	527.5 ± 353 nM	34 ± 3 nM	223 ± 57 nM
UUU*UAUU*UUUUUU	66 ± 2 nM	612 ± 92 nM	51 ± 4 nM	222 ± 21 nM

We found that mutation of the glutamate of ZF2 R(K)YKTEL motif (TIS11d E195K, TTP E145K) had a limited effect on substrate binding. The TTP ZF2 E145K mutation increases the RNA binding affinity of ZF2 for not only the UAUU halfsite, but also the UUUU halfsite. Therefore, changing the electrostatics of ZF2 to make it more positive mildly enhances the affinity of TTP for negatively charged RNA. Conversely, TTP ZF1 E107R mutation in the adenine binding pocket decreases the TZF affinity of TTP for all RNA substrates. To a smaller extent, this is also observed for the TIS11d E157R mutant of ZF1, which decreases the TZF affinity of TIS11d for all substrates by approximately half. We therefore sought to understand why mutations in ZF1, but not ZF2, lower the affinity of both TIS11d and TTP for all RNA substrates.

Structural analysis explains the loss of affinity observed when the ZF1 glutamate is mutated. The NMR solution structure of TIS11d shows that backbone hydrogen bonds from E157, L158, and R160 in ZF1 and E195 L196, and R198 in ZF2 coordination of the adenine. Of particular interest to our findings, the E157 side chain carboxyl in ZF1 forms

a hydrogen bond with the exocyclic amine of the adenosine base stabilizing the adenosine interaction with ZF1. This hydrogen bond is absent in ZF2 potentially explaining the lack of an effect on affinity observed with mutation of the Glu of ZF2 to Lys. The homology model of the E157R/E195K mutation based on the TIS11d TZF structure suggests that substituting the glutamate in ZF1 with arginine results in a loss of base-specific hydrogen bonds, where the side chain carboxyl can no longer bind to the exocyclic amine of the adenosine base (Figure 3.2). Our studies of TTP indicate that RNA is necessary to promote the folding transition of ZF2, as predicted by the induced-fit model. Mutations that destabilize the interaction of the folded ZF1 with RNA, such as TTP E107R that disrupt the adenine binding pocket, have a strong negative effect on RNA binding since binding induces folding of ZF2. In TIS11d where both ZF1 and ZF2 are folded in the absence of RNA, such a strong deleterious effect on RNA-binding is not observed upon mutation of E157 to an arginine residue. Therefore, the different structure and stability observed for the TZF domains of TTP and TIS11d affect how these proteins respond to mutations of residues critical for RNA binding.

Figure 3.2: Adenine binding pocket of E157R/E195K mutation. A) A homology model of E157R/E195K (purple) bound to ARE9- 5′UUAUUUAUU3′(yellow) overlayed onto the surface structure of the solved TIS11d structure (gray) (PDB access code: 1RGO). The red box highlights TIS11d ZF1 adenine recognition pocket. B) Close up view of the adenine binding pocket of TIS11d ZF1. The adenosine base is in yellow. E157 is represented in gray. E157 side chain carboxyl forms a hydrogen bond (black) with the exocyclic amine of the adenosine base. When the glutamate (gray) is replaced with a bulky arginine residue (purple) in ZF1, this hydrogen bond is lost.
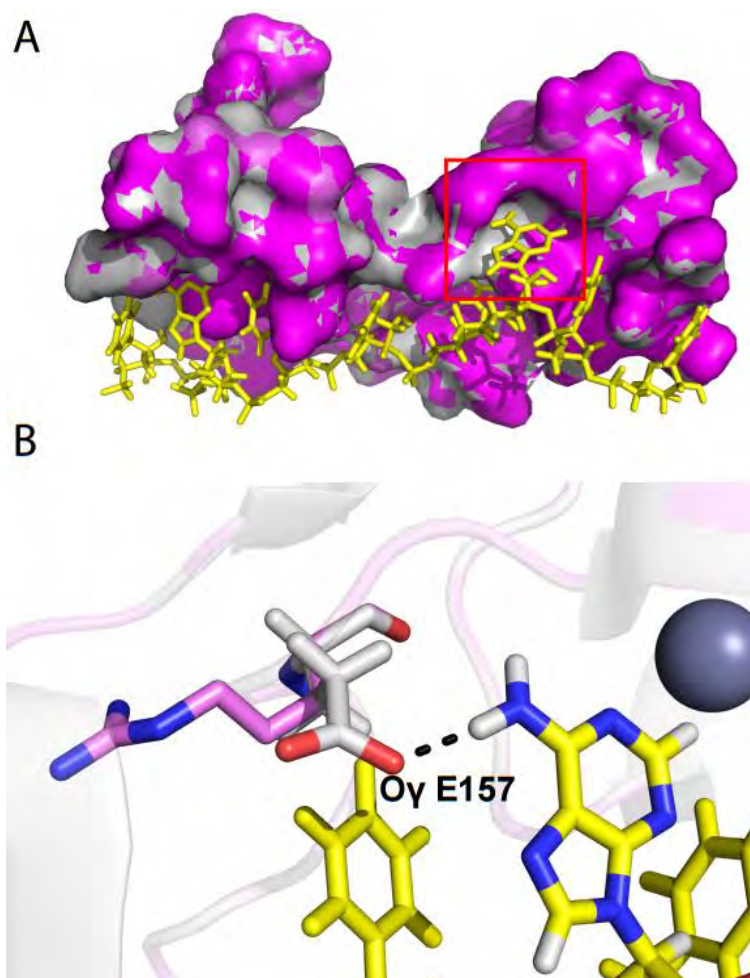
Replacing the glutamates in of the conserved R(K)YTEL sequence affects TTP HSQC

Previous studies of the human TTP TZF in our lab and others have found that ZF2 undergoes a large conformational change upon RNA binding. In the RNA-free state, only ZF1and the first half of the linker of TTP are clearly resolved in the spectra. However, the missing peaks from the linker and ZF2 appear in the spectrum upon addition of RNA, indicating that these residues become more ordered upon RNA binding. This is also observed in the E145K mutant of TTP, thus mutation of the glutamate at ZF2 does not affect the ability of ZF2 to fold and bind RNA (Figure 3.4). The ^{15}N-^{1}H HSQC spectra of E107R mutant TTP and E107R/E145K double mutant are similar to that of TTP, indicating that the mutations do not affect the structure of the protein in solution (Figure 3.3). Addition of RNA to ZF1 E107R mutant and E107R/E145K double mutant, however, causes precipitation of the proteins. The precipitation the E107R and E107R/E145K proteins observed upon addition of RNA in the NMR experiment suggests that the proteins are not stable in solution in the presence of RNA at the concentrations used in this experiments (50 μM). Although the protein concentration was much lower (2 μM), we cannot exclude that there is some precipitation of these proteins in the FP RNA binding assay, explaining the low measured RNA binding affinity.

Figure 3.3: E107R, E145K, and E107R/E145K mutations have very little effect on TTP fold. ^{15}N-^{1}H HSQC overlays of TTP (red) and E107R/E145K (purple), E107R (cyan), and E145K (blue). Extra peaks in E145K, especially in the 8ppm region, can be due to the presence of a 19 amino acid, MHHHHHHGLEVLFQGPLGS, tag left on the protein to facilitate purification.
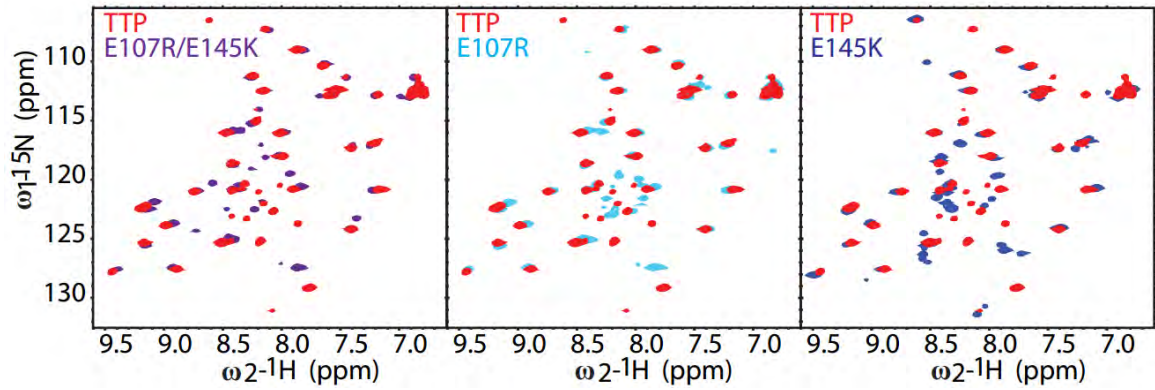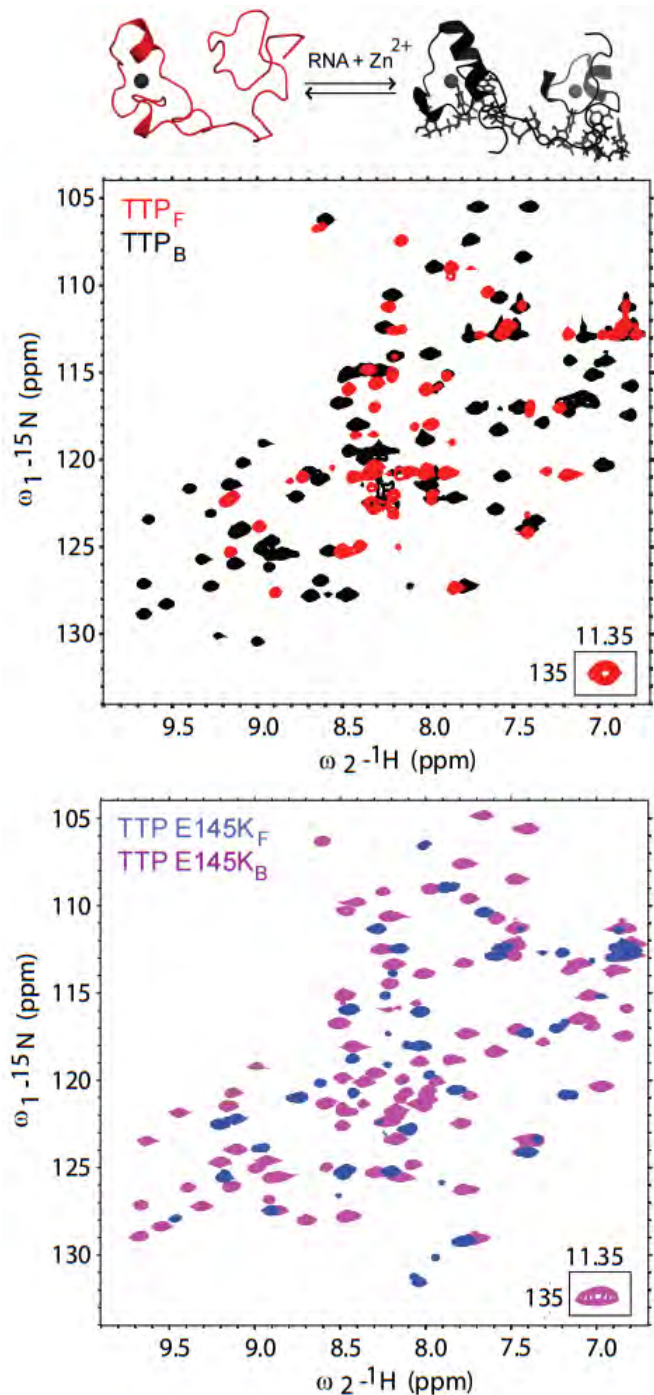
Figure 3.4: E145K mutation has minimal effect on TTP binding to ARE13. Top: ^{15}N-^{1}H HSQC spectra of TTP (red) bound to ARE13 - 5´UUUUAUUUAUUUU3´ (black). Above the HSQC is a cartoon representation of TTP binding to RNA. TTP undergoes an unfolding/ folding transition upon RNA binding. Bottom: HSQC spectrum of TTP E145K (blue) and TTPE145K: ARE13 (magenta) demonstrates the same unfolding/folding transition as that seen for TTP.

Examining the ability of the mutants to degrade TNF-α in HEK cells

A luciferase reporter assay shows that targeted mutations affect TTP cellular function (Figure 3.5). HEK293 cells were co-transfected with a plasmid containing individual TTP mutants and a reporter gene encoding Renilla luciferase fused to the 3′UTR of TNF-α, a known recognition site for the TTP family. In this assay, decreased
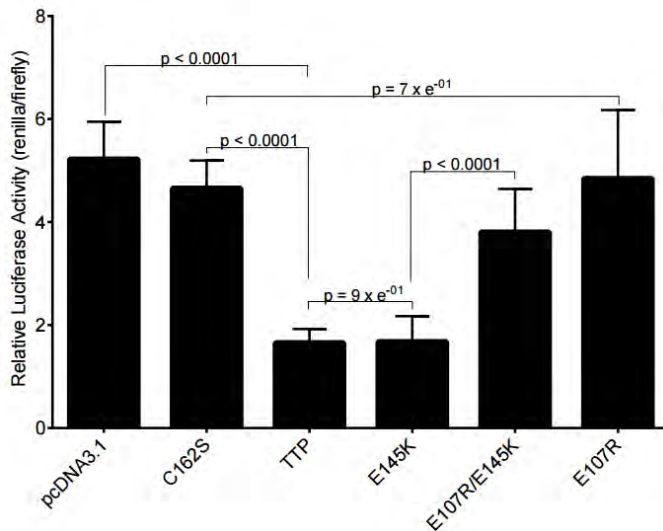
Figure 3.5: Measurements of the cellular activity of WT TTP and E107R/E145K mutations. The E107R mutation of TTP affects the mRNA destabilizing activity of TTP in HEK293 cells. The plot shows the relative luciferase activity measured for HEK293 cells incubated for 48 hours with empty pcDNA 3.1 plasmid, WT TTP, C162S, E107R, E145K, or E107R/E145K -mutations.

Renilla luciferase expression is indicative of luciferase mRNA turnover in the cell, and therefore increased TTP activity. As expected the ZF2 mutation E145K, which does not affect the RNA binding affinity nor specificity of the protein, has similar luciferase activity to wild type TTP. A previously characterized mutant, C162S, which cannot bind RNA due to the loss of zinc coordination in ZF2, shows increased luciferase activity. E107R and dual E107R/E145K mutant forms of TTP display elevated luciferase activity on par with C162S. We therefore conclude that the ZF1 E107R mutation in TTP displays an increase in luciferase activity due to its inability to bind properly to ARE RNA. Therefore, consistent with our *in vitro* RNA binding data, changes in the conserved

R(K)YKTEL sequence preceding ZF1 impair TNF-α turnover by TTP due to the

decreased ability of the protein to bind the target RNA sequence.

Changes in the R(K)YKTEL sequence preceding each zinc finger have a small effect on chemical shift perturbations of apo TIS11d

In order to characterize the effect of E157R, E195K, and E157R/E195K

mutations on TIS11d we used NMR spectroscopy. ^{15}N-^{1}H HSQC spectra collected for

E157R, E195K, and E157R/E195K are similar to that of WT TIS11d, indicating that the

mutations do not affect the overall structure of the protein (Figure 3.7a). The overall

chemical shift perturbations (CSPs) observed between wild-type TIS11d and E157R,

E195K, and E157R/E195K were small. As expected, CSPs for TIS11d ZF2 E195K are

observed at or near the mutation site. In TIS11d ZF1 E157R mutation CSPs are not only

observed for residues that are in close proximity to the mutation, either in space or

primary sequence, but also in ZF2 (Figure 3.6). This observation suggests that this

mutation affects the conformation of the flexible linker that allows a different

arrangement of ZF1 and ZF2 in solution relative to the wild type protein. In addition to

perturbing the adenine binding site, this mutation might also affect RNA-binding through

its effect on the orientation of the ZFs in the free state.

Figure 3.6: Chemical Shift Perturbations (CSPs) of RNA free TIS11d, E157R, E195K, and E157R/E195K. A) ^{15}N-^{1}H HSQC overlays of TIS11d (red) and E157R/E195K (purple), E157R (cyan), and E195K (blue). Below are Chemical Shift Perturbation (CSPs) plots of TIS11d minus each R(K)YKTEL mutation. B) CSPs of TIS11d minus E157R are mapped onto the solution structure of bound TIS11d (1RGO). Zinc is shown as gray spheres. White indicates minimal chemical shift variations between TIS11d and E157R spectra, while red residues are those with higher chemical shift differences. G179 has the highest chemical shift variation, since it is adjacent to the mutated site. However, chemical shift variations are mapped through the length of TIS11d TZF.
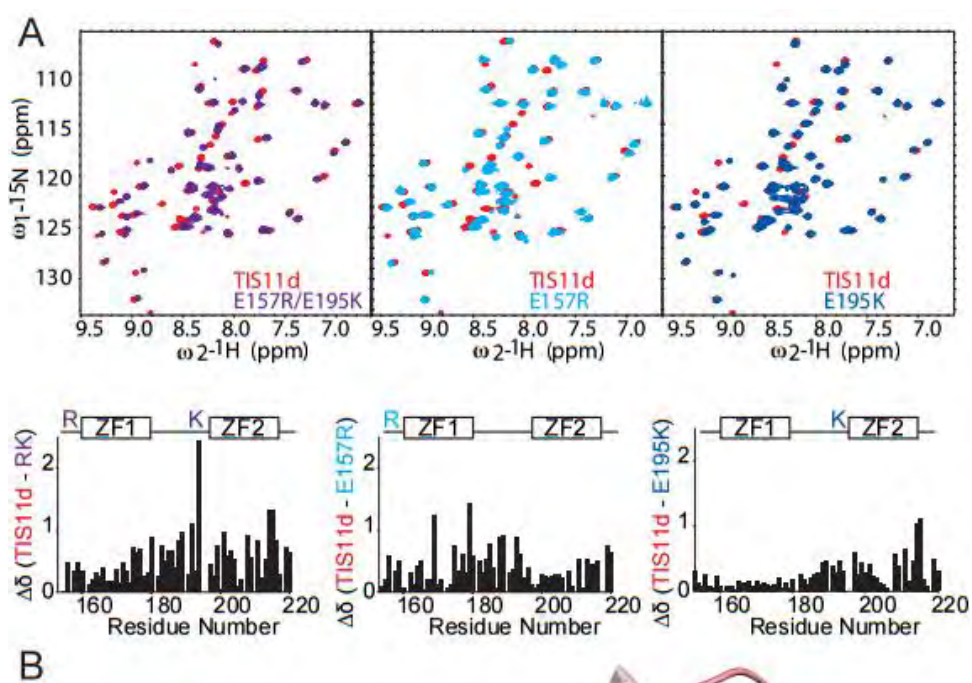
Changes in the R(K)YKTEL sequence preceding each zinc finger do not alter

TIS11d binding registry

Chemical shift difference maps were calculated from ^{15}N-^{1}H HSQCs of WT and

E157R/E195K TIS11d mutant RBDs between the free and ARE13-bound states (Figure

3.7). Chemical shift difference of E157, E195K and E157R/E195K bound to RNA

indicate that the mutations have little effects on cognate ARE13 (UUUUAUUUAUUUU)

binding. Although present in the WT spectrum, in the ^{15}N-^{1}H HSQC spectrum of TIS11d

ZF1 E157R mutation, cross-peaks for R160 and R198 are low in the noise and therefore

are absent in the chemical shift analysis. Peaks for R160 and R198 are present in the

ARE13 bound E157R/E195K dual mutant; however are also low in intensity. In the

^{15}N-^{1}H HSQC spectrum taken for TIS11d ZF2 E195K mutation, these peaks are present

with similar intensity to WT TIS11d. In the NMR structure of TIS11d, R160 and R198

form hydrogen bonds when bound to the ARE sequence and consequently shift upfield in

the bound ^{15}N-^{1}H HSQC spectrum (boxed in ^{15}N-^{1}H HSQC spectrum). Given the signal

to noise ratio of these experiments, we cannot determine if the E157R mutation weakens

the hydrogen bonds between R160 and R198 and the RNA. More work will be needed to

determine if this is the case.

Figure 3.7: Mutations of the highly conserved sequence have little effects on the overall conformation of ARE13 bound TIS11d. ^{15}N-^{1}H HSQC overlays of TIS11d (red) and E157R/E195K (purple), E157R (cyan), and E195K (blue) overlaid with their ARE13 bound ^{15}N-^{1}H HSQCs (gray). In the right hand corner of each spectra, with exception of E157R with peaks absent in its ^{15}N-^{1}H HSQC) there is an inset representing peaks R198 (left) and R160 (right). In the dual RK (E157R/E195K) mutation the R160 peak appears absent; however, this peak is in the noise. Below are Chemical Shift Perturbation (CSPs) plots of TIS11d minus TIS11d ARE13 bound spectra.
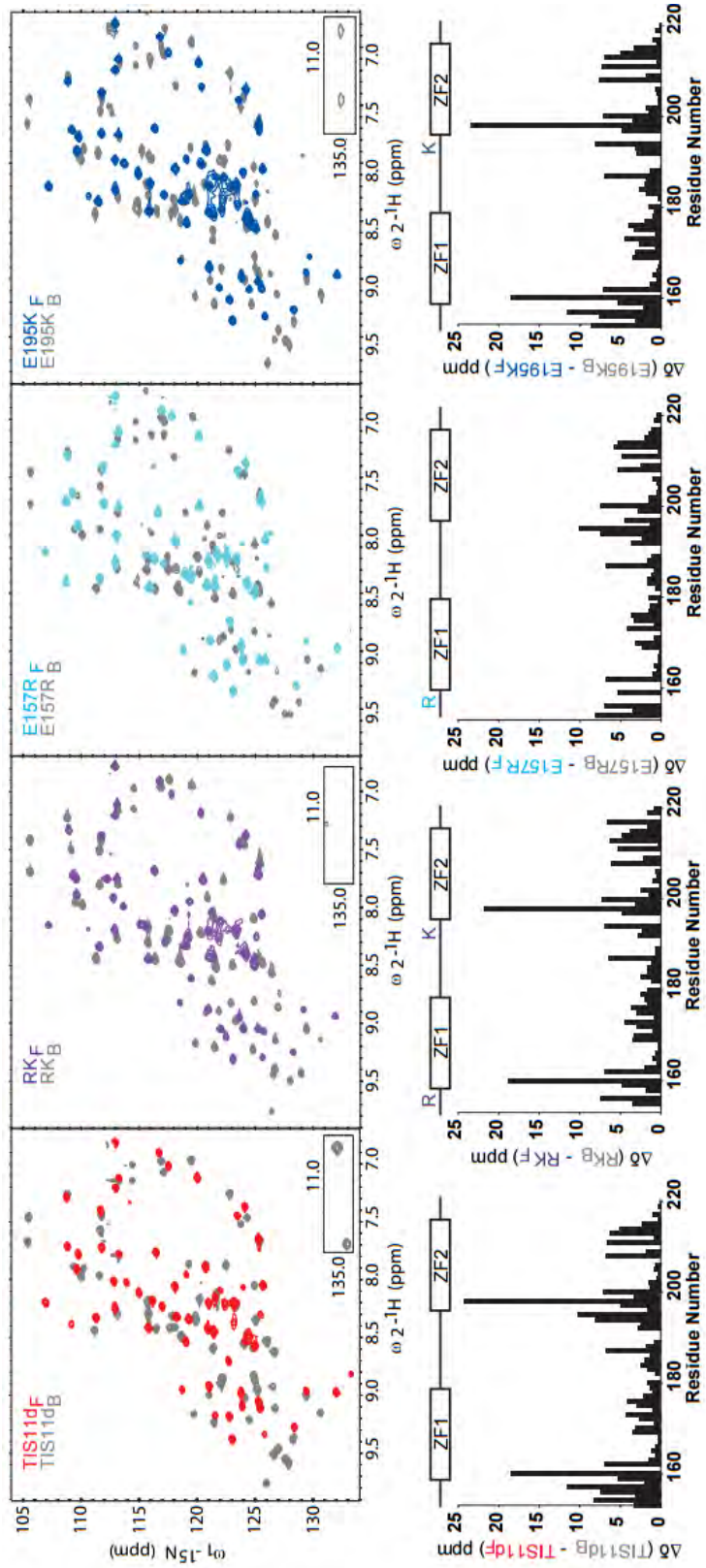
Previous work in our lab determined that TIS11d ZF1 binds the 3′ U6-A7-U8-U9 half-site and ZF2 binds the 5′-U2-A3-U4-U5 half-site of the ARE9 (U1-U2-A3-U4-U5-U6-A7-U8-U9) RNA sequence. Here we investigate chemical shift differences associated with E157R and E195K bound to different RNA sequences to test if these mutants bind RNA with a similar 3′ to 5′ binding registry. In these experiments we compared chemical shifts associated with ARE13 (UUUU**A**UUU**A**UUUU) binding to uracil substitutions for one or both RNA adenosines. Relative to ARE binding to E157R/E195K TIS11d, binding of 5U13 (UUUU**U**UUU**A**UUUU) shows larger chemical shift changes at ZF2, whereas binding of 3U13 (UUUU**A**UUU**U**UUUU) shows larger chemical shift changes in ZF1 (Figure 3.8). TIS11d binding to U13 (UUUU**U**UUU**U**UUUU) is associated with the combined chemical shift changes that we observe for 5U13 and 3U13, in that larger chemical shift changes are observed for both ZF1 and ZF2 relative to ARE13. These results are consistent with all the mutant proteins binding the four different RNA sequence using the same register of the WT protein, thus binding the 3′ half-site with ZF1 and the 5′ halfsite with ZF2 regardless of uracil substitution. Therefore the mutations do not alter TIS11d RNA binding register.

a

5′UUUUAUUUAUUUU3′
5′UUUUUUUUAUUUU3′

5′UUUUAUUUAUUUU3′
5′UUUUAUUUUUUUU3′

5′UUUUAUUUAUUUU3′
5′UUUUUUUUUUUUU3′

b

5′UUUUAUUUAUUUU3′
5′UUUUUUUUAUUUU3′

5′UUUUAUUUAUUUU3′
5′UUUUAUUUUUUUU3′

5′UUUUAUUUAUUUU3′
5′UUUUUUUUUUUUU3′

80
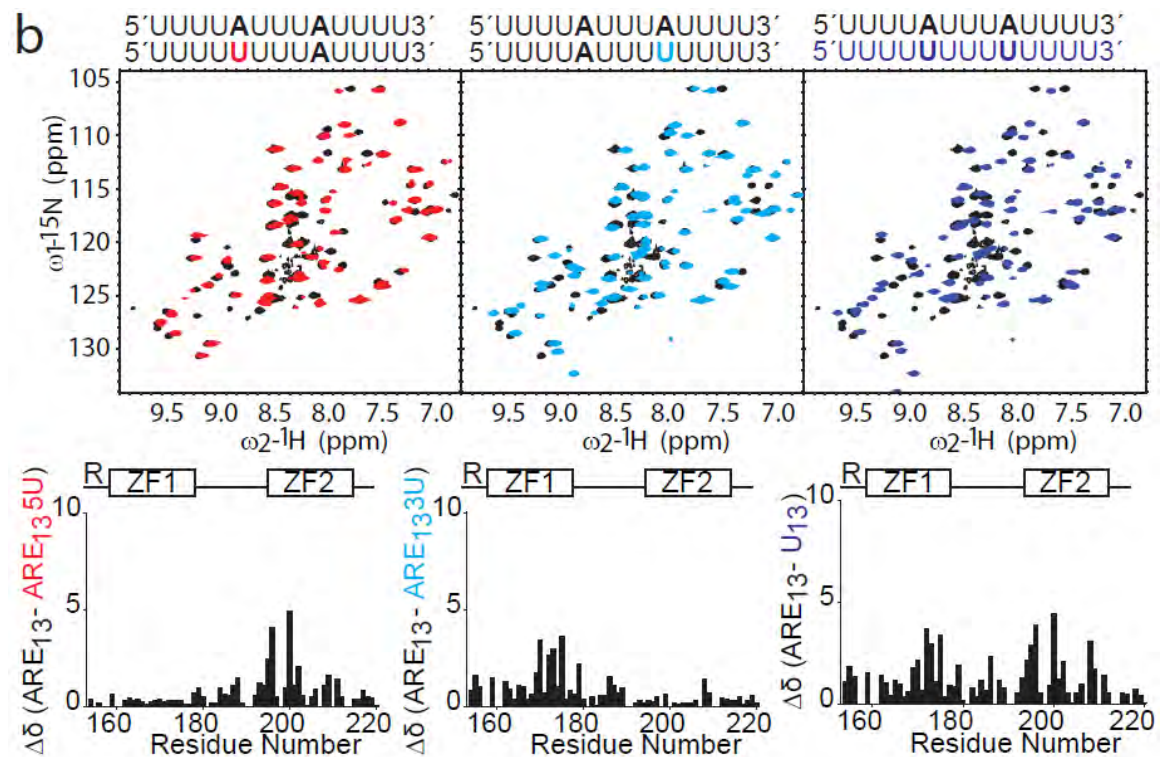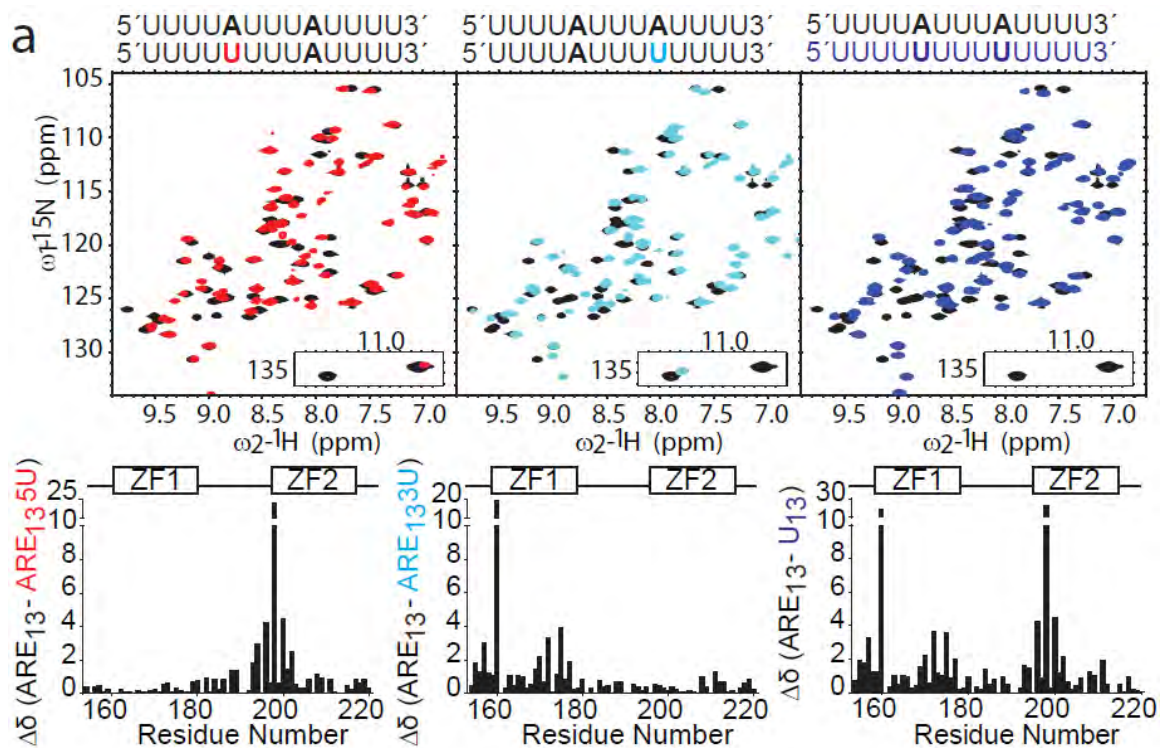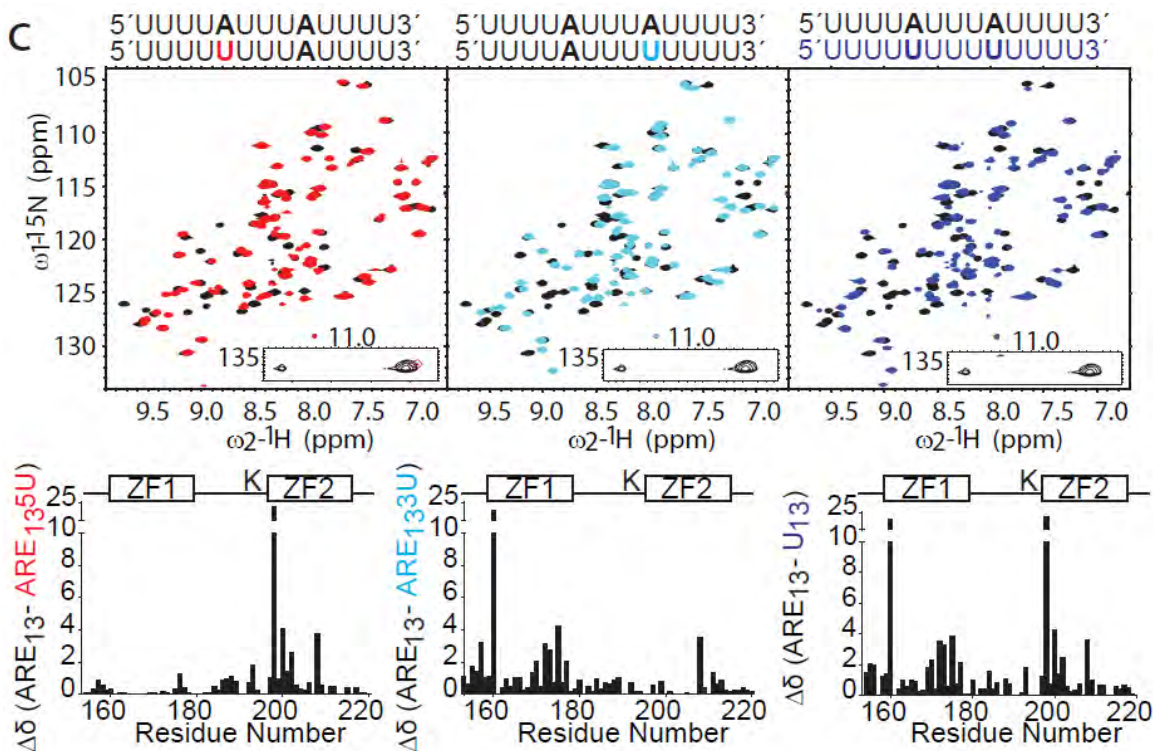
Figure 3.8: TIS11d, E157R, E195K recognition RNA with a 3′ to 5′ polarity regardless of uridine substitution of the UAUU subsite. **a)** HSQCs of TIS11d bound to ARE13 5′U - 5′UUUUUUUUUAUUUU3′ (red), ARE13 3′U - 5′UUUUAUUUUUUUU3 (cyan), and U13 – 5′ UUUUUUUUUUUUU3′ (blue) overlaid with TIS11d in complex with ARE13 – 5′UUUUAUUUAUUUU3′(black). Beneath each HSQC are their respective chemical shift perturbation plots, each with a schematic representation of the TZF motif of TIS11d. **b)** HSQCs of E157R bound to each RNA sequence with its corresponding chemical shift perturbation plots below. **c)** E195K in complex with RNA variants overlaid with ARE13. CSP maps give similar profile as those seen for WT TIS11d.

Conclusions

The TZF domain of the *C. elegans* protein MEX-5 binds RNA with high affinity and low specificity to uridine rich stretches. In contrast, the mammalian proteins TIS11d and TTP bind to 5′UUUUAUUUAUUUU′3 with high affinity and specificity. The relaxed binding specificity seen in MEX-5 is attributed to the Arg/Lys (R274/K318) in the fifth residue (X) of the highly conserved R(K)YKTXL motif preceding each zinc

finger in the CCCH TZF. In the mammalian proteins the fifth residue (X) is always a glutamate, whereas in *C.elegans* proteins, this position is less uniform. In this study we explored the effects on the RNA-binding activity of the equivalent mutations in TTP and TIS11d, E107R/E145K and E157R/E195K. We found that mutations of the R(K)YKTEL in the first finger are detrimental to both TIS11d and TTP UAUU binding activity. Mutating the glutamate in ZF1 to a bulky arginine residue resulted in a loss of RNA binding affinity. These results exemplify the challenges associated with defining the recognition code for all CCCH tandem zinc fingers since what is applicable for one CCCH family member may not be true for all CCCH members. As the field advances, and more structures are deposited for CCCH proteins in complex with their cognate RNA sequences, we can begin to understand how structure as well as primary sequence changes of more than one amino acid, influences RNA specificity for all of the CCCH family.

For TIS11d and TTP, the integrity of the conserved R(K)YKTEL eukaryotic sequence is essential for high affinity RNA binding. This sequence motif makes necessary interactions with RNA seen in the NMR structure of TIS11d in complex with high affinity UUAUUUAUU sequence. In this study we show that mutation of the glutamate residues at position 157 (107) to arginine severely impacts the ability of TIS11d (TTP) to bind RNA with high affinity. Mutation of E195 (E145) does not affect the RNA binding affinity of TIS11d (TTP). This is reflected in the cellular luciferase reporter assays which determine that E107R of ZF1 impairs TNF-α degradation by TTP. Homology modeling of E157R and E195K mutations onto the published TIS11d

structure suggests that TTP E107R and TIS11d E157R mutations may cause changes to the adenine binding pocket that preclude RNA binding at ZF1 due to the increase in size of the side chain moiety. This finding contradicts our original hypothesis, which was that the positively charged residues would form more favorable interactions with the negatively charged RNA backbone to allow more promiscuous binding. Furthermore, this finding suggests that not only electrostatic, but also steric interactions between the RNA and protein play a large role in mRNA specificity.

Consistent with the biophysical and biochemical data, mutation of the third position of the R(K)YKTEL motif (K105) in TTP is linked to bladder urothelial carcinomas, and mutation of the fifth motif position in TIS11d (E157) is observed in patients with bladder, breast, liver and lung carcinomas[102]. Mutations associated with the adenine-coordinating residues in ZF1 are detrimental to TIS11d (TTP) RNA binding activity. Our work suggest that mutations of the conserved R(K)YKTEL motif in ZF1 decrease the affinity of TIS11d for its targets thereby impeding its activity and ultimately resulting in cancerous phenotypes.

Materials and Methods

Sample preparation for NMR

WT TTP, WT TIS11d, E157R, E195K, and E157R/E195K were cloned, expressed and purified similar to Chapter II. TTPK was subcloned into a modified pGEX6P1 vector minus coding region for GST tag. To simplify the purification process the His tag in the

MHHHHHHHGLEVLFQGPLGS tag was not removed. TTPK was expressed and lysed similar to Chapter II. Lysates were centrifuged at 19500 RPM for 1 hr at 4°C and passed through a 20 mL pre-packed PrepEase His Tagged resin (Affymetrix), washed with 5 column volumes of 50 mM Tris HCl, pH 8.0, 50 mM NaCl, 5 mM imidazol, and eluted with 50 mM Tris HCl, 5 pH 8.0, 50 mM NaCl, 350 mM imidazol. The protein was then passed through a 5 mL HiTRAP Q (GE health are Life Science) pre-equilibrated with a buffer containing 50 mM Tris HCl, pH 8.0, 50 mM NaCl. Flow through was buffer exchanged into 10 mM Tris, pH 6.2, 20 mM KCl, 2 mM DTT, 0.1 mM ZnSO4 by dialysis and concentrated to using a 3 KDa Centriprep concentrator (Millipore).

Sample preparation for FP assays

The RBD of human TIS11d (residues 152-220) was synthesized by Genescript and cloned into the pHMTC vector between BamHI and HindIII restriction sites. Constructs containing arginine/lysine mutations in TTP and TIS11d were generated using the QuikChange Site-Directed Mutagenesis Kit from Stratagene. TIS11d and mutated constructs were expressed in BL21 (DE3) E. coli competent cells. Isotopic labeling with ^{15}N was performed by growing the cells in M9 enriched with 1 g of ^{15}NH$_4$Cl per liter. Carbon labeling is performed by growing cells in M9 containing ^{13}C-glucose. The cells were grown at 37°C to an OD$_{600}$ of 0.8 and then induced for 4 hours with 1 mM Isopropyl β-D-1 thiogalactopyranoside (IPTG) and 0.1 mM ZnSO$_4$ at the same temperature. Harvested cells were then passed through a cell disrupter in 50 ml lysis buffer containing 50 mM Tris HCl, pH 8.0, 100 mM NaCl, 100 μM ZnOAc, 2 mM dithiothreitol (DTT)

and 1 EDTA free Complete protease inhibitor tablet (Roche). Lysate was centrifuged at 19500 RPM for 1hr at 4°C and passed through a 20 ml Amylose column pre-equilibrated with wash buffer (50 mM Tris HCl, pH 8.0, 100 mM NaCl, 100 μM ZnOAc and 2 mM DTT). The column was washed with 10 column volumes of wash buffer. The protein was eluted with 10 mM Maltose in wash buffer. The eluent was then placed over a 5 ml Hi TRAP Q column (GE healthcare Life Science) pre-equilibrated with the same wash buffer used above. The column was washed with 3 column volumes of wash buffer. The protein was eluted with a gradient of NaCl from 0-1 M; the peptides typically eluted at 0.3-0.5 M NaCl. Fractions containing our protein were combined, concentrated and dialyzed in 50 mM Tris HCl, pH 8.0, 100 mM NaCl, 100 μM ZnOAc and 2 mM DTT.

Measurements of RNA-binding affinity

The RNA-binding activity of the MBP tagged protein samples was determined using fluorescent polarization with fluorescein 5′ end labeled RNA as previously described Briefly, the affinities of TTP and TIS11d for variants of the cognate RNA sequence: 5′-UUUUAUUUAUUUU-3′ (ARE_{13}) were measured by direct titration of 3 nM labeled RNA with increasing concentrations of protein. Varying concentrations of the protein were incubated for 3 hours at room temperature with 3nM fluorescently labeled RNA in a buffer solution containing 10 mM TRIS (pH 8), 100 μM $Zn(OAc)_2$, 100 mM NaCl, 0.01 mg tRNA, 0.01% (v/v) IGEPAL, and 2 mM TCEP. To detect the fluorescently labeled RNA, the gel was imaged using a Fuji FLA-5000 laser imager. The apparent dissociation constant $K_{d,app}$ was determined by fitting to the quadratic equation

$$f = \frac{m-b}{2R}\left(K_d + P + R - \sqrt{[K_d + P + R]^2 - 4RP}\right) + b,$$

where m and b are the maximum and base signals, K_d is the dissociation constant, and P

and R are the concentrations of protein and labeled RNA in the sample, respectively. The

reported data was done in triplicate.

NMR spectroscopy

All ^{15}N-^1H HSQC experiments were collected on a Varian Innova spectrometer operating

at 600 MHz equipped with a triple-resonance cold probe. The temperature was calibrated

using a sample of 100% methanol. Data processing was performed using NMRPipe [145]

and Sparky software[146]. The chemical shift differences, Δ, were determined using $\Delta =$

$(\delta_H^2 + (\delta_N \gamma_N / \gamma_H)^2)^{1/2}$, where δ_H is the chemical shift difference of ^1H, δ_N is the chemical

shift difference of ^{15}N and γ_N, γ_H are the gyromagnetic ratio of ^1H and ^{15}N atoms.

Luciferase reporter assay

The pcDNA3.1 His-C-TTP (TTP) expression construct was kindly given to us by Dr.

Seth Brooks[48]. C162S, E107R, E145K, and E107R/E145K mutantions of TTP was

generated using Q5-mutagenesis kit (NEB). Luciferase reporter constructs harboring

cDNA of TNFα 3′UTR (nucleotides 1,231-1,506) was generated by gblock synthesis

(IDT) and was inserted into the psicheck™-2 construct at restriction sites XhoI and NotI.

Human embryonic kidney (HEK) 293 cells were plated at a density of 300,000 cells/well

in 6 well plates, with Dulbecco′s Modified Eagle′s Medium (DMEM) containing 100

units/mL penicillin and 100 μg/mL streptomycin and 10% fetal bovine serum (FBS). The

plates were incubated for 24 hours in a humidified 5% CO_2 incubator set at 37° C. When

the cells were 60-70% confluent each well was cotransfected with 0.25 µg

psicheck2_TNFalpha and 0.5 µg of pcDNA3.1-His-C (empty plasmid), pcDNA3.1 TTP,

pcDNA3.1 TTP (E107R), , pcDNA3.1 TTP (E145K), pcDNA3.1 TTP (E107R/E145K),

or pcDNA3.1 TTP (C162S) using Dharmafect Duo protocol (Thermo-Scientific).

Transfections were performed in triplicate. 48 hours after transfection, cells were

harvested and Luciferase activity was monitored using a Dual-luciferase Reporter Assay

System (Promega) and normalized by the internal control values given by firefly

luciferase. Luciferase activity was monitored in each well 3 times.

Chapter IV: Three residues make an evolutionary switch for folding and RNA-destabilizing activity in the

TTP family of proteins

Abstract

Tristetraprolin (TTP) binds to mRNA transcripts to promote their degradation. The TTP protein family in humans includes two other proteins, TIS11b and TIS11d. All three proteins contain a highly homologous RNA binding domain (RBD) that consists of two CCCH zinc fingers (ZFs). Both ZFs are folded in the absence of RNA in TIS11d and TIS11b. In TTP, however, only ZF1 adopts a stable fold. The focus of this study is to understand the origin and biological significance of the structural differences of the RBD. We identified three residues that affect the affinity for the structural Zn^{2+} and determine the folding of ZF2 in the absence of RNA. We observed that the mRNA destabilizing activity of TTP was increased when the partially disordered RBD of TTP was replaced with the fully structured RBD of TIS11d, indicating that differences in the folded state of the RBD affect the activity of the proteins in the cell.

Significance

Despite the importance of RNA-binding proteins to gene regulation, our understanding of how their structure and dynamics contribute to their biological activity is limited. In this study we focus on two related RNA-binding proteins—TTP and TIS11d—that regulate the stability of mRNA transcripts encoding key cancer-related proteins, such as tumor necrosis factor-α and vascular endothelial growth factor. These two proteins display differential folding propensity in the absence of RNA, despite sharing a high sequence identity. Here we identified three residues located at the C-terminal end of an α-helix that determine the folding propensity of the RNA-binding domain in the apo state. We also showed that stabilization of the structure of the RNA-binding domain is associated with increased RNA-destabilizing activity. Phylogenetic analysis indicates that this family of proteins has only recently evolved to be able to modulate its biological activity through its dynamic structure.

Introduction

Tristetraprolin (TTP), also known as TIS11, Nup475, GOS24, and ZFP36[55,100,154-158], is an RNA binding protein that binds to the 3′ UTR of transcripts at AU-rich elements (AREs)[159]. Binding of TTP to these transcripts promotes their fast degradation, as TTP recruits and activates mRNA decay enzymes[60,160,161]. The function of TTP became apparent with the observation that TTP knockout mice quickly develop severe inflammatory phenotypes after birth, a result of the accumulation of several transcripts[67].

The most abundant of these transcripts encodes the proinflammatory cytokine tumor necrosis factor α (TNFα)[55].

In humans, the TTP protein family includes TIS11b and TIS11d, also known as ZFP36L1 and ZFP36L2[118,126], respectively. Based on their primary sequences, these three proteins are predicted to have low structural complexity and high flexibility. They each contain an RNA binding domain (RBD), surrounded by less-structured N- and C-terminal domains. The highly conserved RNA binding domain is a tandem zinc finger (TZF) motif with two $CX_8CX_5CX_3H$ zinc fingers, where X represents amino acids between each zinc coordinating residue. The two zinc fingers are separated by an 18 amino acid linker. A well conserved sequence, (R/K)YKTEL, precedes each finger and has been shown to be important for RNA binding[118,128,162].

In 2004, Wright and coworkers determined the structure of TIS11d bound to the RNA sequence 5′-UUAUUUAUU-3′ (PDB code:1RGO) using NMR spectroscopy[127]. This structure depicts two folded zinc fingers where the zinc ions are coordinated by residues C159, C168, C174, and H178 in the first finger (ZF1) and C197, C206, C212, and H216 in the second finger (ZF2). The protein-RNA complex shows that the structure of the TZF domain of TIS11d is symmetrical, both ZF1 and ZF2 contain a short α-helix between the first two zinc coordinating cysteine residues (spanning residues 160-165 in ZF1 and 198-203 in ZF2). Additionally, both fingers contain a turn of 3_{10}-helix between the second and third cysteine-coordinating resides (amino acids 171-173 in ZF1 and 209-211 in ZF2). The symmetry observed between the structures of the two zinc fingers is not surprising since their primary sequence is ~50% identical. The two zinc fingers are held

together by a flexible linker, which contains a short 3_{10}-helix at residues 179-183 and is involved in forming a small hydrophobic cluster with residues of the first finger. NMR and computational studies have shown that in the absence of RNA, the structure of the two zinc fingers of TIS11d is maintained although their orientation changes, as the linker region is highly flexible[127,128,162]. Despite their high sequence identities, TTP and TIS11d present striking differences in their unliganded structures. The structural symmetry observed for ZF1 and ZF2 in TIS11d is not observed in unliganded TTP. Previous NMR spectroscopic studies of TTP indicated that only ZF1 of TTP may adopt a stable fold in its RNA free state[163,164].

The focus of this study is to understand the origin and biological significance of the structural differences observed between the RNA binding domains of TTP and TIS11d. We used TTP/TIS11d chimeras to identify the regions responsible for these differences. After testing whether these chimeras are still active and capable of binding RNA, we used NMR spectroscopy to determine if ZF2 is folded in the free state. Finally, we determined how a fully folded TZF domain affects the activity of TTP using a luciferase reporter assay, where luciferase was placed under the control of the TNFα 3′UTR. The results reveal that the degree of structure of the RBD affects the activity of these proteins in the cell.

Results and Discussion

Despite the importance of RNA-binding proteins to gene regulation, our understanding of how their structure and dynamics contribute to their biological activity

92

is limited. In this study we focus on two related RNA-binding proteins—TTP and TIS11d—that regulate the stability of mRNA transcripts encoding key cancer-related proteins, such as tumor necrosis factor-α and vascular endothelial growth factor. TTP and TIS11d display differential folding propensity in the absence of RNA, despite sharing a high sequence identity. To understand the origin of the different folding propensities and how the activities of the two proteins are affected, we used an interdisciplinary approach that included biochemical and biophysical methods, cell-based assays and phylogenetic analysis.

The TZF domains of TTP and TIS11d share high sequence identity but differ in their RNA-free structures.

Although the TZF domains of TTP and TIS11d share 70% sequence identity, we observe that their solution structures differ dramatically in the apo state. The well-dispersed ^{15}N-^{1}H HSQC spectra of the TZF domains of TIS11d (residues 151-220) and TIS11b (residues 200-270) indicate that the structures of both ZF1 and ZF2 are preserved
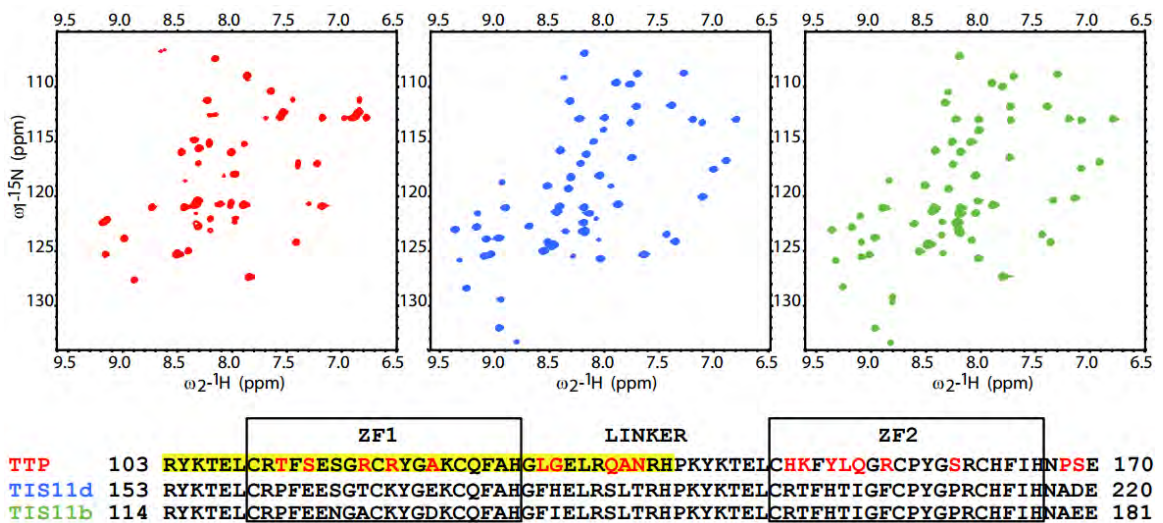
Figure 4.1. The C-terminal ZF of TTP is unstructured in the free state. A) ^{15}N-^{1}H HSQC spectra of the TZF domains of TTP (red), TIS11d (blue) and TIS11b (green). B) Sequence alignments of TZF domains of TTP, TIS11d, and TIS11b. Sequence differences between TTP, TIS11d and TIS11b are highlighted in red. Residues with cross-peaks present in the ^{15}N-^{1}H HSQC spectrum of TTP collected in the absence of RNA are highlighted in yellow.

in the absence of RNA (Figure 4.1). In contrast, the ^{15}N-^{1}H HSQC spectrum of the TTP

TZF domain (residues 102-174) contains only cross peaks from residues of ZF1 and from

the first nine residues of the linker (Figure 4.1 and Figure 4.2). The lack of backbone

amide (N-H^{N}) cross peaks for ZF2 from the spectrum of TTP in the absence of RNA is

the result of a chemical exchange process that is intermediate on the NMR chemical shift

time scale, likely due to the flexibility of ZF2 that samples different

conformations[115,165,166]. Cross-peaks from the C-terminal part of the linker and from ZF2

appear in the ^{15}N-^{1}H HSQC spectrum of TTP only upon addition of RNA (Figure 4.3A).

The overall increase in chemical shift dispersion observed upon addition of RNA results

from the increased number of cross-peaks (cross-peaks from the linker and ZF2 are now

present in the ^{15}N-^{1}H HSQC spectrum) and from the chemical shift changes of ZF1, due

to RNA-binding. These data suggest that in the absence of RNA, ZF2 of TTP is in a

molten globule state and that RNA is needed to stabilize ZF2 in a folded state, in

agreement with the findings of Brewer *et al.*[167] In a previous study, Berg and coworkers

have shown that the TZF domain of murine TTP could bind 1.7 ± 0.4 equivalents of Co^{2+}

[26] which suggests that both ZF1 and ZF2 of murine TTP can bind Zn^{2+} in the absence of

RNA. In the same report, however, NMR spectroscopic studies of the TZF domain of

murine TTP containing a single point mutation introduced to enhance solubility (Y143K),

showed that only ZF1 could stably bind Zn^{2+} while ZF2 was unstructured[168], in

agreement with our observations in human TTP.
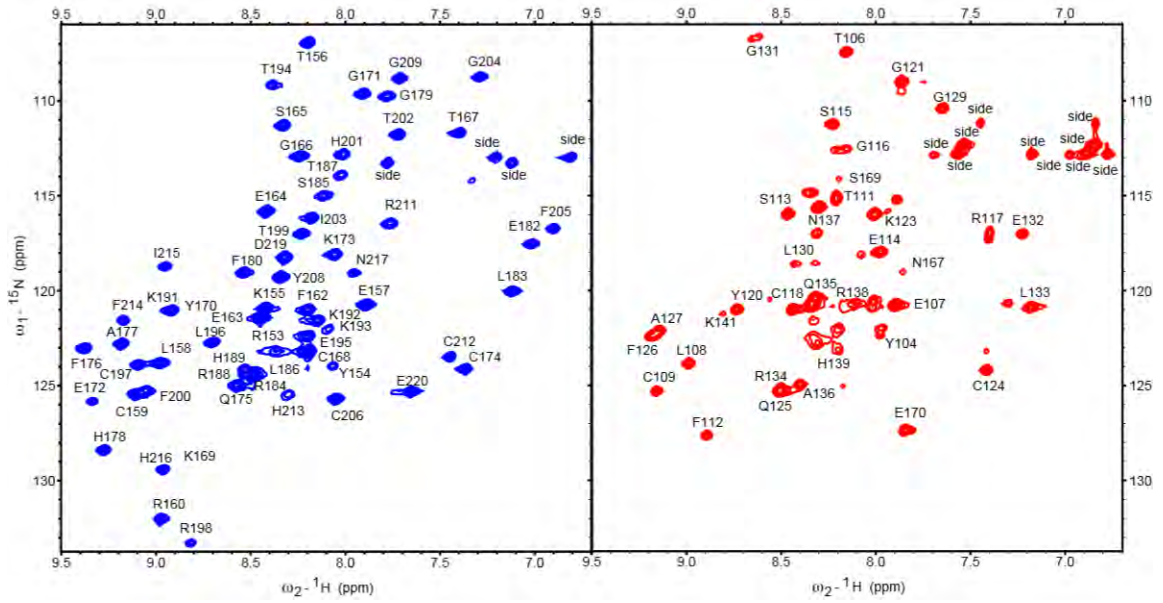
Figure 4. 2. ^{15}N-^{1}H 2D HSQC spectra of TIS11d and TTP. ^{15}N-^{1}H HSQC spectra of TIS11d and TTP are shown in blue and red, respectively. The resonance assignments are indicated on each spectrum.
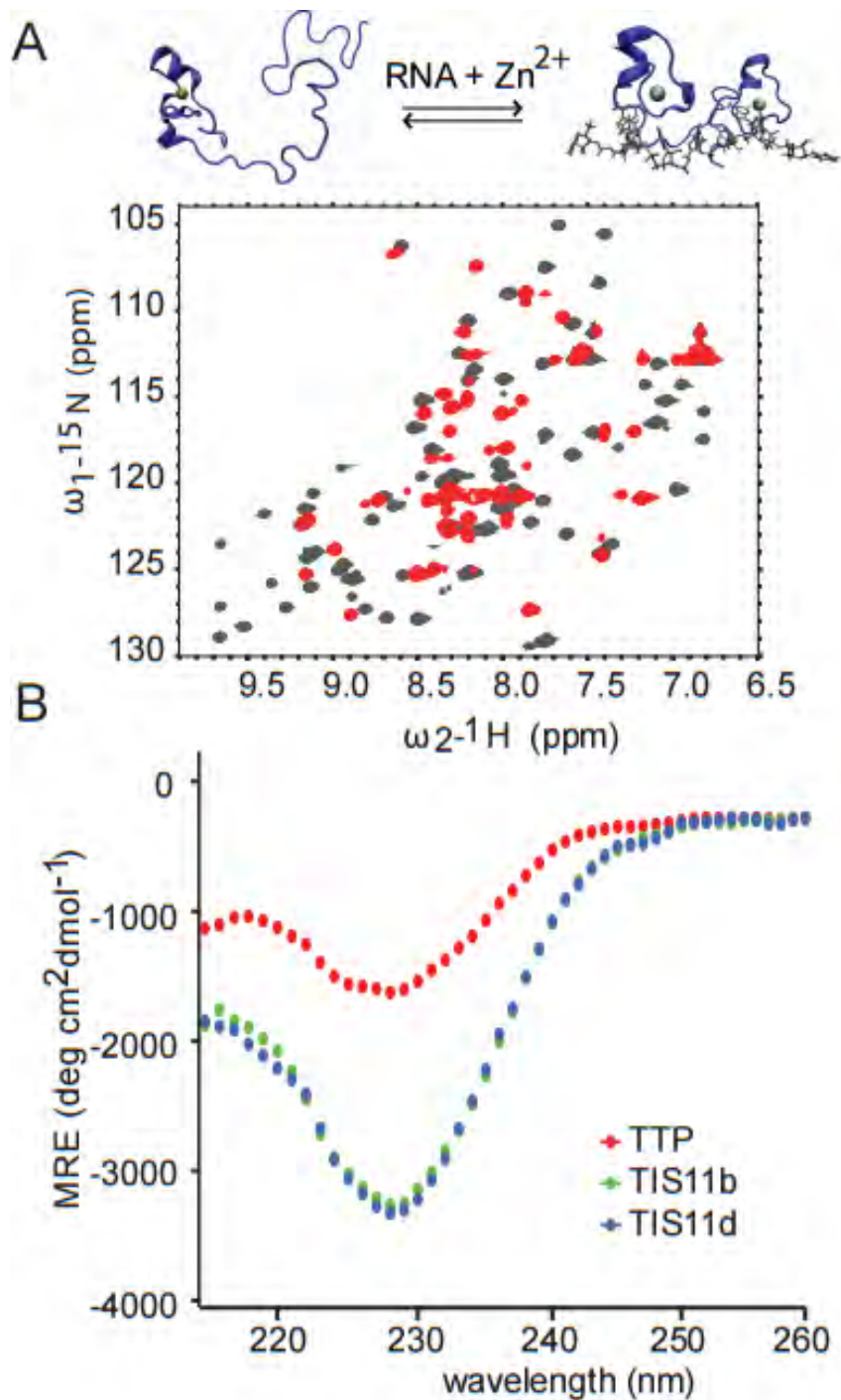
Figure 4.3. In TTP ZF2 is unstructured in the unbound state but folds upon RNA-binding. a) ^{15}N-^{1}H HSQC spectra of RNA free (red)/RNA bound TTP (gray). New cross-peaks, corresponding to residues of the linker and ZF2 of TTP, appear upon addition of RNA. The structural transition occurring upon RNA-binding is depicted on top. The 3D structure of TTP was modeled from that of TIS11d (PDB id: 1RGO)[19]. b) Far-UV circular dichroism (CD) spectra of TTP (red), TIS11d (blue) and TIS11b (green). The CD spectra of TIS11b and TIS11d are almost entirely overlapped.

96

Due to chemical exchange line broadening, cross-peaks from ZF2 are absent in the ^{15}N-^{1}H HSQC spectrum of TTP, thus no structural information can be determined for this part of the domain using NMR spectroscopy. In order to test the hypothesis that ZF2 is in a molten globule state, we used several experimental approaches, including mutagenesis, CD spectroscopy and metal analysis, where we estimated the $[Zn^{2+}]/[TZF]$ ratio for both TTP and TIS11d.
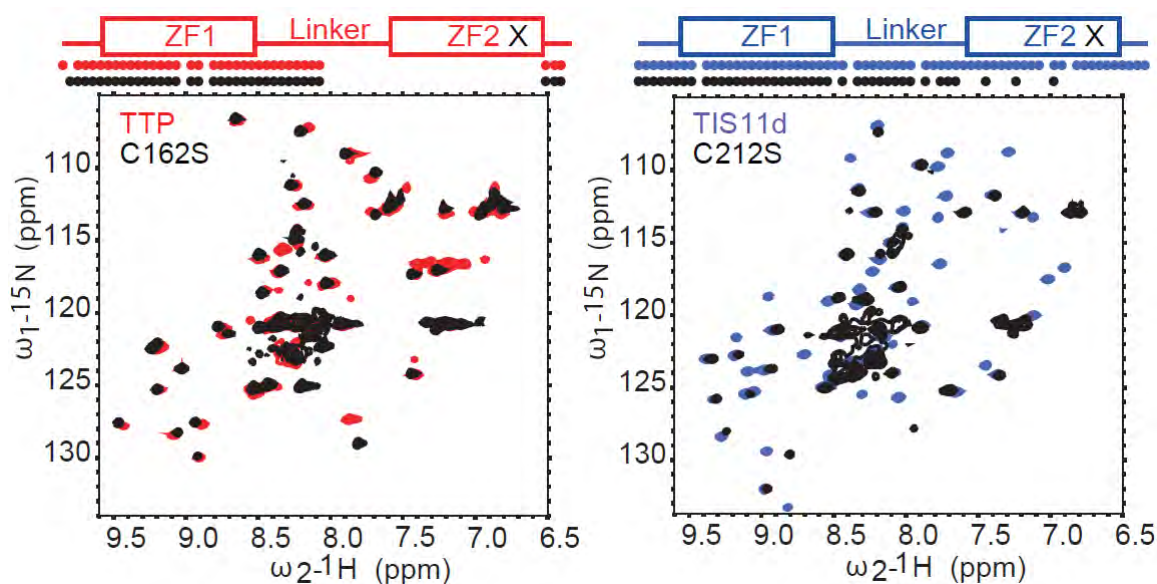
Figure 4.4. ^{15}N-^{1}H HSQC spectra of TTP, C162S TTP mutant, TIS11d and C212S TIS11d mutant.
Left: Overlay of ^{15}N-^{1}H HSQC spectra of TTP (red) and C162S TTP mutant (black), whose C-terminal ZF cannot fold due to a missing Zn-coordinating Cys residue. **Right:** Overlay of ^{15}N-^{1}H HSQC spectra of TIS11d (blue) and C212S TIS11d mutant (black), whose C-terminal ZF cannot fold due to a missing Zn-coordinating Cys residue shows that only the N-terminal ZF of the mutant protein adopts a stable fold. On top, a schematic representation of the TZF domain shows the zinc fingers as rectangles and the linker as line. The black X is representative of the cysteine zinc coordinating residue that is mutated in this experiment. The dots indicate residues along the sequence with a cross-peak in the ^{15}N-^{1}H HSQC spectrum.

NMR spectroscopy was used to determine the effect of a single point mutation, the third zinc-coordinating Cys to Ser, on the structure of TTP and TIS11d: C162S and C212S in TTP and TIS11d, respectively. These mutant proteins are lacking one of the

zinc-coordinating Cys residues in ZF2, thus ZF2 cannot stably bind Zn^{2+} and fold (Figure 4.4). The ^{15}N-^{1}H HSQC spectra of wild-type (WT) TTP and C162S mutant TTP are nearly identical (Figure 4.4), with the exception of a few cross-peaks originating from presence of four extra residues at the C-terminus of the C162S mutant construct used. The ^{15}N-^{1}H HSQC spectrum of C212S TIS11d resembles that of wild-type TTP, as cross-peaks from the unstructured ZF2 are missing (Figure 4.4). These results support the hypothesis that in the absence of RNA, ZF2 of TTP cannot stably bind Zn^{2+}. As a result, ZF2 of TTP samples many partially structured states on a time-scale that is intermediate relative to the chemical shift differences, thus cross-peaks from ZF2 are broadened beyond detection[24]. In addition, these mutant proteins showed that in both TTP and TIS11d, ZF1 can independently adopt a stable fold when ZF2 is unfolded (Figure 4.4).

The CD spectra of TTP, TIS11b and TIS11d show that the TZF domain of TTP is less structured than that of TIS11d and TIS11b, as evidenced by the difference in CD signal peak intensities between 220-240 nm (Fig. 4.3B). In addition, Zn^{2+} titrations of TIS11d and TTP, monitored by CD spectroscopy, show that TIS11d coordinates two equivalents of Zn^{2+}, one ion for each finger. TTP, however, only coordinates one zinc cation, indicating that ZF2 is disordered in solution (Figure 4.5). The same result was obtained when the $[Zn^{2+}]/$ $[TZF]$ ratio was determined for both TTP and TIS11d using inductively coupled plasma-optical emission spectrometry (ICP-OES), $[Zn^{2+}]/[TIS11d] = 1.8 \pm 0.1$ and $[Zn^{2+}]/[TTP] = 1.1 \pm 0.1$.
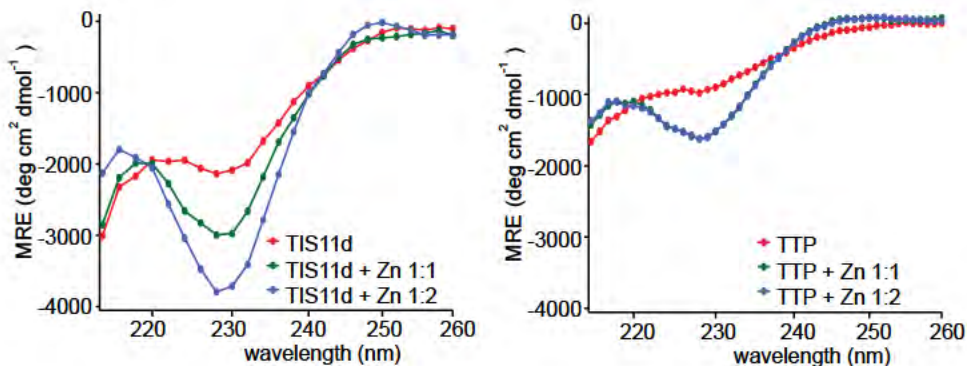
Figure 4.5. CD spectra of TIS11d and TTP at different concentration of Zn^{2+}. Far-UV circular dichroism (CD) spectra of TIS11d (left) and TTP (right) collected with different amounts of Zn^{2+}. The three spectra are collected at different values of the concentration ratio $[Zn2^+]/[TZF]$: 0 (red), 1 (green) and 2 (blue).

Taken together, these findings demonstrate that only the N-terminal ZF, ZF1, of TTP adopts a stable fold in the unbound state, and that RNA binding, in the presence of Zn^{2+}, induces the folding of ZF2. While TIS11d is fully folded, TTP is partially unfolded and requires RNA-binding to promote a transition to a fully folded state. Therefore, RNA recognition by TTP is achieved through an RNA-dependent conformational adaptation of the TZF domain.

The affinity for Zn^{2+} of different types of zinc fingers is known to differ over a range that spans about 7 orders of magnitude, with zinc fingers coordinating the zinc cation with four cysteine residues (Cys_4-type) binding Zn^{2+} with the highest affinity[169,170]. In an attempt to increase the affinity of TTP ZF2 for Zn^{2+} the last Zn^{2+} - coordinating residue of ZF2 was mutated from a His (His 166) to a Cys, to make it into a Cys_4-type zinc finger. The ^{15}N-^1H HSQC spectrum of the mutated TZF domain was still missing all the cross-peaks from the C-terminal half of the domain, as in the WT, suggesting that the mutated ZF2 (now Cys_4-type) is still unable to stably bind Zn^{2+}. This result is not

surprising considering that engineered zinc fingers constructed from the same amino acid sequence except for the Zn^{2+} coordinating residues (Cys_4, Cys_3His and Cys_2His_2 were tested) have similar affinity for Zn^{2+}[169,171]. These and our results indicate that differences in Zn^{2+} binding affinity arise not primarily from the particular atoms that coordinate the Zn^{2+}, the first solvation shell, but mostly from the second coordination sphere[27]. Thus, the particular primary, secondary and tertiary structures of a protein determine the affinity for Zn^{2+} of the zinc finger.

The predicted secondary structure for ZF1 of TTP is the same as that observed for ZF1 of TIS11d.

Small backbone chemical shift differences are observed for ZF1 and the linker of TTP and TIS11d, suggesting that ZF1 of these two proteins have similar structures (Figure 4.6). This is not surprising since ZF1 of TTP and TIS11d (159-179 TIS11d/109-129 TTP) share 81.5% sequence identity. To support this conclusion, the backbone resonances of TTP ($C\alpha$, $C\beta$, CO, N, and H^N) were used to predict the secondary structure elements of ZF1 using δ2D software[172,173]. The predicted secondary elements are the same as those observed in the solution NMR structure for TIS11d. To understand how the primary sequence of ZF1 affects the observed chemical shifts, the residues that differ between TIS11d and TTP were mutated in TIS11d and chemical shift perturbations were calculated (Figure 4.6). From this data we determined that many differences observed between the spectra of TTP and TIS11d ZF1 arise from the identity of one residue, P161 in TIS11d and T111 in TTP. In TIS11d, this proline is in a short α-helix (residues 160-

165) located between the first two zinc coordinating cysteine residues of the first finger. Mutation of residue P161 to T in TIS11d alone can capture many of the differences observed between the spectra of TIS11d and TTP and recapitulate most of the changes observed in the ^{15}N-^{1}H HSQC spectrum when we mutated all the residues of TIS11d ZF1 to those found in TTP (P161T, E163S, T167R, K169R, E172A), Figure 4.6. In TIS11d, F162 forms a hydrogen bond with the side chain of C159 that stabilizes the conformation of ZF1. We hypothesize that mutation of the preceding residue, P161T, affects the conformation of F162 and the hydrogen bond that it forms with C159, thus affecting the structure of many residues in ZF1 and their chemical shifts.
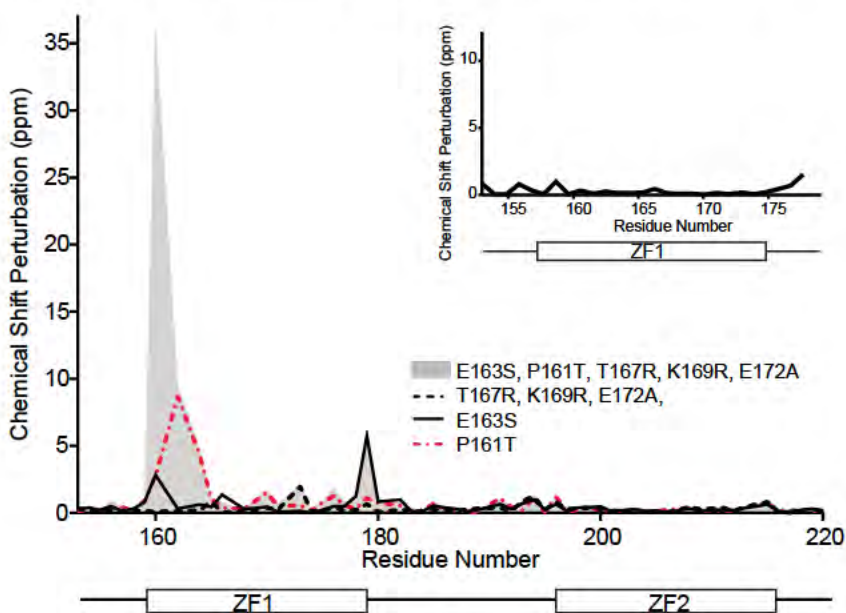
Figure 4.6. Chemical shift perturbation of TIS11d mutant proteins. The chemical shift difference between WT TIS11d and different mutant proteins containing one or more single point mutations in ZF1 is plotted as a function of residue number. All mutations transform WT residues in TIS11d to the corresponding residue in TTP. The largest differences in chemical shifts are observed upon mutation of P161 to the corresponding residue in TTP (T111). The inset shows the chemical shift difference observed between TTP and the mutant protein of TIS11d where we mutated all the residues of TIS11d ZF1 to those found in TTP (P161T, E163S, T167R, K169R, E172A). A schematic representation of the TZF domain that shows the zinc fingers as rectangles and the linker as line is depicted below the x-axis.

Identifying the origin of the difference in structures of TTP and TIS11d using

chimeras.

Many of the residues that differ between the TZF motif of TTP and TIS11d span the

length of the motif, thus it is not easy to identify the residues that stabilize the structure of

ZF2 from a simple analysis of the primary sequence. For this reason, chimeric proteins

were constructed by combining the linker and/or zinc fingers of TTP and TIS11d to

identify the role that different residues have in determining the structure of the zinc

fingers (Figure 4.7). Folding of each chimera was monitored using NMR spectroscopy to

detect structural changes from the wild-type proteins with residue resolution. The absence

of N-H^N cross peaks for the residues of ZF2 and part of the linker from the ^{15}N-^{1}H HSQC

spectrum, due to intermediate exchange line broadening, is an indication of lack of

structure or partial folding of ZF2 (Figure 4.7). From the data we can conclude that

switching the linkers of TTP and TIS11d does not affect the structure of ZF2. However,

the primary sequence of ZF2 affects its structure. Replacing the primary sequence of ZF2

of TTP with that of TIS11d increases the number of resonance peaks observed in the

spectrum, with these cross-peaks corresponding to the C-terminal half of the domain that

now folds into a stable structure. The converse is also true: changing the primary

sequence of TIS11d ZF2 into that of TTP increases the propensity for intrinsic disorder of

the chimera, and cross peaks from ZF2 are broadened beyond detection in the ^{15}N-^{1}H

HSQC spectrum. Altogether, these findings show that the primary sequence of ZF2 alone

determines its structure or lack thereof.
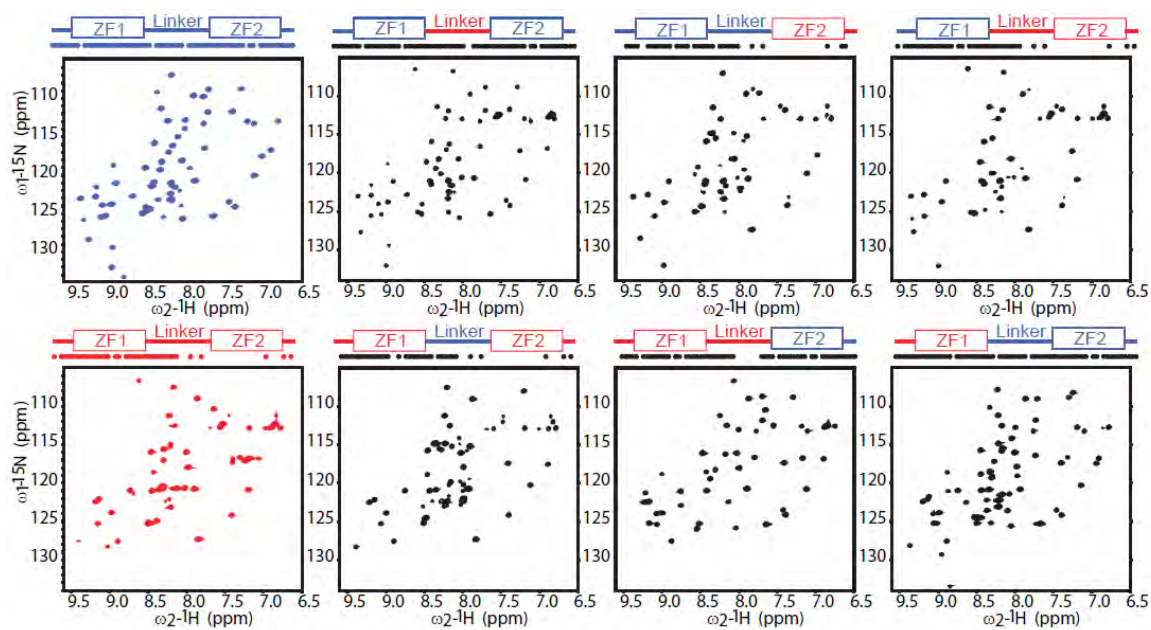
Figure 4.7. ¹H-¹⁵N HSQC spectra of TTP/TIS11d chimeras. Backbone amide cross peaks represented for TTP (red), TIS11d (blue), and chimeras (black). A schematic representation of the TZF domain (amino acid sequences from TIS11d and TTP shown in blue and red, respectively) and the residues that have a cross-peak in the ¹⁵N-¹H HSQC (represented by dots) is depicted on top of each spectrum. Lack of amide cross peaks is due to chemical exchange process that is intermediate on the chemical shift time scale resulting from the flexibility of the unstructured ZF2.

All TTP/TIS11d chimeras bind to the ARE13 sequence with similar affinities.

To determine if the chimeras retain RNA binding activity, we determined the equilibrium dissociation constant of each chimera using fluorescent electrophoretic mobility shift assays[174]. All of the chimeras bind to a model ARE sequence (ARE13: 5′-UUUUAUUUAUUUU-3′) with similar affinity, indicating that the folded/unfolded character of the second zinc finger does not strongly affect the RNA binding activity of the protein, Table 4.1. Analysis of the primary sequence shows that TTP has a net charge of 8.2, while TIS11d has a net charge of 3.3 at pH 7 (Innovagens - peptide properties

calculator, http://www.innovagen.com/custom-peptide-synthesis/peptide-property-calculator/peptide-property-calculator-notes.asp). The more basic nature of TTP may result in enhanced attractive Coulomb interaction with the RNA and a more favorable enthalpy of binding thus compensating for the entropic penalty associated to folding of ZF2 upon RNA binding. This entropy-enthalpy compensation in the free energy of RNA-binding was observed for TIS11d and a mutant of TIS11d where residues D219 and E220 were deleted, thus changing the total net charge of the TZF domain[175].

Table 4.1. Table of the RNA binding activity of TTP/TIS11d chimeras. Electrophoretic mobility shift assays (EMSA) with labeled ARE13 were used to determine the RNA binding activity of each chimera, all chimeras are active. Each of the chimera is made by fusing ZF1, the linker, or ZF2 from either TTP (red) or TIS11d (blue). Left is a representative gel shift for TIS11d binding to ARE13.
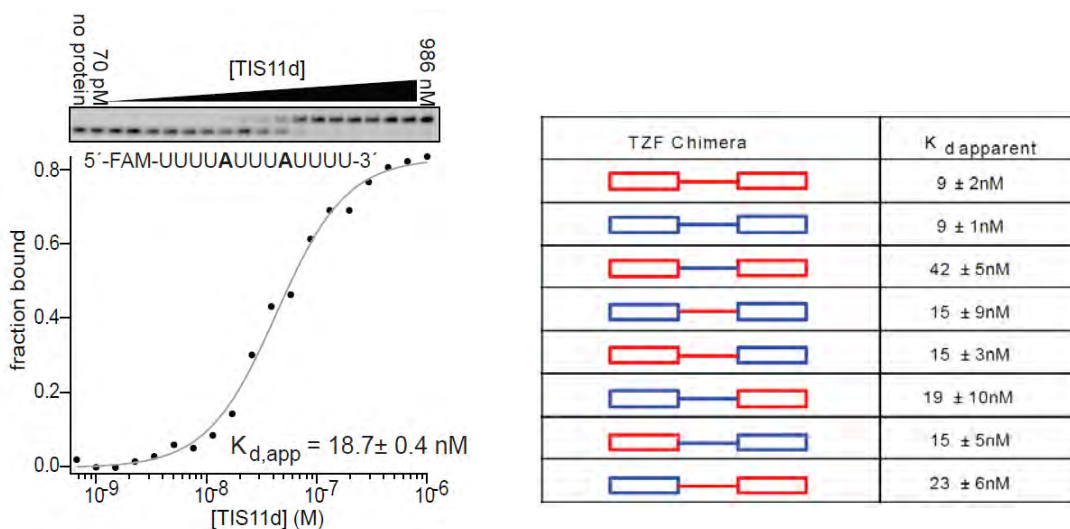
Understanding how the amino acid composition of ZF2 determines the unfolded/folded character of the zinc finger.

We found that the primary sequence of ZF2 determines the structure of ZF2. In order to dissect what accounts for a stably folded ZF2, we made mutations within the second zinc finger where residues of TIS11d were mutated to the equivalent residues in

TTP (Figure 4.8 and Figure 4.9). Most of the differences in amino acid sequence between TTP and TIS11d ZF2 are observed in the region that is helical in TIS11d[117] (Figure 4.1). Mutation of the residues of this region of TTP (residues 148-155) into those of TIS11d (residues 198-205) results in the presence of cross-peaks from ZF2 and the second half of the linker in the ^{15}N-^1H HSQC spectrum, indicating that ZF2 is now stably folded (Figure 4.8, top). Furthermore, mutation of the residues in the second half of the α-helix of TIS11d (residues H201, T202 and I203) to those of TTP (residues Y151, L152, Q153) results in loss of signal from almost all residues of ZF2 and the second part of the linker (Figure 4.8, bottom), indicating loss of structure in ZF2. Mutating the first two residues of the α-helix (R198 and T199) of TIS11d to those of TTP does not affect the structure of ZF2 (Figure 4.9). There are two other residues that are different between ZF2 of TIS11d and TTP (Figure 4.1): F205 and P210. Mutation of F205 to R and of P210 to S in TIS11d did not change the structure of the finger indicating that these two residues do not affect the stability of ZF2 (Figure 4.9).

Figure 4.8. Helicity differences are responsible for the difference in fold observed for TTP and TIS11d. (Top) Overlay of the ^{1}H-^{15}N HSQC spectrum of WT TTP (red) with that of the mutant protein containing the TIS11d amino acid sequence at the α-helical region of ZF2, residues 148-153, (black). (Bottom) Overlay of the ^{1}H-^{15}N HSQC spectrum of WT TIS11d (blue) with that of the mutant protein containing the TTP amino acid sequence at the second half of the α-helical region of ZF2, residues 200-203, (black). On top, a schematic representation of the TZF domain shows the zinc fingers as rectangles and the linker as line. The dots indicate residues along the sequence with a cross-peak in the ^{1}H-^{15}N HSQC spectrum.
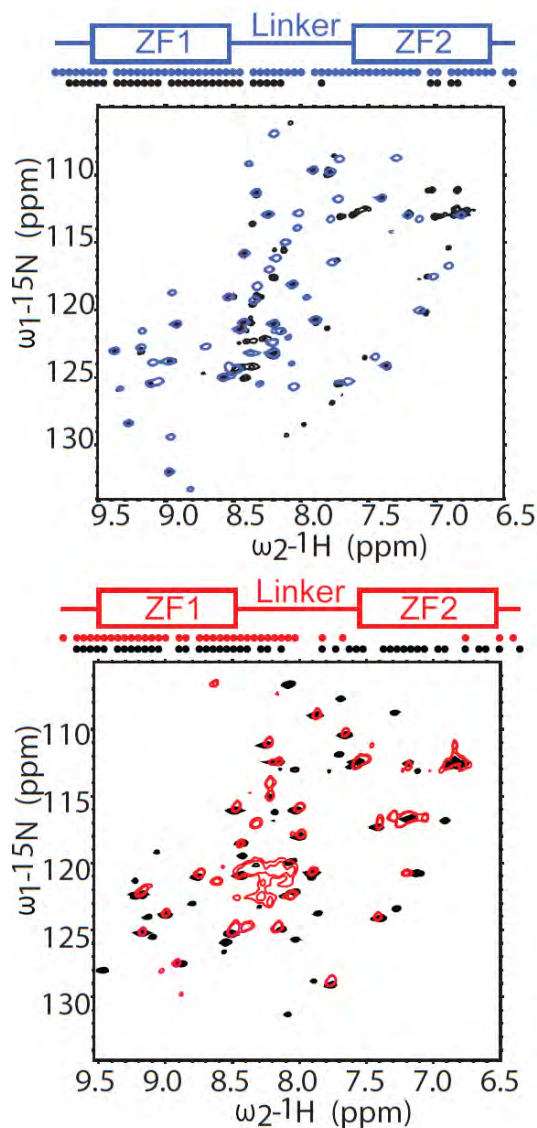
We also investigated how the C-terminal tail of the TZF domain (Figure 4.1) affects the overall stability of ZF2. Previous experimental and molecular dynamics (MD)

studies of TIS11d have shown how the two conserved negatively charged residues flanking ZF2 (D219 and E220) contribute to the stabilization of the TZF structure through their electrostatic interaction with the positively charged residues of the linker and that disruption of these interactions results in a more flexible but still folded ZF2[175,176]. Here we show that mutation of A218 and D219 in TIS11d to the corresponding residues of TTP (P168 and S169, respectively) result in the disappearance of a few cross-peaks in the linker (188-189) and in ZF2 (216-219), Figure4.9. In agreement with our previous studies[117,176], this result indicates that the residues of the C-terminal tail affect the dynamics of the linker region and those of ZF2 but do not affect its folding.

Figure 4.9. ^{15}N-^{1}H HSQC spectra of TIS11d mutants. The figure shows ^{15}N-^{1}H HSQC spectra of the TIS11d mutants designed to identify the residues important for stabilizing the structure of ZF2. On top of each spectrum the sequence of ZF2 is represented in black. Point mutations to the ZF2 are highlighted in red. The amino acid sequence of WT TIS11d is shown for reference in blue. The residues that have a cross-peak in the HSQC are represented by black dots. Black triangles represent the CCCH zinc coordinating residues.
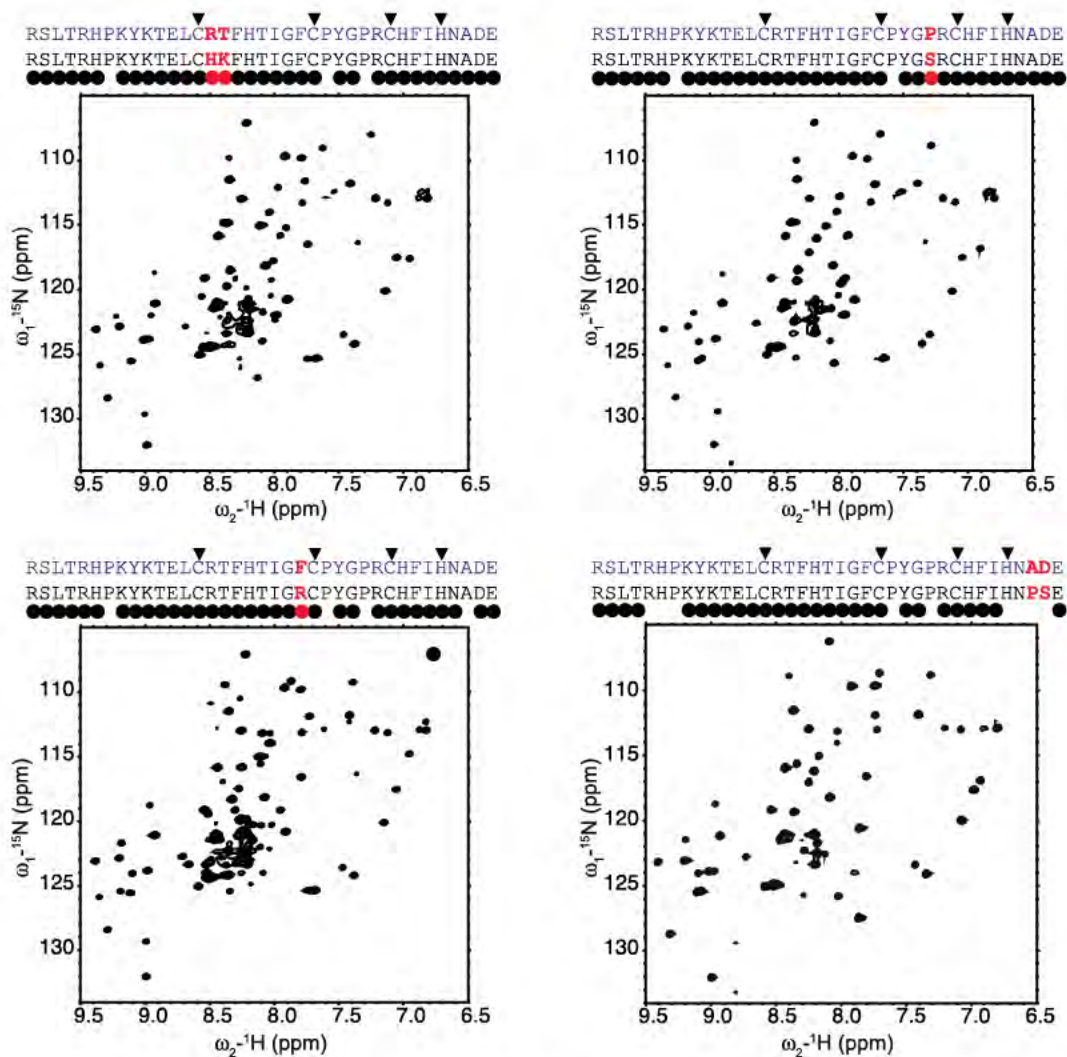
From these experiments, we conclude that the most important region to stabilize the structure of ZF2 comprises residues 151-153 in TTP (residues 201-203 in TIS11d). In TIS11d these three residues are located on the second half of the α-helix between the first two zinc coordinating cysteine residues[117]. Secondary structure prediction (data not

shown) for TTP bound to RNA (ARE13: 5′-UUUUAUUUAUUUU-3′), from the backbone and C_β chemical shifts using $\delta 2D^{173}$ and SPARTA+[177] software, shows that the α-helix between the first two zinc coordinating cysteine residues in ZF2 is shorter in TTP (residues 148-150) than what is observed in TIS11d (residues 198-203). Our experimental results support the recent computational model of TTP bond to RNA bound developed by Blackshear and coworkers[178]. These computational studies suggested that while TIS11d forms two alpha helical turns in this region, TTP only forms one helical turn. Taken together these studies indicate that the ability to form a longer α-helix affects the ability of the finger to stably coordinate the Zn^{2+} ion and fold into a unique structure in the absence of RNA.

Comparative genomics

Comparison of the amino acid sequences of TIS11d and TTP from vertebrates from 100 species[179-182] (Figure 4.10) indicates that the TZF domain of TIS11d is likely always folded, as the three residues of the α-helix that alone stabilize the structure of ZF2 (residues 201-203, HTI) are absolutely conserved. In TTP homologs, however, the corresponding three residues (res. 151-153, YLQ, associated with the disorder of the TZF domain) are only conserved in mammals (Figure 4.10). In fish, reptiles, amphibians and birds these three residues are the same as in TIS11d, thus, from our studies (Figure 4.8), we predict that ZF2 is folded in these vertebrates. Comparative genomics suggests that TTP has evolved more recently in mammals to modulate its folding through Zn^{2+} and RNA binding. In addition, we observed that the presence of the HTI amino acids, which stabilize the structure of ZF2 (Figure 4.8), correlates with the presence of two acidic

amino acid residues at the tail of the TZF domain (Figure 4.10). Our previous studies have shown that these two acidic residues are important to stabilize the structure of the folded TZF domain of TIS11d in an RNA-binding competent state[117]. These data suggest that they are not conserved when ZF2 is unstructured.
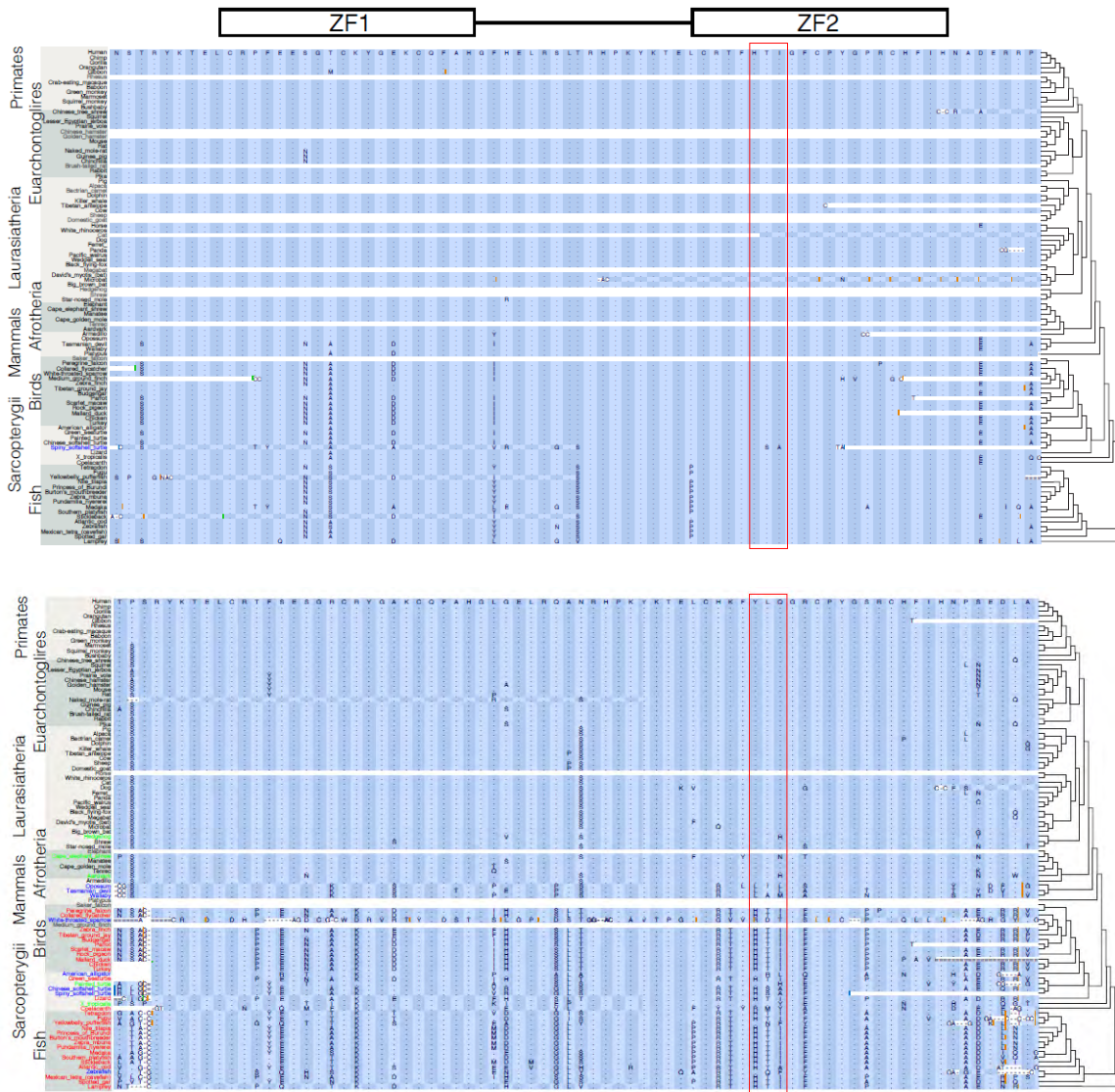
Figure 4.10. Sequence alignment of the TZF domain of TIS11d and TTP. Sequence alignment of the TZF domain of TIS11d (top) and TTP (bottom) taken from 100 vertebrate species. The alignment was generated from the Genome browser (http://genome.ucsc.edu/). The three residues located at the C-terminal half of the α-helix of ZF2, that alone determine the structure or lack of structure of ZF2, are highlighted by a red box. Additional residues flanking the TZF domain that are important for stabilizing TIS11d ZF2 are shown in red. A schematic representation of the TZF domain depicting the zinc fingers as rectangles and the linker as line is shown on top.

Determining the effect of the structure of the TZF domain on the cellular activity of TTP.

To determine whether the structure of the TZF domain of TTP affects its mRNA destabilizing activity in cells, we employed a reporter assay where luciferase was placed under the control of the TNFα 3′UTR. HEK293 cells (which do not express TTP constitutively) were co-transfected with a plasmid containing full length TTP or chimeric variants and a plasmid encoding both Renilla and firefly luciferase. The Renilla luciferase gene was fused to the 3′UTR sequence of TNFα, while the firefly luciferase was fused to a control vector 3′UTR. The ratio of Renilla to firefly luciferase reveals TTP variant activity normalized by transfection efficiency. Differences in luciferase activity observed between cells that expressed wild-type TTP or TTP$_{TZF\_TIS11d}$ fusion protein, where the TZF domain of TTP has been replaced with that of TIS11d, assess the degree to which intrinsic disorder of the TZF domain affects the regulatory activity of the protein. The TTP$_{TZF\_TIS11d}$ fusion protein, which has a stably folded ZF2, led to a two-fold reduction in luciferase activity compared to wild-type TTP (Figure 4.11). Having a structured ZF2 decreased the expression of the protein in cells (decreased luciferase activity), therefore, the TTP$_{TZF\_TIS11d}$ fusion protein has higher activity than WT TTP (Figure 4.11). As expected, high luciferase activity was observed when the cells were transfected with a plasmid containing the mutant protein C162S of TTP, where the third zinc-coordinating cysteine has been mutated to a serine in ZF2 and thus cannot fold even in the presence of RNA (Figure 4.11). Although we expected C162S TTP to be completely inactive, a residual mRNA destabilizing activity was observed for this mutant protein. This residual

activity has been previously observed,[183] suggesting that mutation of the zinc-coordinating residues in ZF1 might be necessary to completely inactivate the protein. Together, the results show that the mRNA destabilizing activity of TTP in the cell is affected by the structure of ZF2 in the RNA binding domain, and increasing the structure of the TZF domain of TTP increases the RNA-destabilizing activity of the protein in the cell.
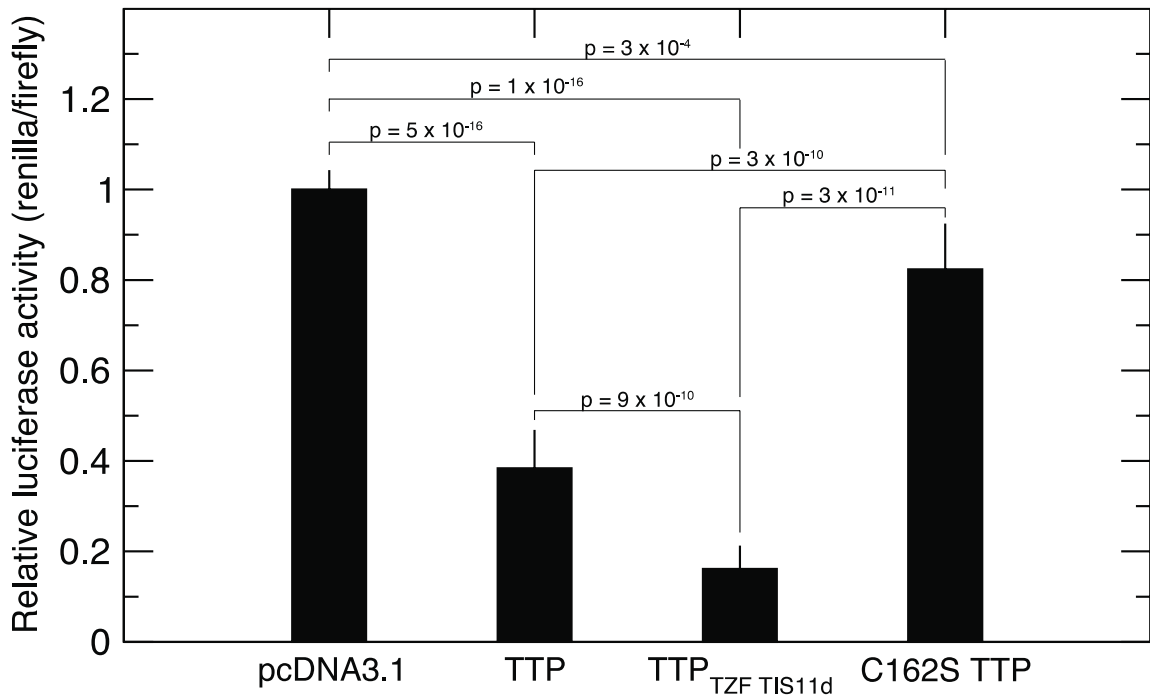
Figure 4.11. Measurements of the cellular activity of TTP and TTP/TIS11d chimeras. The structure of the TZF domain of TTP affects the mRNA destabilizing activity of TTP in HEK293 cells. The plot shows the relative luciferase activity measured for HEK cells incubated for 48 hours with empty pcDNA3.1HISC plasmid, WT TTP, TTP chimera (TTP containing the TZF domain of TIS11d, TTP$_{TZF\ TIS11d}$), and TTP C162S mutation.

There are several possible explanations for this observation. 1) Disorder in the TFZ domain may trigger TTP degradation, lowering its cytoplasmic concentration[184]. 2) The cytoplasmic concentration of TTP may also be decreased by an increased import into the nucleus. The nuclear transport protein importin has been shown to bind to the basic

residues R134 and R137 of the linker region of the TZF[185], thus the structure of ZF2 might affect the recognition and transport of TTP into and out of the nucleus. 3) The structure of the TZF domain may affect how the protein interacts with other enzymes of the RNA degradation machinery[124]. 4) A fully structured TZF domain may increase the RNA-binding affinity in cells. Any or all of these explanations may account for the increased cellular activity associated with a fully folded RNA binding domain. Differential folding propensities of ZFs may explain observations of TZF proteins in other species, as well. The CCCH-type TZF domain of the TTP family of protein was first identified in the murine TTP[163], and has since been found in more than 3600 proteins[186]. Analysis of the *C. elegans* genome has revealed the presence of an unusually high number of proteins (16) containing a TZF domain homologous to TTP. Several of these proteins (OMA-1, OMA-2, MEX-5, MEX-6, PIE-1, POS-1 and MEX-1) have a known function as mRNA regulators at the onset and during the early stages of embryogenesis[187]. Experimental evidence indicates that the two zinc fingers of these TZF domains play different functions during embryogenesis[188]. While the N-terminal zinc finger of POS-1, PIE-1 and MEX-1 has been demonstrated to be necessary and sufficient for degradation in somatic blastomeres, the C-terminal zinc finger is necessary and sufficient to target these proteins to P granules, which are germline cytoplasmic structures rich in RNA[45]. These findings suggest that the two fingers in the CCCH-type TZF domain may function independently and that the structure, or lack thereof, of each finger might affect the activity and/or localization of the protein within the cell. This independence may apply to the human TZF domains of the TTP family, thus the

increased propensity for intrinsic disorder of TTP relative to TIS11b and TIS11d may indicate that the proteins have evolved to be able to modulate their activity through their thermodynamic stability.

Summary

In conclusion, our studies reveal 1) that the three residues located in the α-helical region of ZF2 alone determine if the TZF domain is fully or partially folded, 2) that the degree of structure of the TZF domain affects the activity of the protein in the cell and 3) this family of proteins has only recently evolved to be able to regulate its activity through modulation of its folding. It will be interesting to determine whether the structural disorder of the TZF domain affects binding partner recognition in the cell, cellular stability and localization, or all the above.

Methods

Protein expression and purification

The RBD of human TTP (residues 102-170) and TIS11d (residues 152-220) was synthesized by Genscript and cloned into the pet21b vector between Nde1 and Xho1 restriction sites. Chimeras of TTP and TIS11d were generated via Quikchange mutagenesis. TTP, TIS11d and chimeras were expressed within BL21(DE3) *E. coli* competent cells. Isotopic labeling with ^{15}N was performed by growing the cells in M9 enriched with 1 g of ^{15}NH$_4$Cl per liter. Carbon labeling was performed by growing cells in ^{13}C-glucose. The cells were grown at 37° C to an OD$_{600}$ of 0.8 and then induced for 4 hours with 1 mM Isopropyl β-D-1 thiogalactopyranoside (IPTG) and 0.1 mM ZnSO$_4$ at the same temperature. Harvested cells were passed through a cell disrupter in 50 mL lysis

buffer containing 50mM Tris HCl, pH 8.0, 50 mM NaCl, 2 mM dithiothreitol (DTT) and

1 *EDTA free Complete protease inhibitor* tablet (Roche). Lysates were centrifuged at

19500 RPM for 1 hr at 4° C and passed through a 20 mL DEAE column pre-equilibrated

with 50 mM Tris HCl, pH 8.0, 50 mM NaCl and 2 mM DTT. The flow through was

dialyzed overnight in 25 mM sodium phosphate, pH 6.5, 50 mM NaCl and 2 mM DTT

and passed through a *HiTRAP SP* 10mL column (GE healthcare Life Science)

preequilibrated with 25 mM sodium phosphate, pH 6.5, 50 mM NaCl and 2 mM DTT.

The peptides were eluted with a gradient of NaCl from 0-1 M; the peptides typically

eluted at 0.2-0.6 M NaCl. Fractions with peptide were combined and concentrated to 2

mL using a 3 KDa Centriprep (Millipore) and further purified using a 1.6 X 60 cm

Superdex-75 size exclusion column (Amersham Bio\sciences) equilibrated with 50 mM

Tris HCL pH 7, 300 mM NaCl, 2 mM DTT. For NMR analysis fractions with TTP,

TIS11d or chimeras were buffer exchanged into 10 mM Tris pH 6.2, 20 mM KCl, 2 mM

DTT, 0.1 mM $ZnSO_4$. Protein concentrations were determined via Ninhydrin assay.

Measurements of RNA-binding affinity

The RNA-binding activity of the samples was determined using fluorescent

electrophoretic mobility shift assays (EMSA) with fluorescein end labeled RNA as

previously described[4]. Briefly, the affinities of TTP, TIS11d, and chimeras for the

sequence 5′-UUUUAUUUAUUUU-3′ (ARE_{13}) were measured by direct titration of 3 nM

labeled RNA with increasing concentrations of protein. Varying concentrations of the

protein were incubated for 3 hours at room temperature with 2 nM fluorescently labeled

RNA in a buffer solution containing 10 mM TRIS (pH 8), 100 μM Zn(OAc)$_2$, 100 mM

NaCl, 0.01 mg tRNA, 0.01% (v/v) IGEPAL, and 2 mM DTT. After addition of 10 μL of

0.005%(w/v) bromocresol green in 30% glycerol to 100 μL of each sample, 50 μL of

each mixture were loaded onto a 1% agarose, 1Å~TB gel and run for 35 min at 120 V at

room temperature to separate bound from free RNA. To detect the fluorescently labeled

RNA, the gel was imaged using a Fuji FLA-5000 laser imager. The apparent dissociation

constant K$_{d,app}$ was determined by fitting to the quadratic equation[31],

$$f = \frac{m-b}{2R}\left(K_d + P + R - \sqrt{[K_d + P + R]^2 - 4RP}\right) + b,$$

where m and b are the maximum and base signals, K$_d$ is the dissociation constant, and P

and R are the concentrations of protein and labeled RNA in the sample, respectively.

NMR spectroscopy

Three dimensional triple resonance (^{1}H-^{13}C-^{15}N) experiments, including HNCO,

HN(CA)CO, HNCA, HN(CO)CA, HNCACB, and CBCA(CO)NH, were collected at 14.1

T and 298 K to assign the backbone ^{1}H, ^{13}C, and ^{15}N resonances of [U-^{13}C, U-^{15}N] TTP

and TIS11d in 92% H$_2$O/8% D$_2$O buffer solution (10 mM Tris, 20 mM KCl, 2 mM DTT,

0.1 mM ZnSO$_4$ at pH 6.2). Additional 3D ^{15}N edited ^{1}H–^{1}H NOESY and HMQC-

NOESY-HSQC experiments were collected at 14.1 T and 298 K and used to aid in the

backbone resonance assignment of the chimeras.

Folding of each chimera was monitored via NMR spectroscopy. ^{15}N-^{1}H HSQC

spectra were collected at 298 K for each chimera. All NMR triple-resonance and ^{15}N-^{1}H

HSQC experiments were collected on a Varian Inova spectrometer operating at 600 MHz

equipped with a triple-resonance cold probe. The temperature was calibrated using a

sample of 100% methanol. Data processing was performed using NMRPipe [145] and

Sparky software[146].

Sample Preparation for Trace Metal Analysis

The RBD of human TIS11d (residues 152-220) and TTP (residues 102-170) were cloned

into the pHMTC vector between BamHI and HindIII restriction sites. Constructs were

expressed in BL21(DE3) E. coli competent cells. The cells were grown in Luria Broth

(LB) media at 37°C to an OD_{600} of 0.6 and then induced for 3 hours with 1 mM IPTG and

0.1 mM $ZnSO_4$ at the same temperature. Harvested cells were then passed through a cell

disrupter in 50 ml lysis buffer containing 50 mM Tris HCl, pH 8.0, 100 mM NaCl, 100

μM ZnOAc, 2 mM DTT and 1 *EDTA free Complete protease inhibitor* tablet (Roche).

Lysate was centrifuged at 19500 RPM for 1hr at 4°C and passed through a 20 ml

Amylose column pre-equilibrated with wash buffer (50 mM Tris HCl, pH 8.0, 100 mM

NaCl, 100 μM ZnOAc and 2 mM DTT). The column was washed with 10 column

volumes of wash buffer. The protein was eluted with 10 mM Maltose in wash buffer. The

eluent was then placed over a 5 ml Hi TRAP Q column (GE healthcare Life Science) pre-

equilibrated with the same wash buffer used above. The column was washed with 3

column volumes of wash buffer. The protein was eluted with a gradient of NaCl from 0-1

M; the peptides typically eluted at 0.3-0.5 M NaCl. Fractions containing our protein were

combined, concentrated and dialyzed in 50 mM Tris HCl, pH 8.0, 150 mM NaCl, trace

amounts of ZnOAc and 0.1% β-mercaptoethanol (BME), and protein concentrations were

determined by UV absorption. The concentration of Zn^{2+} in the samples was determined using inductively coupled plasma-optical emission spectrometry (ICP-OES) at the Center for Applied Isotope Studies at the University of Georgia.

CD spectroscopy

Far-UV circular dichroism (CD) spectra were recorded for TTP (50 µM) and TIS11d (18 µM) in 50 mM HEPES pH 7.0, 20 mM KCl and 1 mM TCEP using a Jasco-810 spectropolarimeter (Jasco Inc., Easton, MD). Curves were monitored from 200-260 nm in a 0.1 cm path length quartz cuvette using a scan rate of 20 nm min^{-1} and a response time of 8 s. The sample temperature for all CD measurements was maintained at 293 K.

Luciferase reporter assay

The pcDNA3.1 His-C-TTP (TTP) expression construct was kindly given to us by Dr. Seth Brooks[159]. The cDNA for the fusion protein containing the N- and C- terminal domain of TTP and the TZF domain of TIS11d was generated by Genscript and contained flanking EcoR1 restriction sites for subsequent cloning into pcDNA3.1 His-C-TTP. C162S mutant of TTP was generated using Q5-mutagenesis kit (NEB). Luciferase reporter constructs harboring cDNA of TNFα 3′UTR (nucleotides 1,231-1,506) was generated by gblock synthesis (IDT) and was inserted into the psicheck™-2 construct at restriction sites XhoI and NotI.

Human embryonic kidney (HEK) 293 cells were plated at a density of 300,000 cells/well in 6 well plates, with Dulbecco′s Modified Eagle′s Medium (DMEM) containing 100

units/mL penicillin and 100 µg/mL streptomycin and 10% fetal bovine serum (FBS). The

plates were incubated for 24 hours in a humidified 5% CO_2 incubator set at 37° C. When

the cells were 60-70% confluent each well was cotransfected with 0.25 µg

psicheck2_TNFalpha and 0.5 µg of pcDNA3.1-His-C (empty plasmid), pcDNA3.1 TTP,

pcDNA3.1 TTP$_{TZF\_TIS11d}$, or pcDNA3.1 TTP (C162S) using Dharmafect Duo protocol

(Thermo-Scientific). Transfections were performed in triplicate. 48 hours after

transfection, cells were harvested and Luciferase activity was monitored using a Dual-

luciferase Reporter Assay System (Promega) and normalized by the internal control

values given by firefly luciferase. Luciferase activity was monitored in each well 3 times.

Chapter V: Missense mutations in the TZF

of TIS11d affect fold and cellular localization

Abstract

TIS11d is a member of the post transcriptional regulator TTP family whose function is to bind adenine-uracil rich elements in the 3′ UTR of many different cytokine, growth factor, and proto-oncogenes encoding mRNAs to regulate intracellular turnover. Missense mutations of TIS11d have been associated with many different types of leukemias in patients. Here we show that two missense mutations, P190L and D219E, located in the RNA binding domain (RBD) of TIS11d affect its structural flexibility while maintaining RNA binding activity similar to that of wild type TIS11d. However, while in HEK293 cells GFP tagged TIS11d is uniformly distributed in the cytoplasm, P190L and D219E mutants display a markedly distinct phenotype consisting of puncta within the cytoplasm. This result suggests that the increased flexibility of the RBD affects the localization of TIS11d in the cell and plays a role in disease pathogenesis.

Introduction

Cytokines and growth factors function to regulate and maintain normal growth, cellular differentiation and development, and tissue homeostasis[189]. Misregulation of cytokines can lead to development of autoimmune diseases and cancer pathogenesis[190]. Therefore, growth factors and cytokines and their respective signaling pathways are tightly regulated at the transcriptional and post-transcriptional level.

Several transcripts encoding immune proteins contain A-U-rich elements (AREs) in their 3′ untraslated regions (UTRs)[191]. One protein that binds to AREs is tristetraprolin

(TTP), the prototype of the CCCH-type zinc finger family of proteins, to promote

degradation of the transcript. This process provides an important mechanism for

reducing the synthesis of key cytokines, such as tumor necrosis factor (TNF) -α and

granulocyte-macrophage colony stimulating factor (GM-CSF)[75,121]. In humans, the TTP

protein family has two other members, TIS11b and TIS11d. The RNA binding domain

(RBD) of TIS11b and TIS11d consists of two CCCH zinc fingers (ZFs) that share a high

degree of sequence identity to TTP (71%) and have TTP-like activity, yet neither TIS11b

nor TIS11d can replace TTP function in TTP knockout mice, indicating that they are not

functionally equivalent to TTP[140]. To date, the biological functions of TIS11d and

TIS11b are not fully defined.

Mutations in the TTP family that result in cancerous phenotypes in humans,

suggesting their role in controlling proto-oncogenic mRNAs[192]. Breast and prostate

cancers are characterized by their inability to express the protein TTP[74]. Misregulation of

identified TTP - regulated transcripts, such as *FOS*, *MYC*, and *COX-2,* results in

uncontrolled cell proliferation, insensitivity to pro-apoptotic stimuli, and

angiogenesis[84,85,193,194]. Recent mice knockout experiments determine that TIS11b/d are

required for proper thymocyte development and, when depleted, result in T-

lymphoblastic leukemia[104]. Leukemia in these mice is associated with overexpression of

the transmembrane protein Notch1, which acts as an oncogenic transcription factor as it

controls many cell fate pathways[104]. Further work is required to understand the TTP

family's role in the early stages of cancer pathogenesis. The study herein focuses on two

missense mutations, P190L and D219E, located in the RNA binding domain (RBD) of

TIS11d that are found in patients tissues with acute myeloid leukemia and acute

lymphoblastic leukemia, respectively[103]. Despite the critical role that TTP proteins play

in controlling normal homeostasis of the cell, little is understood of how missense

mutations in the RBD lead to disease. To understand how these mutations affect the

biological function of TIS11d, we used NMR and biochemical assays to characterize the

structure and RNA binding activity of the RDB, and we collected fluorescence confocal

images to determine the subcellular distribution. We observe that the mutations affect the

structure and dynamics of the RDB and cause mislocalization of the protein in the cell

that might interfere with its normal function and lead to pathogenesis.

Results

TIS11d missense mutations show ZF2 structural flexibility by NMR.

In 2004 Wright and coworkers determined the structure of TIS11d when bound to

the single stranded RNA sequence 5′-UUAUUUAUU-3′ (PDB code:1RGO) using NMR

spectroscopy[127]. This structure depicts two folded zinc fingers where the zinc ions are

coordinated by residues C159, C168, C174, and H178 in the first finger (ZF1) and C197,

C206, C212, and H216 in the second finger (ZF2), respectively. The protein-RNA

complex shows that the structure of the tandem zinc finger (TZF) domain of TIS11d is

rather symmetrical, in that both ZF1 and ZF2 contain a short α helix (spanning residues

160-165 in the first finger and 198-203 in the second finger) sandwiched between the first

two zinc coordinating cysteine residues[130]. Additionally, both fingers contain a 3_{10}-helix

between the second and third cysteine coordinating resides (amino acids 171-173 in the first finger and 209-211 in the second finger). The two zinc fingers are held together by a flexible linker whose only form of secondary structure element is a 3_{10}-helix at residues 179-183 and is involved in forming a small hydrophobic cluster with residues of the first finger. NMR and computational studies have shown that in the absence of RNA, the structure of the two zinc fingers of TIS11d is maintained although their orientation changes, as the linker region is highly flexible[128]. We sought to understand how these missense mutations affect the fold and of TIS11d using NMR spectroscopy.
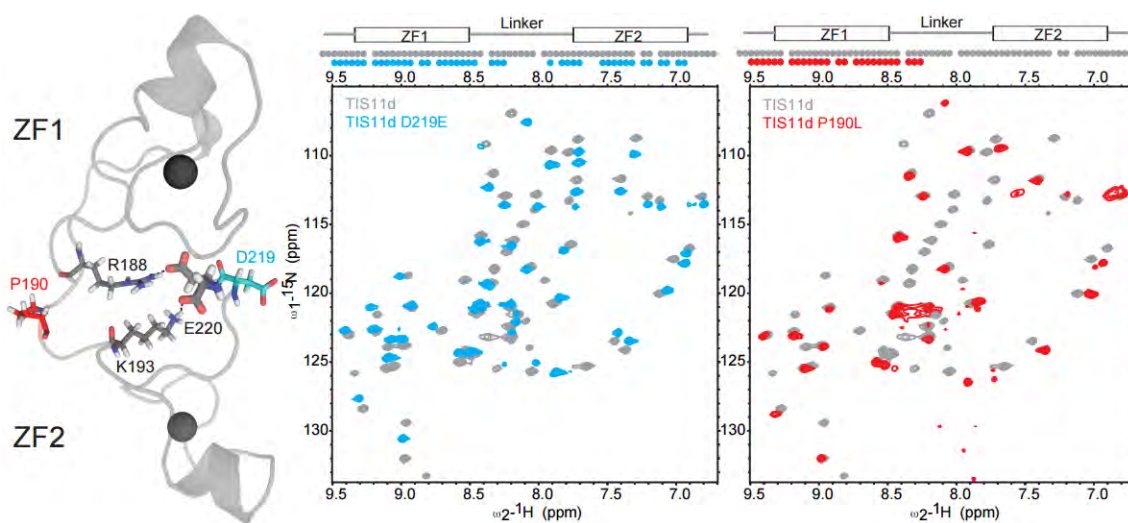
Figure 5.1: Overlay of 1H-15N HSQC spectra of TIS11d and TIS11d missense mutations that cause leukemia. The position of P190 (red) and D219 (cyan) are depicted in a conformation of TIS11d taken from an MD trajectory of TIS11d in the free state. Residues R188 and K193 that participate in the hydrogen bonding network with E220 are shown in gray. ^{15}N-^{1}H HSQC spectra overlays of TIS11d with P190L (right spectrum) and D219E (left spectrum) show the loss of cross-peaks from ZF2, as indicated by the cartoon above each ^{15}N-^{1}H HSQC. The dots indicate residues along the sequence with a cross-peak in the ^{15}N-^{1}H HSQC spectrum.

The ^{15}N-^{1}H HSQC spectrum of the P190L and D219E mutations of TIS11d are missing cross-peaks from the linker and ZF2 indicating that these regions sample multiple states and as a consequence cross-peaks are broadened beyond detection (Figure

5.1). P190L mutation gave a much more pronounced change in the ^{15}N-^{1}H HSQC spectrum as all peaks from the linker and ZF2 are missing in the ^{15}N-^{1}H HSQC spectrum. Previous MD simulation work performed in our lab of wild type (WT) TIS11d showed that removal of RNA results in formation of hydrogen bonds between ZF1 and ZF2 and the C-terminal tail and linker, specifically E220 of ZF2 with K193 and R198 of the linker. Additionally, NMR and MD simulation studies of the mutants TIS11d-E220A and TIS11d-ΔD219/E220 (where D219 and E220 were deleted) showed that both mutations increased the flexibility of the linker region indicating that these two negative residues contribute to the overall stability of the structure of TIS11d TZF domain[151,195]. It is our hypothesis then that the P190L and D219E mutations disrupt the hydrogen bond network between ZF2 and the linker region resulting in more flexible, less structured domain. All together this data suggests that the stability of TIS11d ZF2 is necessary for normal cell growth and proliferation, and when it is mutationally disrupted it results in cancerous phenotypes.

Secondary structural of WT TIS11d, and D219E and P190L mutations.

To determine whether the secondary structure of ZF2 is perturbed by the D219E TIS11d mutation, we used circular dichroism (CD) spectroscopy. Unlike most proteins which give a signature CD spectra with minimum at 190 nm for random coil, 215 nm for beta sheet, and double minima at 205 and 225 nm for alpha helical structures, the TIS11d protein displays a small minimum at 220-240 nm which is indicative of aromatic stacking interactions associated with the minimal secondary structure observed for TIS11d[130]. D219E, however, does not have such a severe effect in secondary structure by CD only

indicates loss of peaks of the linker and ZF2 in the ^{15}N-^{1}H HSQC spectrum (Figure 2). Future work will focus on characterizing the secondary structural elements present in the P190L mutation, which has been shown to contain less structure than WT TIS11d as suggested by NMR analysis. These finding demonstrate that the accurate fold of TIS11d ZF2 is essential for its normal activity. Mutations that influence structural flexibility, such as D219E are found in leukemias genetically linked to human patients.
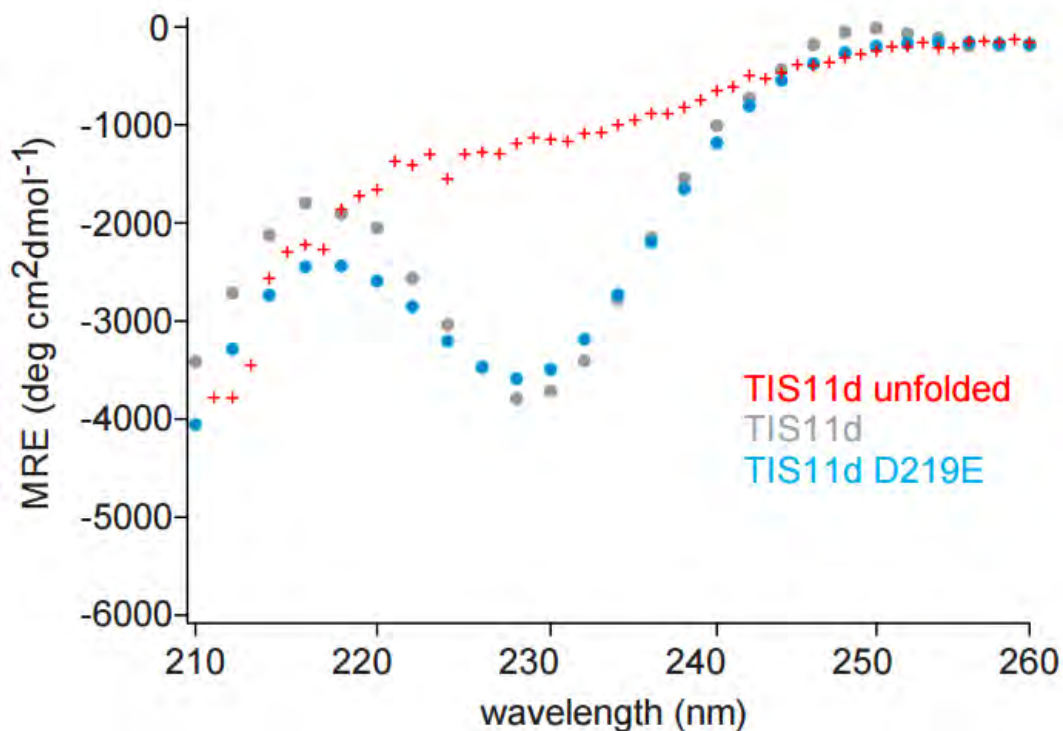
Figure 5.2: Structural studies of D219E mutant of TIS11d. CD spectra of TIS11d wild type (gray), D219E (cyan) and unfolded TIS11d (red).

RNA binding activity of WT TIS11d, and mutants P190L and D219E are similar despite increased structural flexibility at ZF2

We expected that disrupting the fold of the TZF would result in loss of RNA binding activity to the cognate RNA sequence, UUUUAUUUAUUUU. To determine the affinity of each TIS11d mutation to RNA we used a combination of electrophoretic
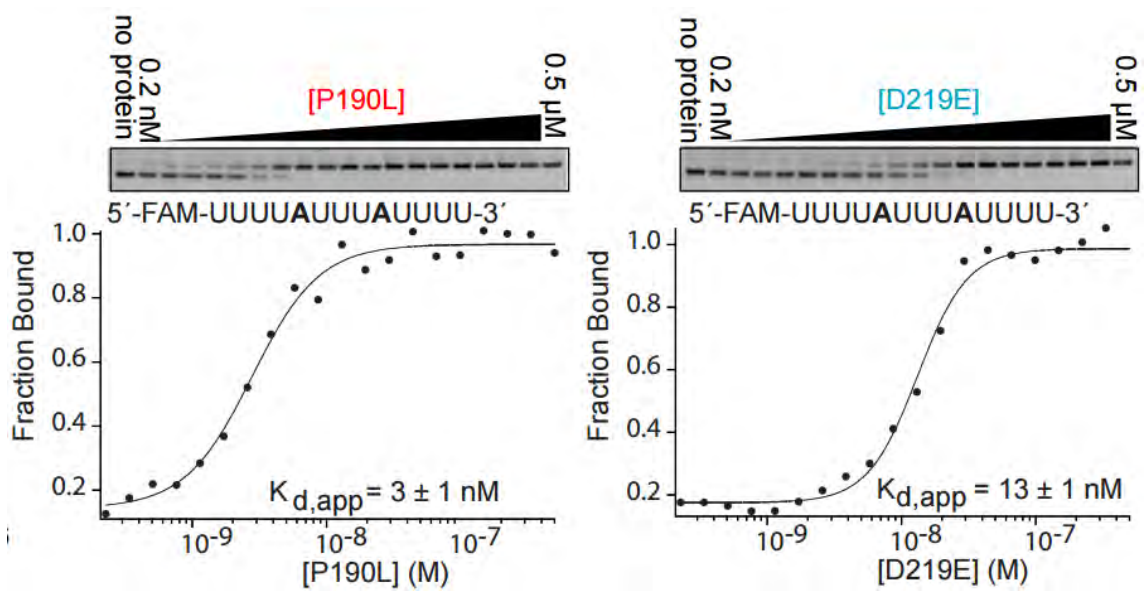
Figure 5.3: RNA binding activity of mutant proteins binding to ARE13 by electrophoretic mobility shift. The ARE13 sequence is show. A plot of fraction bound RNA as a function of mutant TIS11d concentration is present below each gel. The fit of the $K_{d,app}$ and error is given for the specific gel.
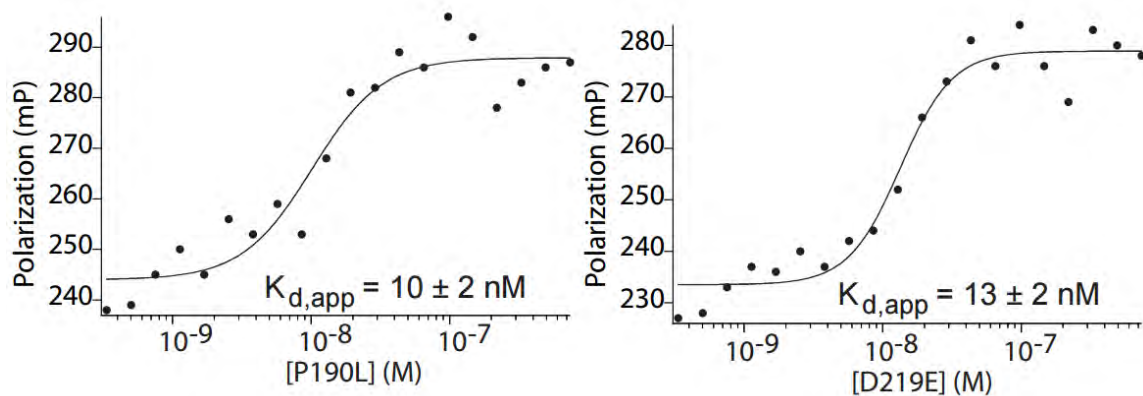
Figure 5.4: RNA binding activity of TIS11d mutations P190L and D219E measured by fluorescence polarization. Fluorescence polarization analysis of TIS11d mutations binding to ARE13 RNA. Raw polarization values are presented. A fit of the data is shown as well as the $K_{d,app}$ and error.

mobility shift assays (EMSA) (Figure 5.3) with untagged proteins, and fluorescence polarization (Figure 5.4) with maltose binding protein (MBP) - tagged protein constructs. The apparent equilibrium dissociation constants (K_d) were similar between what is reported for WT TIS11d in previous chapters of 9.1 ± 2 nM and D219E and P190L mutations of approximately 10 nM. These experiments suggest that although both mutations affect the structural flexibility of the TZF of TIS11d, they do not affect the binding affinity to the cognate RNA sequence. The high affinity measured for TIS11d missense mutations suggest that these proteins can still fold to form a stable complex with RNA, as mutations that disrupt fold of TIS11d ZF2 (such as the C212S zinc coordination mutation) are not RNA binding competent. The high RNA-binding affinity measured for these mutant proteins suggest that the mechanism by which P190L and D219E disrupt TIS11d wild type activity is not through RNA binding of ARE13.

Sub-cellular localization of WT TIS11d, mutants P190L and D219E and control GFP show different phenotypes in HEK293 cells.

Since the P190L and D219E mutations in TIS11d do not affect RNA binding, we suppose the phenotype resulting from these mutations was directly related to the cellular biology. We used confocal microscopy to determine whether GFP-tagged P190L and D219E mutants had a different-subcellular localization in HEK293 cells than the WT. It is important to note that the fusion protein containing a GFP tag does not alter shuttling of the TTP family between the nucleus and cytoplasm[196]. The TTP family members are all nucleocytoplasmic shuttling proteins, with a leucine rich $L_{xxx}L_{xx}L_xL$ N terminal nuclear export signal (NES)[197]. The nuclear localization signal (NLS) was mapped to the basic residues R134 and R137 of the linker region of the TZF[196]. Mutations of these arginines to alanines results in the mislocalization of TTP; however, RNA binding is not affected. Given the role the TTP linker plays in subcellular localization, we hypothesized that P190L and D219E may also affect localization. We use HEK293 cells for our experiments as they do not endogenously express TIS11d. Confocal images taken for
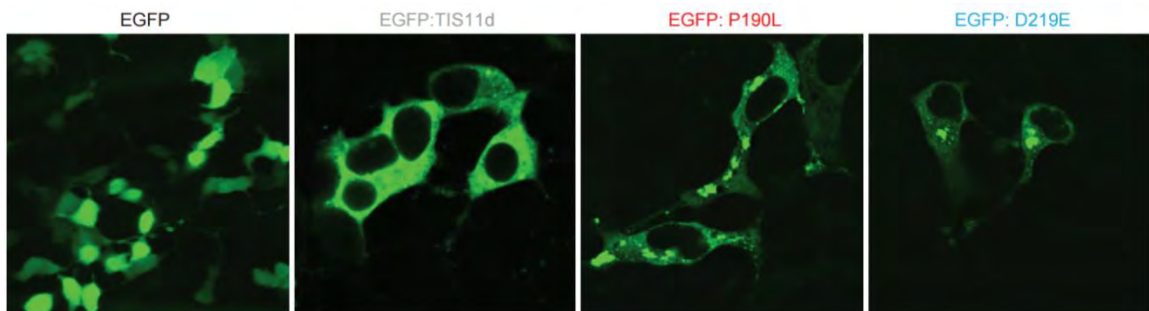
Figure 5.5: Sub cellular localization of GFP, TIS11d, P190L and D219E. Confocal images of HEK293 cells transiently transfected with EGFP tagged full length TIS11d, and P190L and D219E mutations. Subcellular localization of GFP-labeled proteins were observed 24 hours after transfection into HEK293 cells using fluorescence confocal microscopy.

HEK293 cells of GFP alone showed evenly distributed fluorescence throughout the cytoplasm and nucleus (Figure 5.5). Consistent with mRNA destabilizing activity of TIS11d, GFP-tagged TIS11d was dispersedly localized throughout the cytoplasm. In contrast, overexpression of D219E and P190L TIS11d mutants results in the presence of puncta within the cytoplasm (Figure 5.5). This data supports a mechanism by which single nucleotide polymorphisms within the RBD of TIS11d can affect activity by altering cellular localization.

Conclusions and future directions:

We sought to understand the mode by which missense mutations in TIS11d, D219E and P190L, affect its folding, RNA binding activity, and subcellular localization. We determined that the structural flexibility, and possibly destabilization of the structure of ZF2 as seen with P190L, may play a role in disease pathogenesis. The structure of the RBD affects TIS11d localization as GFP - tagged wild type TIS11d has a disperse pattern in the cytoplasm of HEK293 cells; however, TIS11d P190L - and D219E - tagged GFP constructs localize to unidentified puncta within the cell.

The localization into foci observed for P190L and D219E could be due to 1) stress granules since in response to cellular stress, unphosphorylated/active TTP is known to colocalize with these transient mRNA storage vesicles, or 2) processing bodies (P-bodies)[198] since when TTP is phosphorylated it is excluded from stress granules and released into p-bodies, the site of mRNA turnover[72]. However, many of the observed foci

131

are larger than what would be expected for p-body, suggesting that they may be: 1) aggresomes generated from misfolding TIS11d which result after overwhelming the cells protein degradation machinery[199], or 2) autophagosomes which carry abnormal intracellular proteins to lysomes for degradation[200]. In order to fully understand how and why these cytoplasmic puncta are formed in TIS11d mutant variants, further studies are required to identify these puncta using co-immunofluorescence experiments of known protein target antibodies at each suspected localization site.

Taken together, this study highlights how small changes in primary sequence of the essential post-transcriptional regulator TIS11d can affect its protein flexibility and activity, which can then manifest into disease. The cancer genomics database Cbioportal was used to identify frameshift and point mutations throughout TIS11d and TTP gene locus, which have been observed in tissues taken from leukemia patients. Interestingly, more mutations linked to various leukemias and cancers have been mapped throughout the length of TIS11d RBD in comparison to TTP, suggesting that the structural integrity of TIS11d is important for its functions[101]. Curiously, the prototype of this family, TTP, unlike TIS11d, always has a partially folded RBD, unless bound by RNA, and has diffuse cytoplasmic localization when tagged with GFP[185]. These results suggest that TTP and TIS11d have evolved to have divergent modes by which they execute cellular activities. Our results suggest that the appropriate folding of the RBD is coupled with the proper translocation of TIS11d, since mutations that affect TIS11d TZF structural integrity become mislocalized to cytoplasmic foci in the cell. Our lab and others have shown that RNA free form of TTP is partially folded and folds completely upon RNA binding,

which suggests a possible control mechanism of TTP/mRNA translocation and subsequent mRNA decay. RNA association with TTP may be required for its translocation into the cytoplasm for mRNA degradation. The work presented in this chapter warrants future experiments designed to test the extent of TZF folding on localization and mRNA turnover *in vivo*.

Methods and Materials

Expression and Purification of TIS11d, P190L and D219E:

Cloning, Expression and Purification of the TZF of TIS11d and mutants

The RBD of human TIS11d (residues 152-220) was synthesized by Genescript and cloned into the pHMTC vector between BamHI and HindIII restriction sites. TIS11d-E220A and TIS11d- Δ D219/E220 (152-218) constructs were generated using the QuikChange Site-Directed Mutagenesis Kit from Stratagene. TIS11d and mutated constructs were expressed in BL21(DE3) E. coli competent cells. Isotopic labeling with ^{15}N was performed by growing the cells in M9 enriched with 1 g of ^{15}NH$_4$Cl per liter. Carbon labeling is performed by growing cells in M9 containing ^{13}C-glucose. The cells were grown at 37°C to an OD$_{600}$ of 0.8 and then induced for 4 hours with 1 mM isopropyl β-D-1 thiogalactopyranoside (IPTG) and 0.1 mM ZnSO$_4$ at the same temperature. Harvested cells were then passed through a cell disrupter in 50 ml lysis buffer containing 50 mM Tris HCl, pH 8.0, 100 mM NaCl, 100 μM ZnOAc, 2 mM dithiothreitol (DTT) and 1 EDTA free Complete protease inhibitor tablet (Roche). Lysate was centrifuged at

19500 RPM for 1hr at 4°C and passed through a 20 ml amylose column pre-equilibrated with wash buffer (50 mM Tris HCl, pH 8.0, 100 mM NaCl, 100 μM ZnOAc and 2 mM DTT). The column was washed with 10 column volumes of wash buffer. The protein was eluted with 10 mM maltose in wash buffer. The eluent was then placed over a 5 ml Hi TRAP Q column (GE healthcare Life Science) pre-equilibrated with the same wash buffer used above. The column was washed with 3 column volumes of wash buffer. The protein was eluted with a gradient of NaCl from 0-1 M; the peptides typically eluted at 0.3-0.5 M NaCl. Fractions containing our protein were combined, concentrated and dialyzed in 50 mM Tris HCl, pH 8.0, 300 mM NaCl, 100 μM ZnOAc and 2 mM DTT in the presence of TEV at 1:10 ratio and left to proteolyses for 24 hours. The protein was further purified using a 1.6 X 60-cm Superdex-75 size exclusion column (Amersham Bio\sciences) equilibrated with 50 mM Tris HCl pH 7, 300 mM NaCl, 2 mM BME to separate the 8.5 KDa fragments. For NMR analysis fractions with TIS11d or mutant forms of TIS11d were buffer exchanged into 10 mM Tris pH 6.2, 20 mM KCl, 2 mM DTT, 0.1 mM $ZnSO_4$.

RNA binding activity measured by fluorescence polarization and EMSA

Fluorescence Polarization (FP) RNA binding assays were performed with uncleaved Maltose Binding Protein (MBP) tagged protein for accurate determination of protein concentration via absorbance at 280 nm. Optimal binding of the TZF domains to RNA was measured in the presence of 10 mM Tris HCl, pH 8.0, 100 mM NaCl, 0.1 mM $Zn(OAc)_2$, 0.01% IGEPAL CA630, and 2 mM DTT. The affinities of TIS11d, TIS11D-

E220A and TIS11d-Δ D219/E220 (152-218) for the sequence:

5′−UUUUAUUUAUUUU−3′ (ARE$_{13}$) were measured by direct titration of 3 nM labeled

RNA with increasing concentrations of protein using fluorescence polarization.

Electrophoretic Mobility Shift Assays (EMSA), unlike FP, RNA binding assays

were performed with cleaved Maltose Binding Protein (MBP) tagged protein for accurate

determination of protein concentration via absorbance at 280 nm were conducted as

discussed previously. Optimal binding of TIS11d to RNA was measured in the presence

of 2 mM dithiothreitol, DTT. The affinities of TIS11d, K$_{d\ (apparent)}$ for the sequence: 5′-

UUUUAUUUAUUUU-3′ (ARE$_{13}$), was measured by direct titration of 3 nM labeled

RNA with increasing concentrations of TIS11d as described in Pagano *et al*[174]. The K$_{d,app}$

of TIS11d to ARE$_{13}$ is not fit to the quadratic equation but to the quadratic equation

$$f = \frac{m-b}{2R}\left(K_d + P + R - \sqrt{[K_d + P + R]^2 - 4RP}\right) + b,$$

where m and b are the maximum and base signals, K$_d$ is the dissociation constant, and P

and R are the concentrations of protein and labeled RNA in the sample, respectively.

NMR spectroscopy

Folding of TIS11d and TIS11d P190L and D21E mutations were monitored via NMR

spectroscopy. ^{15}N-^{1}H HSQC spectra were collected at 298 K for each chimera. All NMR

triple-resonance and ^{15}N-^{1}H HSQC experiments were collected on a Varian Inova

spectrometer operating at 600 MHz equipped with a triple-resonance cold probe. The

temperature was calibrated using a sample of 100% methanol. Data processing was performed using NMRPipe [145] and Sparky software[146].

CD spectroscopy

Far-UV circular dichroism (CD) spectra were recorded for D219E (60 μM) and TIS11d (18 μM) in 50 mM HEPES pH 7.0, 20 mM KCl and 1 mM TCEP using a Jasco-810 spectropolarimeter (Jasco Inc., Easton, MD). Curves were monitored from 200-260 nm in a 0.1 cm path length quartz cuvette using a scan rate of 20 nm min^{-1} and a response time of 8 s. The sample temperature for all CD measurements was maintained at 293 K.

Confocal Microscopy

The pDEST53 and pDEST53TIS11d mammalian expression construct were made using the Gateway cloning system. pDEST53D219E and pDEST53P190L were then generated using Q5-mutagenesis kit (NEB). Human embryonic kidney (HEK) 293 cells were plated at a density of 300,000 cells/well in glass bottom plates (MatTek), with Dulbecco′s Modified Eagle′s Medium (DMEM) containing 100 units/mL penicillin and 100 μg/mL streptomycin and 10% fetal bovine serum (FBS). The plates were incubated for 24 hours in a humidified 5% CO_2 incubator set at 37° C. When the cells were 60-70% confluent each were transiently transfected with 1 μg of pcDNA3.1-His-C (empty plasmid), pcDNA3.1 TTP, pcDNA3.1 TTP$_{TZF\_TIS11d}$, or pcDNA3.1 TTP (C162S) using lipofectamine 2000 (Sigma). 48 hours after transfection, cells were imaged via

fluorescence confocal microscopy using a Leica TCS SP5 confocal Scanning microscope

at UMass Medical School.

Chapter VI: Discussion

Tristetraprolin (TTP) and its family members, TIS11d and TIS11b, are essential RBPs, known to regulate gene expression in order to maintain cellular homeostasis. Dysregulation of TTP expression and function is associated with chronic inflammation and cancer due to the aberrant expression of tightly-regulated genes. Many cancer cells have shown decreased expression levels of TTP, which has arisen as a common prognostic indicator for breast cancer[201]. Understanding how TTP, and its family members, bind to and regulate their mRNA targets will help define their role in human pathology.

Identifying TIS11d Targets

In Chapter II, we discovered the role primary and secondary structural elements in the TTP family of proteins plays on their target mRNA binding and selectivity. Explicitly, we found, that the post-transcriptional RNA binding proteins (RBPs), TTP and TIS11d, have different RNA sequence specificities despite sharing large primary sequence identity. This finding exemplifies how changes in protein sequence can influence the protein structure and propagate to differences in RNA binding specificity. By substituting adenine nucleotides for uridines in the canonical 3'-UTR sequence, we identified the RNA specificity determinants required by TTP and TIS11d. These results highlighted the need for identifying RNA sequence determinants in the regulation of RNA-binding. Peak intensity differences in the ^{15}N-^{1}H heteronuclear single quantum coherence (HSQC) spectrum mapped to the adenine coordination sites of the TZF domain suggested degeneracy in TTP RNA binding that was not observed with TIS11d – consistent with a more "relaxed" binding structure. Comparing the binding affinities of

TTP and TIS11d for various lengths of RNA targets by fluorescence polarization and NMR spectroscopy established that TTP specifically coordinates an adenine nucleotide at residues just preceding ZF1, whereas TIS11d was not found to require this same specific RNA sequence. We concluded that the difference in specificity of TTP for the 5'UAUU3' half site at ZF1 is due to differences in TIS11d and TTP RBD stability. TTP, unlike TIS11d, needs RNA to stably fold ZF2, as described through an induced-fit mechanism. Specifically, we determined that an extra hydrogen bond formed between TTP ZF1 and RNA by residue E107, is required for TTP-RNA interaction where it serves as an anchor for ZF2 binding/folding on the RNA. The ZF2 of TIS11d is already folded in its ligand-free state and therefore does not require a stable interaction between ZF1 and RNA to fold. Because TIS11d lacks the same adenine coordination constraint in ZF1 as TTP, this may allow for it to be more promiscuous in binding biological targets. A key gap in our understanding is whether this mechanism is applicable in other RBPs, specifically proteins containing one or more CCCH-type zinc finger domains.

With the confirmation of ARE13 (5´UUAUUUAUU3´) and uridine substituted (5´UUUUUUAUU3´, 5´UUAUUUUUU3´ and 5´UUUUUUUUU3´) binding sites, several approaches can be implemented to identify "true" biologically relevant mRNA targets of TIS11d from a complex pool of cellular transcripts. Determining TIS11d targets with the strict criterion of measuring *in vivo* mRNA stabilization in cells derived from TIS11d knockout mice is a time-intensive process. Bioinformatics has made the ability to predict potential targets more time efficient; however, this method requires confirmation of all predictions and is limited to identification only. Fortunately, genome-wide approaches

allow for the identification of thousands of target transcripts simultaneously in response to altered levels of TIS11d expression. Microarray profiling identified 250 of 40,000 probed 3' UTRs in TTP knockout mice fibroblasts that demonstrated increased RNA lifetimes compared to wild-type fibroblasts after stimulation with epithelial growth factor for various time intervals followed by treatment with actinomycin D to halt additional mRNA synthesis[98]. This study was encouraging as Northern blots confirmed TTPs interaction with these 3'UTRs; showing the utility of genome-wide analyses to study mRNA decay. However, targets that did not strictly conform to the 5'UUAUUUAUU3' sequence, may have been missed during the bioinformatics analysis which make it an imperfect strategy for RBPs that bind with relaxed specificity as seen with TIS11d. A more recent study using RNA immunoprecipitation and microarray analysis (RIP)-Chip on TTP to compare wild-type and TTP-knockout embryonic fibroblasts identified 137 full-length transcripts that are associated with TTP[77]. This approach is advantageous over traditional microarray because it can identify sequence elements that are enriched among TTP-associated mRNAs. Alternatively, TTP directly-associated mRNA targets can be identified utilizing Photoactivatable-Ribonucleoside-Enhanced Crosslinking and Immunoprecipitation (PAR-Clip). The exact position of the crosslink can be determined by mutations in the cDNA, where base pairs of 4-thiouridine are made only with guanidine, incorporating a T to C mutation in the cDNA library that can be identified using deep sequencing[202]. Using this technique in HEK cells, 5-fold more mRNAs were identified than by the previously described techniques[99]. Combining PAR-Clip with secondary screens to demonstrate biological relevance will allow the identification of

other targets of TIS11d. These targets can then be tested for interaction with TTP by measuring changes in RNA stability, translational activity (repression), differences in subcellular distribution (P-bodies), or global phenotypes (immunocompromised mice), etc, to be classified as truly biologically relevant.

Understanding the physical forces that drive TTP and TIS11d discrimination for their unique mRNA targets is critical for understanding how they regulate RNA turnover in the cell. Many other factors bind the TTP family of proteins for their activation/inactivation, localization, and mRNA degradation activity. Whether RNA induced structural differences that result in the TTP family biological functions is still a mystery and will be an exciting area of research in the future.

Leveraging our knowledge on RNA recognition for therapeutic design

Engineering zinc fingers to bind a particular RNA target is an active goal in developing therapeutics. Since CCCH RBDs are small, uncomplicated protein domains RNA binding specificity is dictated mainly through their primary sequence. Here, we highlight how tertiary structure may also play a role in determining specificity. Therefore, the field must also take into consideration the final folded structure of the CCCH motif when designing new therapeutics.

The results in Chapter II, provides insight into other proteins containing CCCH-type zinc fingers and the role played by primary sequence in determining RNA specificity. Studies done by our lab and others demonstrate that the TZF domain of the *C. elegans* protein MEX-5 binds to uridine stretches high affinity and low specificity. In contrast, the mammalian protein TIS11d binds specifically to 5'UUUUAUUUAUUUU'3

with high affinity. The relaxed binding specificity seen in MEX-5 is attributed to the Arg/Lys (R274/K318) in the fifth residue (X) of the highly conserved R(K)YKT**X**L motif preceding each zinc finger. In mammals, the fifth residue (X) is always a glutamate; whereas in *C.elegans*, this position is less uniform[203]. Indeed, TIS11d mutations at this position are seen in patients with various forms of cancer highlighting the importance of this specific residue in RNA binding. To study the role this residue plays in RNA binding, we generated the equivalent mutations in TTP and TIS11d, E107R/E145K and E157R/E195K, respectively and found that mutations of the R(K)YKTEL in ZF1 are detrimental to TIS11d (TTP) RNA binding, while the mutations in ZF2 do not negatively affect the binding affinity. These findings exemplifies the challenges associated with defining the recognition sequence for all CCCH TZFs, since what is known about the TZF fold and specificity for one CCCH member may not hold true for all CCCH members.

Tumor suppressor therapies though direct protein injection

The loss of TTP expression in cancer cell lines is thought to contribute to tumorigenesis. Recently (2010) researchers were able to successfully inject a recombinant form of the purified TTP family member, TIS11b, into adrenal glands of immunodeficient mice and nude mice with subcutaneous cell carcinomas using a poly-arginine tag (R9) fused to its N terminus[204]. R9-TIS11b treated mice showed decrease angiogenesis and tumor growth as consequence of reduced VEGF mRNA levels, suggesting that using a similar approach to increase TTP protein levels in human cancer cells could be a viable therapeutic technique. Although TTP family members seem to be

excellent targets for antitumor therapies, their off target effects have not been examined. Identifying the specificity determinants for the TTP family will be useful in developing therapies for immune disease and cancers that have as few off target effects as possible. Furthermore, understanding what transcripts are regulated by which protein of a family will allow us to evaluate other genes that may be therapeutic targets of TTP family injection therapies.

Molecular basis for disease

The accurate post-transcriptional regulation of genes by regulatory RNA-binding proteins requires the ability to recognize specific transcripts from a complex pool of cellular mRNAs. This is accomplished through stable sequence- and structure- specific interactions between the RNA binding proteins and their target mRNAs. The RNA binding protein tristetraprolin (TTP), and its homologues TIS11b and TIS11d, are required for post-transcriptional repression of many different genes associated with inflammation and cancer initiation/progression in mammals. TTP family members mediate post-transcriptional repression by binding mRNA targets to promote their degradation. Misregulation of TTP directed mRNA degradation results in a wide array of host-cellular responses including acute inflammatory responses to harmful stimuli. TTP-deficient mice suffer from a systematic inflammatory syndrome characterized by arthritis, autoimmune disorders, and myeloid hyperplasia associated with over-expression of the proinflammatory cytokine TNFα. Therefore, identifying mutations in TTP that increase/decrease its activity can be used to develop therapeutics for inhibiting mRNA

over-biosynthesis which causes toxic accumulation of cytokines and growth factors that lead to chronic inflammation and cancer.

Developing therapeutics to increase TTP activity by folding its RBD

In Chapter III of this thesis, we examined the structural differences observed between the highly identical (72%) RBDs of TTP and TIS11d. NMR data collected for their RBDs determined that TTP is partially unfolded and TIS11d is folded in their RNA free state. NMR and binding assay of chimeric proteins of the TZF domains of TTP and TIS11d established that three residues located at the C-terminal end of the α-helix determine the structure of TZF domain. Using a reporter assay where luciferase expression was under control of the TNFα 3'UTR, we observed that mRNA destabilizing activity of TTP was increased when the partially disordered TZF domain of TTP was replaced with the fully structured domain of TIS11d. These results demonstrate that the degree of structure present in the TZF domain directly affects the function of the protein in the cell and suggests that protein activity is modulated through its structure.

Stabilization of the TTP RBD occurs upon binding to RNA, but also occurs upon zinc coordination. This stabilization may play a role in the cellular localization and mRNA degradation activity of TTP. Analysis of the amino acid sequences of TIS11d and TTP from 100 vertebrate species suggests that the TZF domain of TIS11d is always folds as the three α-helical residues, histidine-threonine-isoleucine, sufficient to stabilize the structure of ZF2, are strictly conserved. In TTP, however, the corresponding three residues, tyrosine-leucine-glutamine, which are associated with the observed disorder in the TZF domain, are only conserved in mammals. In fish and birds these three residues

are the same as in TIS11d, suggesting that the TZF domain of TTP is possibly folded in these vertebrates. Comparative genomics suggests that the activity regulation of TTP through its structure has evolved more recently in mammals.
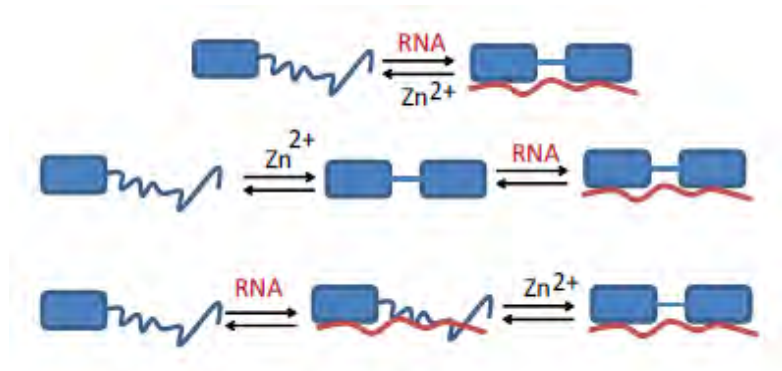
Figure 6.1: Mechanisms of RNA binding. Schematic representation of the three possible scenarios for the mechanism of TTP folding in the presence of RNA and zinc. (Top) Both RNA and zinc bind simultaneously to TTP to form a stable RNA bound complex; (Middle) zinc binds to fold ZF2 after which RNA can bind; (Bottom) RNA binding precedes zinc binding.

Because zinc is a critical mediator of TTP-RNA-binding activity, we sought to investigate the molecular mechanism by which TTP interacts with zinc to form a stable protein-RNA complex. Figure 6.1 depicts the possible mechanisms of TTP ZF2 binding in the presence of zinc and RNA. Three possible scenarios exist for the mechanism of TTP folding in the presence of both cofactors: 1) both RNA and zinc bind simultaneously to TTP to form a stable RNA bound complex; 2) zinc binds to fold ZF2 after which RNA can bind; 3) RNA binding precedes zinc binding. Previous experiments by our lab and others on a TTP mutant (C162S), which cannot coordinate zinc, was found to not bind RNA, thus eliminating the third scenario as a possible mechanism for TTP zinc and RNA binding. In order to determine whether zinc and RNA binding is a concerted versus

146

stepwise reaction process, other biophysical techniques must be employed. One such technique is time - resolved FRET to look at the differences between association with RNA binding of ZF1 and ZF2 since the FRET excited state decays will differ depending on the mechanism as the probes will have different distances in the folded and unfolded states. If ZF1 and ZF2 are folded prior to RNA binding, as in scenario number 2, their FRET associations will be the same. If ZF1 needs to fold before RNA can associate, as in scenario number 1, then their FRET will be different.

Given that mRNA turnover activity of TTP is enhanced when its partially disordered TZF domain is substituted with the fully structured domain of TIS11d and that when the stable folded zinc finger of TIS11d is disrupted it results in disease, future studies must focus on structure based design to identify potential locations for small molecule binding on the partially folded TZF of TTP and misfolded variants of TIS11d. HSQC NMR-based screening would be a powerful way to identify small molecules that can bind and fold TTP. Other high throughput approaches, such as intrinsic tyrosine fluorescence may not allow for the resolution required to couple folding to compound binding. Other methods, such as FRET, that use probes to look at secondary structure changes may also present an issue since they require re-engineering the native protein, which could alter the limited secondary structure available. Screening many different compound libraries could result in the identification of several putative compounds to stabilize ZF2. After defining which compounds bind to induce a fully folded TTP TZF, a more rational based design/optimization of these therapeutics could be explored. Using our biophysical understanding of the partially folded state of TTP and what specific

147

interactions are necessary for it to fold and function, molecular dynamics simulations and modeling techniques can be used to optimize the structure and functional groups of our putative compounds to enhance binding affinity.

Molecules that stabilize the TTP family RBD fold could be further screened utilizing the luciferase reporter system developed by our lab and discussed above. Through the direct measure of enhanced luciferase turnover we can control for issues associated with drug delivery to target TTP folding in the nucleus. Furthermore, the consequences of induced TTP folding upon binding of these small molecules can be tested in mice. Recent advancements in gene editing techniques would allow us to even make changes to TTP *in vivo*. We could use the CRISPER/Cas9 in TTP KO mice, which suffer from systematic inflammatory syndrome, to see if targeted changes to TTP, such as replacing the unfolded YLQ motif with the folded HTI motif from TIS11d, will rescue the mouse phenotype by allowing a more rapid turnover of the toxic TNF-α cytokine mRNA.

Understanding how the structure of the RBD affects the rest of the TTP sequence

Chapter IV investigates the relationship between the structure and function of the TIS11d TZF. Studies using wild-type and disease-associated mutations, P190L and D219E, demonstrated differences in structural flexibility of the RBD of TIS11d. In contrast, both mutations still bound similarly to the cognate RNA sequence. Expression analysis in HEK293 cells using GFP-tagged construct showed TIS11d distributed throughout the cytoplasm. However, P190L and D219E mutants display puncta within

the cytoplasm. These results suggest that the folding and structure of the RBD can affect the regulation and localization of TIS11d in cell culture models.

In this thesis I mainly describe the biochemical and biophysical studies characterizing the RBD of the TTP family; however, it is important to note that the N-and C-terminal domains, which are predicted to be highly disordered, contain important sites for the temporal and spatial regulation of the activity of the TTP family. For example, the translocation of the TTP/RNA complex is achieved through its interaction with many protein partners, including the exportin CRM1, which contains an N terminal hydrophobic $L_{xxx}L_{xx}L_xL$ sequence known as the nuclear export signal (NES)[197]. This is significant as mRNAs bound by TTP are transported to stress granules where they are sequestered from translation machinery or to processing bodies (p-bodies) where they are degraded by various cellular mechanisms. Both p-bodies and stress granules are important for the repression of gene expression.

Understanding how the structure of the RBD affects the rest of the TTP sequence is important to understand how protein-RNA interactions may affect TTP activity in the cell. Interestingly, truncation experiments mapped the TTP nuclear localization signal (NLS) to the interfinger linker region of its TZF/RBD. Further mutational analysis demonstrated that the nuclear transport proteins Importin α/β bind to the basic residues R134 and R137 of the linker region of the TZF[185]. Mutations of these residues to alanines results in the mislocalization of TTP. The fact that the NLS of TTP is also contained in its RBD suggests that the RNA target may play a role in directing TTP into and out of the nucleus. When considered with our research showing that RNA is necessary for TTP

149

folding, this suggests that a fully-folded TTP may be required to ensure the proper cellular localization of TTP.

Biophysical characterization of TTP in complex with other protein-protein interactomes, such as14-3-3 chaperone proteins or importin α/β, in the presence and absence of RNA will allow us to identify the role played by RNA in facilitating TTP protein associations *in vivo*. Since the structures of 14-3-3 chaperone proteins and importin α/β have been solved by x-ray crystallography, co-crystallizing TTP in its RNA free and bound states may provide insight into how RNA stabilizes TTP protein-protein interactions. Additional insights may come from gel mobility shift assays to determine how the addition of RNA enhances TTP-protein complex formation.

Additionally, the ability of TTP to target transcripts for rapid cytoplasmic degradation is regulated via its hyper-phosphorylation at residues S60 and S186, which are directly adjacent to the RBD, by MAPK-AP kinase-2 (MK2). A possible explanation is that phosphorylation of TTP results in its interaction with the chaperone 14-3-3 dimer complex allowing it to be trafficked into p-bodies. TTP interaction with 14-3-3 protein is thought to preclude CAF1 association with the CCR4-NOT1 complex in order to halt mRNA degradation. Dephosphorylation of TTP by protein phosphatase 2A (PP2A) releases the 14-3-3 proteins and restores mRNA degradation activity. The molecular mechanism by which TTP is recognized by the 14-3-3 dimer complex is poorly understood and many unanswered questions remain. Does phosphorylation stabilize the second zinc finger to allow the binding of the 14-3-3 complex? Answering this and other

questions in order to understand how TTP makes critical protein-protein and protein-RNA interactions within the cell will further aid in therapeutic design.

Thesis Summary

The focus of these studies was to understand how the tristetraprolin (TTP) family of proteins regulates RNA at the molecular level. Particular attention was given to determining how the structure of their RNA binding domain (RBD) may affect their activity in the cell. Biophysical studies on two members of this family, TTP and TIS11d, have shown that the RBD of TTP is only partially-folded in the absence of RNA, unlike its homologous family member TIS11d, which is fully folded. A multidisciplinary approach was employed to identify the residues responsible for the structural differences observed for TIS11d and TTP as well as to understand the relationship between their differences in structure, RNA-binding specificity, and cellular activity. Altogether, we conclude that the extent of TZF folding in the TTP family is important for differential RNA recognition, mRNA turnover, and protein localization *in vivo*. Further work to understand how TTP partially folded state influences its activity could be leveraged for future therapeutic design.

Bibliography

1. Jones AR, Francis R, Schedl T. GLD-1, a cytoplasmic protein essential for oocyte differentiation, shows stage- and sex-specific expression during caenorhabditis elegans germline development. *Dev Biol*. 1996;180(1):165-183.

2. Mello CC, Schubert C, Draper B, Zhang W, Lobel R, Priess JR. The PIE-1 protein and germline specification in C. elegans embryos. *Nature*. 1996;382(6593):710-712.

3. Subramaniam K, Seydoux G. Nos-1 and nos-2, two genes related to drosophila nanos, regulate primordial germ cell development and survival in caenorhabditis elegans. *Development*. 1999;126(21):4861-4871.

4. Schubert CM, Lin R, de Vries CJ, Plasterk RH, Priess JR. MEX-5 and MEX-6 function to establish soma/germline asymmetry in early C. elegans embryos. *Mol Cell*. 2000;5(4):671-682.

5. Heasman J. Maternal determinants of embryonic cell fate. *Semin Cell Dev Biol*. 2006;17(1):93-98.

6. Mino T, Takeuchi O. Post-transcriptional regulation of cytokine mRNA controls the initiation and resolution of inflammation. *Biotechnol Genet Eng Rev*. 2013;29:49-60.

7. Muhlrad D, Parker R. Mutations affecting stability and deadenylation of the yeast MFA2 transcript. *Genes Dev*. 1992;6(11):2100-2111.

8. Day DA, Tuite MF. Post-transcriptional gene regulatory mechanisms in eukaryotes: An overview. *J Endocrinol*. 1998;157(3):361-371.

9. Perrone-Bizzozero N, Bolognani F. Role of HuD and other RNA-binding proteins in neural development and plasticity. *J Neurosci Res*. 2002;68(2):121-126.

10. Hu L, Chen Y, Evers S, Shen Y. Expression of fragile X mental retardation-1 gene with nuclear export signal mutation changes the expression profiling of mouse cerebella immortal neuronal cell. *Proteomics*. 2005;5(15):3979-3990.

11. Fan J, Heller NM, Gorospe M, Atasoy U, Stellato C. The role of post-transcriptional regulation in chemokine gene expression in inflammation and allergy. *Eur Respir J*. 2005;26(5):933-947.

12. Chaudhury A, Hussey GS, Howe PH. 3'-UTR-mediated post-transcriptional regulation of cancer metastasis: Beginning at the end. *RNA Biol*. 2011;8(4):595-599.

13. Muto J, Imai T, Ogawa D, *et al*. RNA-binding protein Musashi1 modulates glioma cell growth through the post-transcriptional regulation of notch and PI3 kinase/akt signaling pathways. *PLoS One*. 2012;7(3):e33431.

14. Brinegar AE, Cooper TA. Roles for RNA-binding proteins in development and disease. *Brain Res*. 2016.

15. Day DA, Tuite MF. Post-transcriptional gene regulatory mechanisms in eukaryotes: An overview. *J Endocrinol*. 1998;157(3):361-371.

16. Clery A, Blatter M, Allain FH. RNA recognition motifs: Boring? not quite. *Curr Opin Struct Biol*. 2008;18(3):290-298.

17. Daubner GM, Clery A, Allain FH. RRM-RNA recognition: NMR or crystallography...and new findings. *Curr Opin Struct Biol*. 2013;23(1):100-108.

18. Bou-Nader C, Pecqueur L, Bregeon D, *et al*. An extended dsRBD is required for post-transcriptional modification in human tRNAs. *Nucleic Acids Res*. 2015;43(19):9446-9456.

19. Poulsen H, Jorgensen R, Heding A, Nielsen FC, Bonven B, Egebjerg J. Dimerization of ADAR2 is mediated by the double-stranded RNA binding domain. *RNA*. 2006;12(7):1350-1360.

20. Teplova M, Hafner M, Teplov D, Essig K, Tuschl T, Patel DJ. Structure-function studies of STAR family quaking proteins bound to their *in vivo* RNA target sites. *Genes Dev*. 2013;27(8):928-940.

21. Stoiber MH, Olson S, May GE, *et al*. Extensive cross-regulation of post-transcriptional regulatory networks in drosophila. *Genome Res*. 2015;25(11):1692-1702.

22. Murn J, Teplova M, Zarnack K, Shi Y, Patel DJ. Recognition of distinct RNA motifs by the clustered CCCH zinc fingers of neuronal protein unkempt. *Nat Struct Mol Biol*. 2016;23(1):16-23.

23. Qu J, Kang SG, Wang W, Musier-Forsyth K, Jang JC. The arabidopsis thaliana tandem zinc finger 1 (AtTZF1) protein in RNA binding and decay. *Plant J*. 2014;78(3):452-467.

24. Spike CA, Coetzee D, Nishi Y, *et al*. Translational control of the oogenic program by components of OMA ribonucleoprotein particles in caenorhabditis elegans. *Genetics*. 2014;198(4):1513-1533.

25. Cass D, Hotchko R, Barber P, Jones K, Gates DP, Berglund JA. The four zn fingers of MBNL1 provide a flexible platform for recognition of its RNA binding elements. *BMC Mol Biol*. 2011;12:20-2199-12-20.

26. Phelps KJ, Tran K, Eifler T, Erickson AI, Fisher AJ, Beal PA. Recognition of duplex RNA by the deaminase domain of the RNA editing enzyme ADAR2. *Nucleic Acids Res*. 2015;43(2):1123-1132.

27. Matoulkova E, Michalova E, Vojtesek B, Hrstka R. The role of the 3' untranslated region in post-transcriptional regulation of protein expression in mammalian cells. *RNA Biol*. 2012;9(5):563-576.

28. Glisovic T, Bachorik JL, Yong J, Dreyfuss G. RNA-binding proteins and post-transcriptional gene regulation. *FEBS Lett*. 2008;582(14):1977-1986.

29. Filipowicz W, Bhattacharyya SN, Sonenberg N. Mechanisms of post-transcriptional regulation by microRNAs: Are the answers in sight? *Nat Rev Genet*. 2008;9(2):102-114.

30. Kloc M, Zearfoss NR, Etkin LD. Mechanisms of subcellular mRNA localization. *Cell*. 2002;108(4):533-544.

31. Besse F, Ephrussi A. Translational control of localized mRNAs: Restricting protein synthesis in space and time. *Nat Rev Mol Cell Biol*. 2008;9(12):971-980.

32. Decker CJ, Parker R. P-bodies and stress granules: Possible roles in the control of translation and mRNA degradation. *Cold Spring Harb Perspect Biol*. 2012;4(9):a012286.

33. Walters R, Parker R. Quality control: Is there quality control of localized mRNAs? *J Cell Biol*. 2014;204(6):863-868.

34. Garneau NL, Wilusz J, Wilusz CJ. The highways and byways of mRNA decay. *Nat Rev Mol Cell Biol*. 2007;8(2):113-126.

35. Smith JE, Baker KE. Nonsense-mediated RNA decay--a switch and dial for regulating gene expression. *Bioessays*. 2015;37(6):612-623.

36. Houseley J, Tollervey D. The many pathways of RNA degradation. *Cell*. 2009;136(4):763-776.

37. Yang E, van Nimwegen E, Zavolan M, *et al*. Decay rates of human mRNAs: Correlation with functional characteristics and sequence attributes. *Genome Res*. 2003;13(8):1863-1872.

38. Stoecklin G, Lu M, Rattenbacher B, Moroni C. A constitutive decay element promotes tumor necrosis factor alpha mRNA degradation via an AU-rich element-independent pathway. *Mol Cell Biol*. 2003;23(10):3506-3515.

39. Neininger A, Kontoyiannis D, Kotlyarov A, *et al*. MK2 targets AU-rich elements and regulates biosynthesis of tumor necrosis factor and interleukin-6 independently at different post-transcriptional levels. *J Biol Chem*. 2002;277(5):3065-3068.

40. Peixeiro I, Silva AL, Romao L. Control of human beta-globin mRNA stability and its impact on beta-thalassemia phenotype. *Haematologica*. 2011;96(6):905-913.

41. Caput D, Beutler B, Hartog K, Thayer R, Brown-Shimer S, Cerami A. Identification of a common nucleotide sequence in the 3'-untranslated region of mRNA molecules specifying inflammatory mediators. *Proc Natl Acad Sci U S A*. 1986;83(6):1670-1674.

42. Winstall E, Gamache M, Raymond V. Rapid mRNA degradation mediated by the c-fos 3' AU-rich element and that mediated by the granulocyte-macrophage colony-stimulating factor 3' AU-rich element occur through similar polysome-associated mechanisms. *Mol Cell Biol*. 1995;15(7):3796-3804.

43. Brown CY, Lagnado CA, Goodall GJ. A cytokine mRNA-destabilizing element that is structurally and functionally distinct from A+U-rich elements. *Proc Natl Acad Sci U S A*. 1996;93(24):13721-13725.

44. Chen CY, Chen TM, Shyu AB. Interplay of two functionally and structurally distinct domains of the c-fos AU-rich element specifies its mRNA-destabilizing function. *Mol Cell Biol*. 1994;14(1):416-426.

45. Bakheet T, Williams BR, Khabar KS. ARED 2.0: An update of AU-rich element mRNA database. *Nucleic Acids Res*. 2003;31(1):421-423.

46. Chen CY, Chen TM, Shyu AB. Interplay of two functionally and structurally distinct domains of the c-fos AU-rich element specifies its mRNA-destabilizing function. *Mol Cell Biol*. 1994;14(1):416-426.

47. Wilusz CJ, Wormington M, Peltz SW. The cap-to-tail guide to mRNA turnover. *Nat Rev Mol Cell Biol*. 2001;2(4):237-246.

48. Kim HS, Wilce MC, Yoga YM, *et al*. Different modes of interaction by TIAR and HuR with target RNA and DNA. *Nucleic Acids Res*. 2011;39(3):1117-1130.

49. Yeap BB, Voon DC, Vivian JP, *et al*. Novel binding of HuR and poly(C)-binding protein to a conserved UC-rich motif within the 3'-untranslated region of the androgen receptor messenger RNA. *J Biol Chem*. 2002;277(30):27183-27192.

50. Brooks SA, Blackshear PJ. Tristetraprolin (TTP): Interactions with mRNA and proteins, and current thoughts on mechanisms of action. *Biochim Biophys Acta*. 2013;1829(6-7):666-679.

51. Gratacos FM, Brewer G. The role of AUF1 in regulated mRNA decay. *Wiley Interdiscip Rev RNA*. 2010;1(3):457-473.

52. Dember LM, Kim ND, Liu KQ, Anderson P. Individual RNA recognition motifs of TIA-1 and TIAR have different RNA binding specificities. *J Biol Chem*. 1996;271(5):2783-2788.

53. Garcia-Mayoral MF, Diaz-Moreno I, Hollingworth D, Ramos A. The sequence selectivity of KSRP explains its flexibility in the recognition of the RNA targets. *Nucleic Acids Res*. 2008;36(16):5290-5296.

54. Gardiner AS, Twiss JL, Perrone-Bizzozero NI. Competing interactions of RNA-binding proteins, MicroRNAs, and their targets control neuronal development and function. *Biomolecules*. 2015;5(4):2903-2918.

55. Carballo E, Lai WS, Blackshear PJ. Feedback inhibition of macrophage tumor necrosis factor-alpha production by tristetraprolin. *Science*. 1998;281(5379):1001-1005.

56. King EM, Kaur M, Gong W, Rider CF, Holden NS, Newton R. Regulation of tristetraprolin expression by interleukin-1 beta and dexamethasone in human pulmonary epithelial cells: Roles for nuclear factor-kappa B and p38 mitogen-activated protein kinase. *J Pharmacol Exp Ther*. 2009;330(2):575-585.

57. Chen YL, Jiang YW, Su YL, Lee SC, Chang MS, Chang CJ. Transcriptional regulation of tristetraprolin by NF-kappaB signaling in LPS-stimulated macrophages. *Mol Biol Rep*. 2013;40(4):2867-2877.

58. Taylor GA, Thompson MJ, Lai WS, Blackshear PJ. Mitogens stimulate the rapid nuclear to cytosolic translocation of tristetraprolin, a potential zinc-finger transcription factor. *Mol Endocrinol*. 1996;10(2):140-146.

59. Sanduja S, Blanco FF, Dixon DA. The roles of TTP and BRF proteins in regulated mRNA decay. *Wiley Interdiscip Rev RNA*. 2011;2(1):42-57.

60. Lykke-Andersen J, Wagner E. Recruitment and activation of mRNA decay enzymes by two ARE-mediated decay activation domains in the proteins TTP and BRF-1. *Genes Dev*. 2005;19(3):351-361.

61. Blackshear PJ, Perera L. Phylogenetic distribution and evolution of the linked RNA-binding and NOT1-binding domains in the tristetraprolin family of tandem CCCH zinc finger proteins. *J Interferon Cytokine Res*. 2014;34(4):297-306.

62. Fabian MR, Frank F, Rouya C, *et al*. Structural basis for the recruitment of the human CCR4-NOT deadenylase complex by tristetraprolin. *Nat Struct Mol Biol*. 2013;20(6):735-739.

63. Lai WS, Thompson MJ, Blackshear PJ. Characteristics of the intron involvement in the mitogen-induced expression of zfp-36. *J Biol Chem*. 1998;273(1):506-517.

64. Lai WS, Thompson MJ, Taylor GA, Liu Y, Blackshear PJ. Promoter analysis of zfp-36, the mitogen-inducible gene encoding the zinc finger protein tristetraprolin. *J Biol Chem*. 1995;270(42):25266-25272.

65. Hitti E, Iakovleva T, Brook M, *et al*. Mitogen-activated protein kinase-activated protein kinase 2 regulates tumor necrosis factor mRNA stability and translation mainly by altering tristetraprolin expression, stability, and binding to adenine/uridine-rich element. *Mol Cell Biol*. 2006;26(6):2399-2407.

66. Johnson BA, Stehn JR, Yaffe MB, Blackwell TK. Cytoplasmic localization of tristetraprolin involves 14-3-3-dependent and -independent mechanisms. *J Biol Chem*. 2002;277(20):18029-18036.

67. Carballo E, Gilkeson GS, Blackshear PJ. Bone marrow transplantation reproduces the tristetraprolin-deficiency syndrome in recombination activating gene-2 (-/-) mice. evidence that monocyte/macrophage progenitors may be responsible for TNFalpha overproduction. *J Clin Invest*. 1997;100(5):986-995.

68. la Cour T, Kiemer L, Molgaard A, Gupta R, Skriver K, Brunak S. Analysis and prediction of leucine-rich nuclear export signals. *Protein Eng Des Sel*. 2004;17(6):527-536.

69. Phillips RS, Ramos SB, Blackshear PJ. Members of the tristetraprolin family of tandem CCCH zinc finger proteins exhibit CRM1-dependent nucleocytoplasmic shuttling. *J Biol Chem*. 2002;277(13):11606-11613.

70. Frederick ED, Ramos SB, Blackshear PJ. A unique C-terminal repeat domain maintains the cytosolic localization of the placenta-specific tristetraprolin family member ZFP36L3. *J Biol Chem*. 2008;283(21):14792-14800.

71. Bowden H, Dormann D. Altered mRNP granule dynamics in FTLD pathogenesis. *J Neurochem*. 2016.

72. Stoecklin G, Stubbs T, Kedersha N, *et al*. MK2-induced tristetraprolin:14-3-3 complexes prevent stress granule association and ARE-mRNA decay. *EMBO J*. 2004;23(6):1313-1324.

73. Brennan SE, Kuwano Y, Alkharouf N, Blackshear PJ, Gorospe M, Wilson GM. The mRNA-destabilizing protein tristetraprolin is suppressed in many cancers, altering tumorigenic phenotypes and patient prognosis. *Cancer Res*. 2009;69(12):5168-5176.

74. Milke L, Schulz K, Weigert A, Sha W, Schmid T, Brune B. Depletion of tristetraprolin in breast cancer cells increases interleukin-16 expression and promotes tumor infiltration with monocytes/macrophages. *Carcinogenesis*. 2013;34(4):850-857.

75. Carballo E, Lai WS, Blackshear PJ. Evidence that tristetraprolin is a physiological regulator of granulocyte-macrophage colony-stimulating factor messenger RNA deadenylation and stability. *Blood*. 2000;95(6):1891-1899.

76. Ogilvie RL, Abelson M, Hau HH, Vlasova I, Blackshear PJ, Bohjanen PR. Tristetraprolin down-regulates IL-2 gene expression through AU-rich element-mediated mRNA decay. *J Immunol*. 2005;174(2):953-961.

77. Stoecklin G, Tenenbaum SA, Mayo T, *et al*. Genome-wide analysis identifies interleukin-10 mRNA as target of tristetraprolin. *J Biol Chem*. 2008;283(17):11689-11699.

78. Qiu LQ, Lai WS, Bradbury A, Zeldin DC, Blackshear PJ. Tristetraprolin (TTP) coordinately regulates primary and secondary cellular responses to proinflammatory stimuli. *J Leukoc Biol*. 2015;97(4):723-736.

79. Horner TJ, Lai WS, Stumpo DJ, Blackshear PJ. Stimulation of polo-like kinase 3 mRNA decay by tristetraprolin. *Mol Cell Biol*. 2009;29(8):1999-2010.

80. Sauer I, Schaljo B, Vogl C, *et al*. Interferons limit inflammatory responses by induction of tristetraprolin. *Blood*. 2006;107(12):4790-4797.

81. Emmons J, Townley-Tilson WH, Deleault KM, *et al*. Identification of TTP mRNA targets in human dendritic cells reveals TTP as a critical regulator of dendritic cell maturation. *RNA*. 2008;14(5):888-902.

82. Patino WD, Kang JG, Matoba S, Mian OY, Gochuico BR, Hwang PM. Atherosclerotic plaque macrophage transcriptional regulators are expressed in blood and modulated by tristetraprolin. *Circ Res*. 2006;98(10):1282-1289.

83. Kim CW, Kim HK, Vo MT, *et al*. Tristetraprolin controls the stability of cIAP2 mRNA through binding to the 3'UTR of cIAP2 mRNA. *Biochem Biophys Res Commun*. 2010;400(1):46-52.

84. Marderosian M, Sharma A, Funk AP, *et al*. Tristetraprolin regulates cyclin D1 and c-myc mRNA stability in response to rapamycin in an akt-dependent manner via p38 MAPK signaling. *Oncogene*. 2006;25(47):6277-6290.

85. Young LE, Sanduja S, Bemis-Standoli K, Pena EA, Price RL, Dixon DA. The mRNA binding proteins HuR and tristetraprolin regulate cyclooxygenase 2 expression during colon carcinogenesis. *Gastroenterology*. 2009;136(5):1669-1679.

86. Emmons J, Townley-Tilson WH, Deleault KM, *et al*. Identification of TTP mRNA targets in human dendritic cells reveals TTP as a critical regulator of dendritic cell maturation. *RNA*. 2008;14(5):888-902.

87. Sanduja S, Kaza V, Dixon DA. The mRNA decay factor tristetraprolin (TTP) induces senescence in human papillomavirus-transformed cervical cancer cells by targeting E6-AP ubiquitin ligase. *Aging (Albany NY)*. 2009;1(9):803-817.

88. Frasca D, Landin AM, Alvarez JP, Blackshear PJ, Riley RL, Blomberg BB. Tristetraprolin, a negative regulator of mRNA stability, is increased in old B cells and is involved in the degradation of E47 mRNA. *J Immunol*. 2007;179(2):918-927.

89. Ogilvie RL, Sternjohn JR, Rattenbacher B, *et al*. Tristetraprolin mediates interferon-gamma mRNA decay. *J Biol Chem*. 2009;284(17):11216-11223.

90. Fechir M, Linker K, Pautz A, *et al*. Tristetraprolin regulates the expression of the human inducible nitric-oxide synthase gene. *Mol Pharmacol*. 2005;67(6):2148-2161.

91. Lee HH, Vo MT, Kim HJ, *et al*. Stability of the LATS2 tumor suppressor gene is regulated by tristetraprolin. *J Biol Chem*. 2010;285(23):17329-17337.

92. Al-Souhibani N, Al-Ahmadi W, Hesketh JE, Blackshear PJ, Khabar KS. The RNA-binding zinc-finger protein tristetraprolin regulates AU-rich mRNAs involved in breast cancer-related processes. *Oncogene*. 2010;29(29):4205-4215.

93. Yu H, Stasinopoulos S, Leedman P, Medcalf RL. Inherent instability of plasminogen activator inhibitor type 2 mRNA is regulated by tristetraprolin. *J Biol Chem*. 2003;278(16):13912-13918.

94. Brooks SA, Connolly JE, Rigby WF. The role of mRNA turnover in the regulation of tristetraprolin expression: Evidence for an extracellular signal-regulated kinase-specific, AU-rich element-dependent, autoregulatory pathway. *J Immunol*. 2004;172(12):7263-7271.

95. Brennan SE, Kuwano Y, Alkharouf N, Blackshear PJ, Gorospe M, Wilson GM. The mRNA-destabilizing protein tristetraprolin is suppressed in many cancers, altering tumorigenic phenotypes and patient prognosis. *Cancer Res*. 2009;69(12):5168-5176.

96. Jalonen U, Nieminen R, Vuolteenaho K, Kankaanranta H, Moilanen E. Down-regulation of tristetraprolin expression results in enhanced IL-12 and MIP-2 production and reduced MIP-3alpha synthesis in activated macrophages. *Mediators Inflamm*. 2006;2006(6):40691.

97. Gringhuis SI, Garcia-Vallejo JJ, van Het Hof B, van Dijk W. Convergent actions of I kappa B kinase beta and protein kinase C delta modulate mRNA stability through phosphorylation of 14-3-3 beta complexed with tristetraprolin. *Mol Cell Biol*. 2005;25(15):6454-6463.

98. Lai WS, Parker JS, Grissom SF, Stumpo DJ, Blackshear PJ. Novel mRNA targets for tristetraprolin (TTP) identified by global analysis of stabilized transcripts in TTP-deficient fibroblasts. *Mol Cell Biol*. 2006;26(24):9196-9208.

99. Lu YC, Chang SH, Hafner M, *et al*. ELAVL1 modulates transcriptome-wide miRNA binding in murine macrophages. *Cell Rep*. 2014;9(6):2330-2343.

100. Essafi-Benkhadir K, Onesto C, Stebe E, Moroni C, Pages G. Tristetraprolin inhibits ras-dependent tumor vascularization by inducing vascular endothelial growth factor mRNA degradation. *Mol Biol Cell*. 2007;18(11):4648-4658.

101. Gao J, Aksoy BA, Dogrusoz U, *et al*. Integrative analysis of complex cancer genomics and clinical profiles using the cBioPortal. *Sci Signal*. 2013;6(269):pl1.

102. Cerami E, Gao J, Dogrusoz U, *et al*. The cBio cancer genomics portal: An open platform for exploring multidimensional cancer genomics data. *Cancer Discov*. 2012;2(5):401-404.

103. Iwanaga E, Nanri T, Mitsuya H, Asou N. Mutation in the RNA binding protein TIS11D/ZFP36L2 is associated with the pathogenesis of acute leukemia. *Int J Oncol*. 2011;38(1):25-31.

104. Hodson DJ, Janas ML, Galloway A, *et al*. Deletion of the RNA-binding proteins ZFP36L1 and ZFP36L2 leads to perturbed thymic development and T lymphoblastic leukemia. *Nat Immunol*. 2010;11(8):717-724.

105. Desroches-Castan A, Cherradi N, Feige JJ, Ciais D. A novel function of Tis11b/BRF1 as a regulator of Dll4 mRNA 3'-end processing. *Mol Biol Cell*. 2011;22(19):3625-3633.

106. Varnum BC, Ma QF, Chi TH, Fletcher B, Herschman HR. The TIS11 primary response gene is a member of a gene family that encodes proteins with a highly conserved sequence containing an unusual cys-his repeat. *Mol Cell Biol*. 1991;11(3):1754-1758.

107. Lai WS, Kennington EA, Blackshear PJ. Tristetraprolin and its family members can promote the cell-free deadenylation of AU-rich element-containing mRNAs by poly(A) ribonuclease. *Mol Cell Biol*. 2003;23(11):3798-3812.

108. Baou M, Jewell A, Murphy JJ. TIS11 family proteins and their roles in posttranscriptional gene regulation. *J Biomed Biotechnol*. 2009;2009:634520.

109. Taylor GA, Carballo E, Lee DM, *et al*. A pathogenetic role for TNF alpha in the syndrome of cachexia, arthritis, and autoimmunity resulting from tristetraprolin (TTP) deficiency. *Immunity*. 1996;4(5):445-454.

110. Stumpo DJ, Byrd NA, Phillips RS, *et al*. Chorioallantoic fusion defects and embryonic lethality resulting from disruption of Zfp36L1, a gene encoding a CCCH tandem zinc finger protein of the tristetraprolin family. *Mol Cell Biol*. 2004;24(14):6445-6455.

111. Stumpo DJ, Broxmeyer HE, Ward T, *et al*. Targeted disruption of Zfp36l2, encoding a CCCH tandem zinc finger RNA-binding protein, results in defective hematopoiesis. *Blood*. 2009;114(12):2401-2410.

112. Brennan SE, Kuwano Y, Alkharouf N, Blackshear PJ, Gorospe M, Wilson GM. The mRNA-destabilizing protein tristetraprolin is suppressed in many cancers, altering tumorigenic phenotypes and patient prognosis. *Cancer Res*. 2009;69(12):5168-5176.

113. Edgar RC. MUSCLE: Multiple sequence alignment with high accuracy and high throughput. *Nucleic Acids Res*. 2004;32(5):1792-1797.

114. Varnum BC, Ma QF, Chi TH, Fletcher B, Herschman HR. The TIS11 primary response gene is a member of a gene family that encodes proteins with a highly

conserved sequence containing an unusual cys-his repeat. *Mol Cell Biol*. 1991;11(3):1754-1758.

115. Barbar E. NMR characterization of partially folded and unfolded conformational ensembles of proteins. *Biopolymers*. 1999;51(3):191-207.

116. Blackshear PJ, Lai WS, Kennington EA, *et al*. Characteristics of the interaction of a synthetic human tristetraprolin tandem zinc finger peptide with AU-rich element-containing RNA substrates. *J Biol Chem*. 2003;278(22):19947-19955.

117. Hudson BP, Martinez-Yamout MA, Dyson HJ, Wright PE. Recognition of the mRNA AU-rich element by the zinc finger domain of TIS11d. *Nat Struct Mol Biol*. 2004;11(3):257-264.

118. Lai WS, Kennington EA, Blackshear PJ. Interactions of CCCH zinc finger proteins with mRNA: Non-binding tristetraprolin mutants exert an inhibitory effect on degradation of AU-rich element-containing mRNAs. *J Biol Chem*. 2002;277(11):9606-9613.

119. Glisovic T, Bachorik JL, Yong J, Dreyfuss G. RNA-binding proteins and post-transcriptional gene regulation. *FEBS Lett*. 2008;582(14):1977-1986.

120. Carballo E, Lai WS, Blackshear PJ. Feedback inhibition of macrophage tumor necrosis factor-alpha production by tristetraprolin. *Science*. 1998;281(5379):1001-1005.

121. Lai WS, Carballo E, Strum JR, Kennington EA, Phillips RS, Blackshear PJ. Evidence that tristetraprolin binds to AU-rich elements and promotes the deadenylation and destabilization of tumor necrosis factor alpha mRNA. *Mol Cell Biol*. 1999;19(6):4311-4323.

122. Balakathiresan NS, Bhattacharyya S, Gutti U, *et al*. Tristetraprolin regulates IL-8 mRNA stability in cystic fibrosis lung epithelial cells. *Am J Physiol Lung Cell Mol Physiol*. 2009;296(6):L1012-8.

123. Varnum BC, Lim RW, Sukhatme VP, Herschman HR. Nucleotide sequence of a cDNA encoding TIS11, a message induced in swiss 3T3 cells by the tumor promoter tetradecanoyl phorbol acetate. *Oncogene*. 1989;4(1):119-120.

124. Lykke-Andersen J, Wagner E. Recruitment and activation of mRNA decay enzymes by two ARE-mediated decay activation domains in the proteins TTP and BRF-1. *Genes Dev*. 2005;19(3):351-361.

125. Sandler H, Stoecklin G. Control of mRNA decay by phosphorylation of tristetraprolin. *Biochem Soc Trans*. 2008;36(Pt 3):491-496.

126. Taylor GA, Carballo E, Lee DM, *et al*. A pathogenetic role for TNF alpha in the syndrome of cachexia, arthritis, and autoimmunity resulting from tristetraprolin (TTP) deficiency. *Immunity*. 1996;4(5):445-454.

127. Hudson BP, Martinez-Yamout MA, Dyson HJ, Wright PE. Recognition of the mRNA AU-rich element by the zinc finger domain of TIS11d. *Nat Struct Mol Biol*. 2004;11(3):257-264.

128. Morgan BR, Massi F. A computational study of RNA binding and specificity in the tandem zinc finger domain of TIS11d. *Protein Sci*. 2010;19(6):1222-1234.

129. Pagano JM, Farley BM, McCoig LM, Ryder SP. Molecular basis of RNA recognition by the embryonic polarity determinant MEX-5. *J Biol Chem*. 2007;282(12):8883-8894.

130. Deveau LM, Massi F. Three residues make an evolutionary switch for folding and RNA-destabilizing activity in the TTP family of proteins. *ACS Chem Biol*. 2016;11(2):435-443.

131. Blackshear PJ, Lai WS, Kennington EA, *et al*. Characteristics of the interaction of a synthetic human tristetraprolin tandem zinc finger peptide with AU-rich element-containing RNA substrates. *J Biol Chem*. 2003;278(22):19947-19955.

132. Brewer BY, Malicka J, Blackshear PJ, Wilson GM. RNA sequence elements required for high affinity binding by the zinc finger domain of tristetraprolin: Conformational changes coupled to the bipartite nature of au-rich MRNA-destabilizing motifs. *J Biol Chem*. 2004;279(27):27870-27877.

133. Gubler M, Bickle TA. Increased protein flexibility leads to promiscuous protein--DNA interactions in type IC restriction-modification systems. *EMBO J*. 1991;10(4):951-957.

134. Nobeli I, Favia AD, Thornton JM. Protein promiscuity and its implications for biotechnology. *Nat Biotechnol*. 2009;27(2):157-167.

135. Munz M, Hein J, Biggin PC. The role of flexibility and conformational selection in the binding promiscuity of PDZ domains. *PLoS Comput Biol*. 2012;8(11):e1002749.

136. Pabis A, Kamerlin SC. Promiscuity and electrostatic flexibility in the alkaline phosphatase superfamily. *Curr Opin Struct Biol*. 2015;37:14-21.

137. Patil A, Kinoshita K, Nakamura H. Hub promiscuity in protein-protein interaction networks. *Int J Mol Sci*. 2010;11(4):1930-1943.

138. Gianni S, Dogan J, Jemth P. Coupled binding and folding of intrinsically disordered proteins: What can we learn from kinetics? *Curr Opin Struct Biol*. 2016;36:18-24.

139. Liu Z, Huang Y. Advantages of proteins being disordered. *Protein Sci*. 2014;23(5):539-550.

140. Lai WS, Kennington EA, Blackshear PJ. Interactions of CCCH zinc finger proteins with mRNA: Non-binding tristetraprolin mutants exert an inhibitory effect on degradation of AU-rich element-containing mRNAs. *J Biol Chem*. 2002;277(11):9606-9613.

141. Mukherjee N, Jacobs NC, Hafner M, *et al*. Global target mRNA specification and regulation by the RNA-binding protein ZFP36. *Genome Biol*. 2014;15(1):R12-2014-15-1-r12.

142. Chen CY, Gherzi R, Ong SE, *et al*. AU binding proteins recruit the exosome to degrade ARE-containing mRNAs. *Cell*. 2001;107(4):451-464.

143. Lebedeva S, Jens M, Theil K, *et al*. Transcriptome-wide analysis of regulatory interactions of the RNA-binding protein HuR. *Mol Cell*. 2011;43(3):340-352.

144. Carpenter S, Ricci EP, Mercier BC, Moore MJ, Fitzgerald KA. Post-transcriptional regulation of gene expression in innate immunity. *Nat Rev Immunol*. 2014;14(6):361-376.

145. Delaglio, F, grzesiek, S, vuister, G W, zhu, G., pfeifer, J., and bax, A. (1995) NMRPipe: A multidimensional spectral processing system based on unix pipes, J. biomol. NMR 6, 277-293. .

146. Goddard, T. D., and kneller, D. G. SPARKY 3, university of California, san francisco, CA. .

147. Narayan VA, Kriwacki RW, Caradonna JP. Structures of zinc finger domains from transcription factor Sp1. insights into sequence-specific protein-DNA recognition. *J Biol Chem*. 1997;272(12):7801-7809.

148. Pagano JM, Farley BM, McCoig LM, Ryder SP. Molecular basis of RNA recognition by the embryonic polarity determinant MEX-5. *J Biol Chem*. 2007;282(12):8883-8894.

149. Brewer BY, Malicka J, Blackshear PJ, Wilson GM. RNA sequence elements required for high affinity binding by the zinc finger domain of tristetraprolin: Conformational changes coupled to the bipartite nature of au-rich MRNA-destabilizing motifs. *J Biol Chem*. 2004;279(27):27870-27877.

150. Farley BM, Ryder SP. POS-1 and GLD-1 repress glp-1 translation through a conserved binding-site cluster. *Mol Biol Cell*. 2012;23(23):4473-4483.

151. Kaymak E, Ryder SP. RNA recognition by the caenorhabditis elegans oocyte maturation determinant OMA-1. *J Biol Chem*. 2013;288(42):30463-30472.

152. Zanocco-Marani T. TIS11/TTP gene family: It's never too late for tumor suppressors. *Cell Cycle*. 2010;9(24):4771.

153. Ciais D, Cherradi N, Feige JJ. Multiple functions of tristetraprolin/TIS11 RNA-binding proteins in the regulation of mRNA biogenesis and degradation. *Cell Mol Life Sci*. 2013;70(12):2031-2044.

154. Blackshear PJ. Tristetraprolin and other CCCH tandem zinc-finger proteins in the regulation of mRNA turnover. *Biochem Soc Trans*. 2002;30(Pt 6):945-952.

155. Siderovski DP, Blum S, Forsdyke RE, Forsdyke DR. A set of human putative lymphocyte G0/G1 switch genes includes genes homologous to rodent cytokine and zinc finger protein-encoding genes. *DNA Cell Biol*. 1990;9(8):579-587.

156. DuBois RN, McLane MW, Ryder K, Lau LF, Nathans D. A growth factor-inducible nuclear protein with a novel cysteine/histidine repetitive sequence. *J Biol Chem*. 1990;265(31):19185-19191.

157. Lai WS, Stumpo DJ, Blackshear PJ. Rapid insulin-stimulated accumulation of an mRNA encoding a proline-rich protein. *J Biol Chem*. 1990;265(27):16556-16563.

158. Zhang H, Liu Y, Wen F, *et al*. A novel rice C2H2-type zinc finger protein, ZFP36, is a key player involved in abscisic acid-induced antioxidant defence and oxidative stress tolerance in rice. *J Exp Bot*. 2014;65(20):5795-5809.

159. Brooks SA, Connolly JE, Diegel RJ, Fava RA, Rigby WF. Analysis of the function, expression, and subcellular distribution of human tristetraprolin. *Arthritis Rheum*. 2002;46(5):1362-1370.

160. Sandler H, Kreth J, Timmers HT, Stoecklin G. Not1 mediates recruitment of the deadenylase Caf1 to mRNAs targeted for degradation by tristetraprolin. *Nucleic Acids Res*. 2011;39(10):4373-4386.

161. Fabian MR, Frank F, Rouya C, *et al*. Structural basis for the recruitment of the human CCR4-NOT deadenylase complex by tristetraprolin. *Nat Struct Mol Biol*. 2013;20(6):735-739.

162. Pagano JM, Farley BM, McCoig LM, Ryder SP. Molecular basis of RNA recognition by the embryonic polarity determinant MEX-5. *J Biol Chem*. 2007;282(12):8883-8894.

163. Amann BT, Worthington MT, Berg JM. A Cys3His zinc-binding domain from Nup475/tristetraprolin: A novel fold with a disklike structure. *Biochemistry*. 2003;42(1):217-221.

164. Blackshear PJ, Lai WS, Kennington EA, *et al*. Characteristics of the interaction of a synthetic human tristetraprolin tandem zinc finger peptide with AU-rich element-containing RNA substrates. *J Biol Chem*. 2003;278(22):19947-19955.

165. Kosol S, Contreras-Martos S, Cedeno C, Tompa P. Structural characterization of intrinsically disordered proteins by NMR spectroscopy. *Molecules*. 2013;18(9):10802-10828.

166. Schulman BA, Kim PS, Dobson CM, Redfield C. A residue-specific NMR view of the non-cooperative unfolding of a molten globule. *Nat Struct Biol*. 1997;4(8):630-634.

167. Brewer BY, Malicka J, Blackshear PJ, Wilson GM. RNA sequence elements required for high affinity binding by the zinc finger domain of tristetraprolin:

Conformational changes coupled to the bipartite nature of au-rich MRNA-destabilizing motifs. *J Biol Chem*. 2004;279(27):27870-27877.

168. Worthington MT, Amann BT, Nathans D, Berg JM. Metal binding properties and secondary structure of the zinc-binding domain of Nup475. *Proc Natl Acad Sci U S A*. 1996;93(24):13754-13759.

169. Seneque O, Latour JM. Coordination properties of zinc finger peptides revisited: Ligand competition studies reveal higher affinities for zinc and cobalt. *J Am Chem Soc*. 2010;132(50):17760-17774.

170. Velyvis A, Qin J. LIM domain and its binding to target proteins, in *zinc finger proteins*
. *Springer US, Boston, MA*. 2005:99–105.

171. Reddi AR, Guzman TR, Breece RM, Tierney DL, Gibney BR. Deducing the energetic cost of protein folding in zinc finger proteins using designed metallopeptides. *J Am Chem Soc*. 2007;129(42):12815-12827.

172. Sormanni P, Camilloni C, Fariselli P, Vendruscolo M. The s2D method: Simultaneous sequence-based prediction of the statistical populations of ordered and disordered regions in proteins. *J Mol Biol*. 2015;427(4):982-996.

173. Camilloni C, De Simone A, Vranken WF, Vendruscolo M. Determination of secondary structure populations in disordered states of proteins using nuclear magnetic resonance chemical shifts. *Biochemistry*. 2012;51(11):2224-2231.

174. Pagano JM, Clingman CC, Ryder SP. Quantitative approaches to monitor protein-nucleic acid interactions using fluorescent probes. *RNA*. 2011;17(1):14-20.

175. Morgan BR, Deveau LM, Massi F. Probing the structural and dynamical effects of the charged residues of the TZF domain of TIS11d. *Biophys J*. 2015;108(6):1503-1515.

176. Morgan BR, Massi F. A computational study of RNA binding and specificity in the tandem zinc finger domain of TIS11d. *Protein Sci*. 2010;19(6):1222-1234.

177. Cornilescu G, Delaglio F, Bax A. Protein backbone angle restraints from searching a database for chemical shift and sequence homology. *J Biomol NMR*. 1999;13(3):289-302.

178. Lai WS, Perera L, Hicks SN, Blackshear PJ. Mutational and structural analysis of the tandem zinc finger domain of tristetraprolin. *J Biol Chem*. 2014;289(1):565-580.

179. Siepel A, Haussler D. Combining phylogenetic and hidden markov models in biosequence analysis. *J Comput Biol*. 2004;11(2-3):413-428.

180. Hubisz MJ, Pollard KS, Siepel A. PHAST and RPHAST: Phylogenetic analysis with space/time models. *Brief Bioinform*. 2011;12(1):41-51.

181. Rosenbloom KR, Armstrong J, Barber GP, *et al*. The UCSC genome browser database: 2015 update. *Nucleic Acids Res*. 2015;43(Database issue):D670-81.

182. Blanchette M, Kent WJ, Riemer C, *et al*. Aligning multiple genomic sequences with the threaded blockset aligner. *Genome Res*. 2004;14(4):708-715.

183. Gomperts M, Pascall JC, Brown KD. The nucleotide sequence of a cDNA encoding an EGF-inducible gene indicates the existence of a new family of mitogen-induced genes. *Oncogene*. 1990;5(7):1081-1083.

184. Ngoc LV, Wauquier C, Soin R, *et al*. Rapid proteasomal degradation of posttranscriptional regulators of the TIS11/tristetraprolin family is induced by an intrinsically unstructured region independently of ubiquitination. *Mol Cell Biol*. 2014;34(23):4315-4328.

185. Frederick ED, Ramos SB, Blackshear PJ. A unique C-terminal repeat domain maintains the cytosolic localization of the placenta-specific tristetraprolin family member ZFP36L3. *J Biol Chem*. 2008;283(21):14792-14800.

186. Finn RD, Bateman A, Clements J, *et al*. Pfam: The protein families database. *Nucleic Acids Res*. 2014;42(Database issue):D222-30.

187. Lee MH, Schedl T. RNA-binding proteins. *WormBook*. 2006:1-13.

188. Reese KJ, Dunn MA, Waddle JA, Seydoux G. Asymmetric segregation of PIE-1 in C. elegans is mediated by two complementary mechanisms that act through separate PIE-1 protein domains. *Mol Cell*. 2000;6(2):445-455.

189. Esposito K, Nappo F, Marfella R, *et al*. Inflammatory cytokine concentrations are acutely increased by hyperglycemia in humans: Role of oxidative stress. *Circulation*. 2002;106(16):2067-2072.

190. Mondet J, Hussein K, Mossuz P. Circulating cytokine levels as markers of inflammation in philadelphia negative myeloproliferative neoplasms: Diagnostic and prognostic interest. *Mediators Inflamm*. 2015;2015:670580.

191. Barreau C, Paillard L, Osborne HB. AU-rich elements and associated factors: Are there unifying principles? *Nucleic Acids Res*. 2006;33(22):7138-7150.

192. Ross CR, Brennan-Laun SE, Wilson GM. Tristetraprolin: Roles in cancer and senescence. *Ageing Res Rev*. 2012;11(4):473-484.

193. Sanduja S, Blanco FF, Young LE, Kaza V, Dixon DA. The role of tristetraprolin in cancer and inflammation. *Front Biosci (Landmark Ed)*. 2012;17:174-188.

194. Patino WD, Kang JG, Matoba S, Mian OY, Gochuico BR, Hwang PM. Atherosclerotic plaque macrophage transcriptional regulators are expressed in blood and modulated by tristetraprolin. *Circ Res*. 2006;98(10):1282-1289.

195. Morgan BR, Deveau LM, Massi F. Probing the structural and dynamical effects of the charged residues of the TZF domain of TIS11d. *Biophys J*. 2015;108(6):1503-1515.

196. Frederick ED, Ramos SB, Blackshear PJ. A unique C-terminal repeat domain maintains the cytosolic localization of the placenta-specific tristetraprolin family member ZFP36L3. *J Biol Chem*. 2008;283(21):14792-14800.

197. Phillips RS, Ramos SB, Blackshear PJ. Members of the tristetraprolin family of tandem CCCH zinc finger proteins exhibit CRM1-dependent nucleocytoplasmic shuttling. *J Biol Chem*. 2002;277(13):11606-11613.

198. Franks TM, Lykke-Andersen J. TTP and BRF proteins nucleate processing body formation to silence mRNAs with AU-rich elements. *Genes Dev*. 2007;21(6):719-735.

199. Johnston JA, Ward CL, Kopito RR. Aggresomes: A cellular response to misfolded proteins. *J Cell Biol*. 1998;143(7):1883-1898.

200. Eskelinen EL, Saftig P. Autophagy: A lysosomal degradation pathway with a central role in health and disease. *Biochim Biophys Acta*. 2009;1793(4):664-673.

201. Milke L, Schulz K, Weigert A, Sha W, Schmid T, Brune B. Depletion of tristetraprolin in breast cancer cells increases interleukin-16 expression and promotes tumor infiltration with monocytes/macrophages. *Carcinogenesis*. 2013;34(4):850-857.

202. Freeberg MA, Kim JK. Mapping the transcriptome-wide landscape of RBP binding sites using gPAR-CLIP-seq: Bioinformatic analysis. *Methods Mol Biol*. 2016;1361:91-104.

203. Pagano JM, Farley BM, McCoig LM, Ryder SP. Molecular basis of RNA recognition by the embryonic polarity determinant MEX-5. *J Biol Chem*. 2007;282(12):8883-8894.

204. Planel S, Salomon A, Jalinot P, Feige JJ, Cherradi N. A novel concept in antiangiogenic and antitumoral therapy: Multitarget destabilization of short-lived mRNAs by the zinc finger protein ZFP36L1. *Oncogene*. 2010;29(45):5989-6003.

205. Ohyama T, Nagata T, Tsuda K, *et al*. Structure of Musashi1 in a complex with target RNA: The role of aromatic stacking interactions. *Nucleic Acids Res*. 2012;40(7):3218-3231.

206. Lewis HA, Musunuru K, Jensen KB, *et al*. Sequence-specific RNA binding by a nova KH domain: Implications for paraneoplastic disease and the fragile X syndrome. *Cell*. 2000;100(3):323-332.